Experiments and Modelling of Hydrogen Gas Generation from the Reaction of Aluminium-NaOH Solution and its Application in Sintering Furnace

A Thesis

Submitted in Partial Fulfilment of the

Requirements for the award of the Degree of

DOCTOR OF PHILOSOPHY

by

Biswajyoti Das

(Roll No. 126103009)

Department of Mechanical Engineering

Indian Institute of Technology Guwahati

Guwahati- 781039

Assam, India

December, 2024

ভাৰতীয় প্ৰযুক্তিবিদ্যা প্ৰতিষ্ঠান গুৱাহাটী
INDIAN INSTITUTE OF TECHNOLOGY
GUWAHATI, Assam, India
Department of Mechanical Engineering

CERTIFICATE

This is to certify that the contents embodied in the thesis entitled "**Experiments and Modelling of Hydrogen Gas Generation from the Reaction of Aluminium-NaOH Solution and its Application in Sintering Furnace"** is the outcome of the investigations carried out completely by Mr. Biswajyoti Das (Roll No. 126103009), Department of Mechanical Engineering under our supervision, and is submitted to the Indian Institute of Technology Guwahati, North – Guwahati-781039, Assam, India for the award of degree of *Doctor of Philosophy*. This work has not been submitted elsewhere for any degree or diploma of any institute or university.

Dr. Pinakeswar Mahanta
Professor
Dept. of Mechanical Engineering
IIT Guwahati
……2024

Dr. P. S. Robi
Professor
Dept. of Mechanical Engineering
IIT Guwahati
……2024

ভাৰতীয় প্ৰযুক্তিবিদ্যা প্ৰতিষ্ঠান গুৱাহাটী
INDIAN INSTITUTE OF TECHNOLOGY
GUWAHATI, Assam, India
Department of Mechanical Engineering

DECLARATION

This is to declare that the contents embodied in the thesis entitled "**Experiments and Modelling of Hydrogen Gas Generation from the Reaction of Aluminium-NaOH Solution and its Application in Sintering Furnace"** is the outcome of the investigations carried out completely by myself under the excellent supervision of Prof. P. S. Robi and Prof. Pinakeswar Mahanta, Department of Mechanical Engineering, and is submitted to the Indian Institute of Technology Guwahati, North – Guwahati-781039, Assam, India for the award of degree of *Doctor of Philosophy*. This work has not been submitted elsewhere for any degree or diploma of any institute or university to the best of my knowledge and belief.

In keeping with the general practice of reporting scientific observations, due acknowledgements have been made wherever the work of other investigators are referred and copyright licences have been taken from respective publishers.

Guwahati — Biswajyoti Das

Date:

Dedicated to.....

my dear mother, sister

and

heavenly aboard father

without whom the journey would not have been completed

Acknowledgements

God is almighty

At the foremost, I offer my sincere gratitude to the almighty for his unrestrained blessings. I am thankful to the unseen for his immense support throughout my life.

I am grateful to my supervisors Prof. P. S. Robi and Prof. Pinakeswar Mahanta, Department of Mechanical Engineering, IIT Guwahati, for their excellent guidance. The journey would not have been possible without their reluctant less support.

I take this opportunity to pay my special thanks to the Doctoral Committee members Prof. U. K. Saha, Prof. S. Pal, Department of Mechanical Engineering, and Prof. S. K. Majumder, Department of Chemical Engineering, IIT Guwahati for constantly reviewing my research work and providing valuable suggestions.

I am also thankful to Dr. Anil Borah, Professor, Department of Mechanical Engineering, Assam Engineering College, Jalukbari, Guwahati, Assam, India for recognizing my ability and inspired me to go for research.

I shall always be grateful to all the faculty members, officers, and the staff of the Department of Mechanical Engineering, IIT Guwahati. I am deeply grateful to all the Central Workshop staff of IIT Guwahati for their excellent support. It is my privilege to say thanks to the Centre for Energy, IIT Guwahati for their kind help. I offer my sincere thanks to Assam down town University for giving me the opportunity to continue research work.

I also take this opportunity to pay thanks to all the amazing lab mates, colleagues, hostel mates, and my dear friends for their immense support during my research work.

The last but not the least, I offer my deepest gratitude to my family members. Especially, the sacrifices of my mother and sister during this journey after my father's departure. Every day I start my work remembering my father who is showering his blesses from the heaven. He has been a guide and philosopher to me.

Finally, as a member of the IIT Guwahati fraternity, I wish all-round development of the institute and cherish the moment of my stay during the research period, glorious days of my life, that I can never forget. God Bless All.

Abstract

The power generation using fossil fuels has been practised globally through several hundreds of years. The calorific values of both the fuel are very high to be used as the source of energy. Fossil fuels are limited and require millions of years to be replenished. As of now, the whole planet strives for the energy crisis. Another shortcoming associated with the burning of fossil fuel is the emission of pollutant gases, which hamper the eco-friendly nature of the environment. The emission of CO_x, SO_x, NO_x, *etc.*, cause serious environmental issues. Considering these aspects related to the scarcity and burning of fossil fuels researchers and scientists have focused on the alternate source of energy, which is renewable. There are many green energy sources exist now a day. Solar energy, biogas, hydro energy, wind energy, ocean energy, H_2 energy is some of the examples of new and renewable sources of energy. In this context, H_2 energy has got much attention recently, as the energy density of hydrogen gas is 142 $MJ.kg^{-1}$, the by-product of the combustion of hydrogen gas is only water and heat, environment-friendly, and the most abundant material found in the universe. Hydrogen is primarily found in hydrocarbons in a combined state.

There are many methods of hydrogen production exist. For example, water electrolysis, hydrocarbon synthesis, chemical methods, *etc.* Though different ways of production of hydrogen gas are present, each process has its own merits and demerits. Among these various techniques of hydrogen production, the chemical method appears to be a viable method of gas production. Therefore, the production of H_2 gas using the Al-H_2O reaction has been chosen for the present study. The reasons behind the selection of Al are as follows: it is lightweight with a high energy density of 29 $MJ.kg^{-1}$, Al scrap is available in abundance, *etc.* Moreover, the reaction by-product $Al(OH)_3$, finds many industrial applications.

The major problems responsible to the limited use of hydrogen gas are the storage, and the transportation of H_2. The ignition energy of hydrogen gas is only 0.02 mJ which makes it vulnerable to flammability. Hence, the novel work has been adopted to use on-board hydrogen gas in the sintering tube furnace. Thereby, reducing the disadvantages of storing and transportation of hydrogen gas. In this present work, the aluminium-water reaction in the presence of aq. NaOH has been carried out under different conditions to establish the kinetics of the reaction. The reactions are conducted at concentrations of aq. NaOH varying from 1M

to 5M in a step of 1M and temperature of the solution varies from 303 K to 333 K in a step of 10 K. The effect of volume of aq. NaOH, size of aluminium pellets is also investigated. It is revealed that the reaction follows first-order kinetics. The rate of production of hydrogen gas is found to be increased with the rise in temperature and concentration of aq. NaOH. The maximum amount of hydrogen gas has been obtained as 1322 $ml.g^{-1}$ of Al, which is ~ 97 % of the maximum theoretical yield. The optimum condition for producing hydrogen gas is determined as 5M/333 K. The activation energy is obtained as 57.62 $kJ.\ mol^{-1}$. Activation energy is found to be reduced for finer pellets of Al.

Hydrogen is a good source of energy for different industrial applications. However, the limited data available at the laboratory level for the production of H_2 gas by the chemical reaction between Al and water in the presence of aq. NaOH cannot predict the feasibility of the process in an effective way for real-time applications. Moreover, in-situ production and utilization of H_2 gas in industry needs close monitoring and control systems. Hence, an effective mathematical model is required for its real-time applications. The mathematical simulation for the reaction kinetics of the reaction is carried out using machine learning techniques *viz.* the ANN, and the MLR. The experimental data are trained, tested, and validated to achieve the best mathematical model which can be implemented for the industrial uses.

On-board production and use of hydrogen in a sintering tube furnace has been demonstrated to investigate its thermal efficiency. The temperature profile of the combusted gas inside the sintering tube furnace in the radial and the axial directions are presented. The thermal efficiency of the furnace has been calculated as 76.22 % at corresponding actual fuel-air ratio of 1:60. A comparison study has been carried out for the cost of using the unit price of hydrogen gas with electricity and LPG.

Contents

List of Figures

List of Tables

Nomenclature

A	:	Pre-exponential factor/Collision frequency
AARE	:	Absolute average relative error
Al	:	Aluminium
$Al(OH)_3$	:	Aluminium hydroxide
$Al_2(SO_4)_3$	:	Aluminium sulphate
C	:	Concentration (mol)
^{o}C	:	Degree Celsius
CO_2	:	Carbon dioxide
c_j	:	Centre of the j^{th} RBF node
C_0	:	Initial volume of Al (cc)
C_t	:	Volume of Al at time (cc)
E_a	:	Activation energy ($kJ.mol^{-1}$)
G	:	Constant
$GJ.ton^{-1}$	:	Giga Joule per Ton
H	:	Heat (MJ)
h	:	Hour
H_2	:	Hydrogen
K	:	Kelvin
k	:	Rate constant (min^{-1})
kWh	:	Kilowatt hour
M	:	Mole
min	:	Minute
mm	:	Millimetre
$ml.g^{-1}$	:	Millilitre per gram
NaOH	:	Sodium hydroxide
$NaAl(OH)_4$	:	Sodium aluminate
OH^-	:	Hydroxide
R	:	Universal gas constant ($J.K^{-1}.mol^{-1}$)
R_{cc}	:	Correlation coefficient
RMS	:	Root mean square
s	:	Second

T	:	Temperature (K)
t	:	Time (min)
ΔT	:	Temperature gradient (K)
V	:	Volume (ml)
V_e	:	Experimental value
V_p	:	Predicted value
$\overline{V_e}$	:	Average values of V_e
$\overline{V_p}$	:	Average values V_p
W_{ij}	:	Weight function
y	:	Constant
z	:	The net input to the neuron

Greek symbols

α	:	Constant
β	:	Constant
γ	:	Constant
δ	:	Spread of the j^{th} RBF node
$\zeta_j(x)$	:	The Gaussian function
η	:	Thermal efficiency
θ_j	:	Bias
λ	:	Fuel-air equivalent ratio
μm	:	Micron/Micrometre

Abbreviations

ADT	:	Advanced Digital Technologies
AI	:	Artificial Intelligence
ANN	:	Artificial Neural Network
aq.	:	Aqueous
BD	:	Big Data
BEP	:	Break-Even Point
BPNN	:	Feed-Forward Back-Propagation Neural Network
BTE	:	Brake Thermal Efficiency
CI	:	Compression Ignition
CMI	:	Continuous Manifold Injection
CNG	:	Compressed Natural Gas
CVP	:	Cost-Volume-Profit
EJ	:	Exajoule
EMS	:	Energy Management System
FAR	:	Fuel-air ratio
FAR_{stoic}	:	Stoichiometric fuel-air ratio
FAR_{ac}	:	Actual fuel-air ratio
F.C.	:	Fixed cost
FL	:	Fuzzy Logic
GA	:	Genetic Algorithm
GHG	:	Green-House Gases
HHV	:	Higher Heating value
H_2ICE	:	Hydrogen Internal Combustion Engine
HPDI	:	High-Pressure Direct Cylinder Injection
ICE	:	Internal Combustion Engine
IoT	:	Internet of Things
ITE	:	Indicated Thermal Efficiency
LCA	:	Life Cycle Assessment
LHV	:	Lower Heating value
logsig	:	Log-sigmoid
LPG	:	Liquefied Petroleum Gas
lpm	:	Litre per minute
LPDI	:	Low-Pressure Direct Cylinder Injection

LSF	:	Least Square Fit
ML	:	Machine Learning
MLR	:	Multiple Linear Regression Model
PSO	:	Particle Swarm Optimization
RBFNN	:	Radial Basis Function Neural Network
RD&D	:	Research, Development & Demonstration
ROI	:	Return On Investment
SI	:	Spark Ignition
SVM	:	Support Vector Machine
tansig	:	Tangent sigmoid
T.C.	:	Total cost
TDC	:	Top Dead Centre
TMI	:	Timed Manifold Injection
V.C.	:	Variable cost
WNN	:	Wavelet Neural Network
wt.	:	Weight

Chapter-1

Introduction

1.1 Preface

Fossil fuel technology for power generation have been practised through several hundreds of years around the globe. A survey on the use of different forms of energy have revealed that 84 % of global energy requirement has been fulfilled by fossil fuel in the year 2020 [1]. In a report in 2019, it is mentioned that 490 EJ of energy requirement have been met by energy system operated on fossil fuel [1]. In the present scenario the increasing use of fossil fuel based energy sources have created lot of environmental pollution gases known as green-house gases (GHG). The concomitant effect of using fossil fuel on a large scale throughout the globe has depleted their reservoir [2]. Hence, the scientists and research communities around the world have focused their attention towards the use of new and renewable sources of energy. Scientists are dedicated to inventing cutting edge technology of producing alternate, environment-friendly, low cost, and renewable source of energy for power generation. The concept of using sustainable sources of energy is an another dimension in this study [3], [4]. Industries and educational organizations in the area of energy have also emphasized their research, development & demonstration (RD&D) works on clean and environment-friendly energy sources. The concept of sustainable energy will be more relevant if the energy demand can be fulfilled for several decades to come for the socio-economic benefits and conservation of environmental elements as well [5], [6].

1.2 Extraction of hydrogen energy

Energy at present, is extracted from various sources of new and renewable sources of energy. Some of the alternate energies are solar energy, geo-thermal energy, bio-gas energy, wind energy, ocean energy, H_2 energy, *etc*. All these sources of energy are eco-friendly in nature, and free from any harmful contents. The industrial application of the sources of alternate energy is limited though, due to the inadequacies such as less energy efficient, complicacy in method of production, technical inefficiency, cost of production *etc*. associated with these sources of energy. Among the different sources of new and renewable energy, hydrogen is the most effective form of energy. The advantages of using hydrogen as a fuel are: (a) high calorific

value (141.86 $MJ.kg^{-1}$), (b) non-toxic, (c) no harmful emission, *etc*. Considering these various characteristics, hydrogen is projected as a source of alternate energy for various applications. Hydrogen energy has many potential industrial applications as given below:

1. In powder metallurgy industries hydrogen gas is used in sintering and annealing furnaces where reducing atmosphere is mandatory.
2. Hydrogen gas is mixed with argon gas to weld stainless steel in the welding industries.
3. Fuel cell-powered vehicles and passenger cars are presently trying to convert their engines fuelled by hydrogen gas.
4. On-demand production of hydrogen gas finds applications in industrial gas-fired furnaces which can eliminate the high cost of petroleum and natural gases as well as high cost for hydrogen gas storage.
5. Hydrogen gas has enormous uses in the pharmaceutical and cosmetics industries.
6. In the chemical industries, hydrogen has got applications like making of fertilizers.
7. In aeronautical industries, hydrogen is used as rocket propulsion gas.

Many methods of production of hydrogen gas exists. But most of these methods of production are (a) based on fossil fuel, (b) require sophisticated technical instruments, (c) associated with high cost, and (d) slow energy transfer rate, *etc*. Production of hydrogen gas by chemical method is a viable technique of production. As the process is simple and cost effective yet yield substantial amount of hydrogen. Hydrogen can be produced by reacting metals with water in the presence of a bases. Hydrogen gas generation by the reaction of aluminium and water in the presence of aq. NaOH solution is an effective method of production. The process is environmental friendly and produce only bayerite, which can be recycled. The emission of CO_x, NO_x is nil in this process [7], [8]. Moreover, Al is readily available on the earth crust, light weight, cheap and largely available in scrap [9]. But, the cost of extraction of aluminium is definitely high. However, considering the impact of greenhouse gas emission as well as other advantages like on-demand supply of hydrogen, thereby avoiding the extra cost involved in storing and transportation of hydrogen gas generated by using fossil fuel. Hence, there would be acceptance for using this technique for hydrogen generation at energy needs for small scale industries and electric automobile vehicles who are looking for means of avoiding batteries in EVs.

The storage of hydrogen for different applications is a challenge due to its low density (0.088 kg. m^{-3}), in addition to the fact that it is highly inflammable. Presently, researchers have

emphasized on the production of hydrogen gas on-demand for various applications. In spite of the efforts put by the scientific communities to introduce hydrogen fuel in the market, it has not picked up momentum. The reasons for this can be attributed to (i) techniques of cost-effective production and storage of high purity hydrogen for industrial needs has not been established, (ii) the resistance offered by the existing automobile industries to invest in RD&D for change over their design, (iii) the high pressure and influence by the existing fuel sector on the government policies to continue with the present fuels, (iv) reluctance to use hydrogen fuel in automobile engines due to high risks of explosion, and (v) insufficient RD&D results available in the open literatures.

1.3 Characteristics of hydrogen gas

Hydrogen is the smallest and the lightest element in the periodic table. It remains in the gaseous state under normal conditions. Hydrogen gas is lighter than vapour of air and gasoline by 14 times and 57 times respectively [10]. It is prone to leakage due to its small molecular size and low viscosity. The physical properties of hydrogen are (a) colourless, (b) odourless, (c) tasteless, (d) non-toxic, and (e) non-poisonous. The auto-ignition temperature of hydrogen gas is 585 ^{o}C as reported, which is much higher than that of gasoline {courtesy: https://h2tools.org/bestpractices/hydrogen-compared-other-fuels}. The following fig.1.1 indicates the comparison of the auto-ignition temperature of the different fuels.

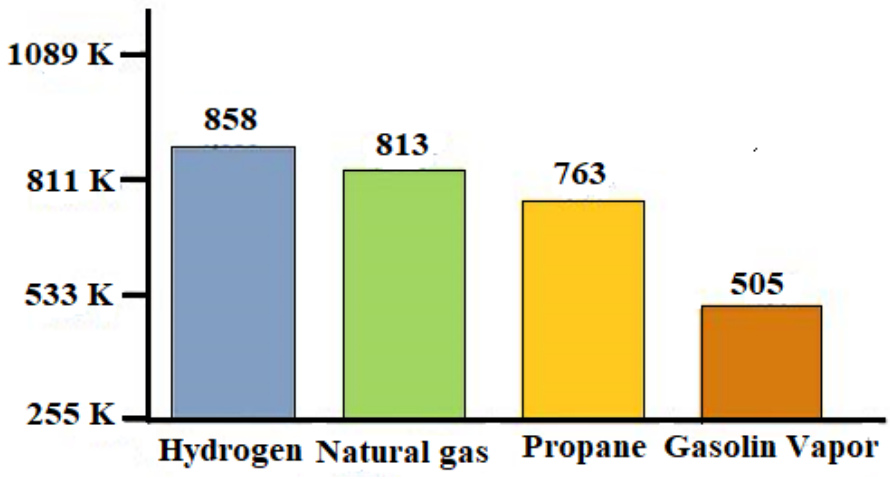

Fig. 1.1 Auto-ignition temperature
{courtesy: https://h2tools.org/bestpractices/hydrogen-compared-other-fuels}

The flammability range of hydrogen varies from 4 % to 75 % compared to other fuels. The optimum condition for which the energy required to combust hydrogen is 29 % hydrogen to

air volume ratio {source: https://h2tools.org/bestpractices/hydrogen-compared-other-fuels}. Hydrogen gas burns with a pale yellow colour which is not possible to detect in daylight.

1.4 Hydrogen energy and Artificial Intelligence

The integration of Artificial Intelligence with the hydrogen energy systems has the potential to be used in the real-world engineering problems. The parametric study of the production of H_2 for industrial applications at an optimum level requires an effective mathematical model. The efficacy of the model depends solely on the numbers of data sets obtained through the actual experiments. However, obtaining a huge number of data by carrying out physical experiments is tedious and time consuming. Besides, in-situ production and utilization of H_2 gas needs to be operated in a loop system for the necessary feedback and control. The constraint of the traditional physics based simulation method is the prerequisite of substantial amount of time for generating data. Hence, Artificial Intelligence (AI) can potentially provide the reasoning and decision support for different engineering and technological challenges in the era of Fourth Industrial Revolution (Industry 4.0). Machine Learning (ML) Techniques emerged as a powerful computing infrastructure to apply to more complex problems in engineering and technology. ML techniques have enabled the industries to better decision making, increasing the productivity and the sustainability of the industrial aspects [11]. ML Techniques are the latest development in the field of computer applications. It can address thorough and accessible information of various technical issues for the research community.

AI gives a real-world applications of the engineering problems by bridging between the practical and imaginary fields. This new and advance method is more efficient than the traditional methods of simulation. It takes in to account of the real-time interconnection of the various input variables to give the output parameter. The non-linear and complex dynamics of the problems can be solved effectively by using the AI tools like the ANN, the RBFNN, the MLR Analysis, Deep Learning, Fuzzy Logic, and Non-linear Fit techniques. These methods offer practical techniques to translating ample amount of information hidden in data into important knowledge [12]. The optimization of the engineering problems now-a-days, is very complex, highly non-linear and hence difficult to map the solution. Artificial Intelligence based multi-objective optimization method (AI-MOO) is an advanced tool to handle this type of problems [13]. The UN Climate Change has taken several initiatives by involving different signatories to mitigate the emission of green-house gases and achieve neutral carbon footprint by 2050 [14]. Computational techniques play a pivotal role and provide cost effective

alternative method to understand the sustainable environmental engineering design through mathematical modelling and simulation [15]. Optimized modelling of energy systems, utilization and storage of the alternate source of energy are some of the highly employed areas of the computational techniques. It has been reported that AI has significant impact on the renewable energy systems [16] which uses data-driven model to predict the sustainability of the source [17]. Quantum computing (QC) [18], [19] has recently attracted the scientific community due to its high computing performances and its wide domain of application starting from (a) cryptography and finance, [20] to (b) molecular design [21], [22], and (c) combating climate change. AI technology has supported the energy industry in growing by integrating Internet of Things (IoT) and Renewable systems [23]. The global economy is strongly dependent on the production of energy, planning and distribution and financial sustainability [16]. This leads to the development of a smart energy systems which comprises of super computers, power electronics, information and control system, cyber security *etc.* [24].

1.5 On-Demand H_2 powered Sintering Tube Furnace

The present study involves the on-demand production and utilization of H_2 energy in a sintering tube furnace and aimed at determining its thermal efficiency. In powder metallurgy industries sintering is an essential process to manufacture different products. Sintering of the powder materials is carried out in furnaces known as sintering tube furnace. Normally, this process requires high temperature. Hence, it is operated using either fossil fuel or electrical energy. H_2 gas is a green source of energy with high calorific values. This energy can effectively be utilised to power a sintering tube furnace in those types of industries. On-demand H_2 gas to be used in the sintering tube furnace requires no means of storage. This method of using H_2 gas in the furnace eradicate the chances of explosion due to gas leakage, high manufacturing cost of storing devices, transportation cost as well as mobility risk.

1.6 Cost Assessment

The analysis of cost associated with a project is important from the economic point of view. It enables to estimate the price of a product, profit margin, loss incurred, break-even-point, *etc.* There exist different methods of finding the various cost components in a project. The return-on-investment, the net present value, the break-even-analysis are some of the widely used cost assessing techniques. Cost estimation also facilitate to compare the effectiveness of a process operated by different modes. This assists in selecting a process with higher level of satisfaction.

1.7 Motivation

The field of new and renewable energy is an emerging field of study. There are lots of studies that have to be envisaged and established. Many scientists and engineers have discovered new technologies to generate power without using fossil fuel based source of energy. In this connection hydrogen gas has got many different uses in the modern era starting from the automobile industries to powder metallurgy industries [25]. Some of the specific uses of hydrogen are in heating, seasonal energy storage, long distant energy transportation, hydrogen vehicle, [26] *etc*. The combustion of hydrogen emits only water. Therefore, to have a pollutant-free atmosphere and to resist the phenomenon like global warming, acid rain, ozone layer depletion, *etc.*, hydrogen is an effective means of energy production. It can also be used as a source of renewable energy [27], [28].

The study of the different literatures reveals that the production of hydrogen by the chemical reaction between aluminium and alkaline water appears to be a viable and cost-effective method. This method has the advantage that high purity hydrogen can be produced and thereby eliminating the impact of the greenhouse gases on the environment due to its combustion. Moreover, the reaction by-product aluminium hydroxide [$Al(OH)_3$] can be recycled. $Al(OH)_3$ has got many practical applications like water treatment, paper making, and fire reticence. Being a light metal with high energy density, Al metal can be put to use in portable devices and in-situ production of hydrogen gas is feasible. Thus, deleting the challenges in connection to its storage. Aluminium scrap is also available in an ample amount. The present topic is therefore, chosen for the research to study the chemical kinetics of the reaction between Al scrap and alkaline water and the on-board use of hydrogen gas for the industrial furnace as well.

1.8 Objectives of the study

The following objectives have been addressed in the present thesis work:

- Study the effect of operating variables on the rate of production of hydrogen gas.
- Determine the kinetic parameters of the chemical reaction.
- Modelling of hydrogen generation by Machine Learning Techniques.
- Determine the thermal efficiency of the hydrogen fuelled sintering furnace.
- Cost estimation of hydrogen gas production.

For the development of a hydrogen fired industrial furnace for mitigating the problems arising due to the use of fossil fuel, optimization of (i) the process variables for the maximum hydrogen gas produced from Al-water reaction and (ii) determination of the fuel to air flow ratio for the maximum furnace efficiency is essential.

1.9 Organisation of the thesis

The present thesis has been organized by the following chapters. A synopsis of the subject matter has been presented concisely. The study incorporates the survey of scientific works carried out by the different researchers and scientists related to the hydrogen energy, its advantages, and disadvantages, method of extracting hydrogen energy from resources by various methods, the environmentally benign characteristics, and effective applications in science and technology. The investigation has been started to gather effective data, a hydrogen generation setup is fabricated and carried out parametric studies under several conditions to find the chemical kinetics of the reaction between Al and water in the presence of aq. NaOH solution. Data obtained from the experiments are used to model kinetics of the reaction by using Machine Learning Techniques. The thesis includes the procedures and experimental instruments used during the time of the experiments. The hydrogen gas is applied in a sintering tube furnace made of stainless steel, where the hydrogen gas is combusted to obtain the thermal efficiency of the furnace and also the cost estimation of hydrogen gas production has been conducted. This thesis consists of five chapters which are summarised as follows:

Chapter 1: The thesis commences with a brief description of the urgency of new and renewable sources of energy in the nearest future due to the rapid depletion of fossil fuel. It states about the different possibilities of alternate sources of energy available. It encompasses the need behind the research work and the primary motivating factor. The eligibility of hydrogen gas as the future fuel or the dream fuel has been justified thoroughly. This chapter includes the integration of chemical kinetics with Artificial Intelligence (AI) techniques and Statistical tool. The main objectives of the present work have been summarised across this particular chapter.

Chapter 2: The detailed study of the literatures available in this area of research has been stated precisely in this chapter. The working procedures, materials used and the experimental results for the production of hydrogen gas by different methods have been mentioned here. This chapter also includes the application base of the hydrogen gas produced by the corrosion reaction of aluminium.

Chapter 3: This chapter incorporates the details of the manufacturing process of experimental setup to conduct the kinetic reaction between aluminium and water. The engineering drawing, materials of the hydrogen generator are mentioned here. The preparation details of the as-received raw materials *i.e.*, the long hollow bars of aluminium is described in this lesson. The details of the experimental procedure with proper instrumentation have been described.

Artificial Intelligence based Machine Learning Techniques such as the ANN modelling, the MLR technique, and the LSF method can be successfully implemented to establish the kinetic equation using the data obtained from the Al-H_2O experimental results. The method of obtaining the best architecture through the various machine learning tools are elucidated through this chapter.

The fabrication of the sintering tube furnace and the details of the experiments conducted on the furnace have been discussed thoroughly. The method of cost analysis relating to the present research work also has been discussed in this chapter along with the cost comparison among H_2 gas, LPG, and electricity.

Chapter 4: The results of H_2 evolution in the aluminium-water reaction in the presence of aq. NaOH at the various conditions have been presented. The procedure for analyzing the data and the summary of results have been put forwarded. The results are also discussed with proper justification. The comparison of the simulated results with the experimental data obtained by the reaction of Al-H_2O in the presence of aq. NaOH using the ANN, the MLR, and the LSF method are presented here. The various Statistical Correlation Factors are found out to establish the best kinetic model for the chemical reaction. The relative influences of the different input variables on the output result are discussed in this chapter.

This chapter also include the application of hydrogen gas in the sintering tube furnace. The temperature profiles of the combustion reaction between H_2 and air at different gas and air flow rate are explained. The optimum fuel-air ratio for which maximum thermal efficiency is attained is discussed in this chapter. Comparison study in terms of cost effectiveness among electric energy, LPG, and hydrogen energy has been conducted further and stated through this chapter.

Chapter 5: The conclusions of the study and the optimum condition for a favourable reaction are presented here. The best kinetic equation for the reaction is established and presented. The accuracy of the data-driven model are stated here. The effectiveness of the hydrogen-fuelled

sintering tube furnace is discussed in this particular chapter. The chapter also includes the outcome of investment analysis. The scope for future works are discussed here followed by references and appendices.

Chapter-2

Literature Survey

2.1 The need for green fuel

The need for a clean and alternate source of energy has been realized around the globe from the last few decades due to the depletion of fossil fuel and the environmental issues related to their combustion [29]. The world population is doubling about every thirty-five years, though the rate of growth is very different in different countries. The world energy use is doubling for every fourteen years and the need still goes on increasing. One of the main energy sources is hydrocarbon oil. Though abundant coal resource is available, the pollution associated with coal is more than oil, leading to acid rain and climate change. Combustion of hydrocarbon fuel and their continuous increase in demand contribute to the global energy crisis. From the literature available, it is reported as of 2017, petroleum provides 34 %, coal provides 28 % and natural gas provides 23 % of the total energy consumption around the world [30].

Fossil fuel has been the major source of energy provider throughout the years. Though it is the major contributor to the world of energy, many drawbacks are related to it. Recently, environmental hazards like global warming, ozone layer depletion, raise in the sea water level, melting of ice glacier, *etc.* are caused by their extensive combustion. The combustion products of fossil fuels are CO_x, NO_x, SO_x, which are the pollutants to the environment [31]. In a report, it is referred that the global emission of CO_2 jumps from 20.7 billion tons in 1990 to 32.5 billion tons in 2006 that corresponds to 35 % faster emission of CO_2 than predicted [32]. This is owing to less efficiency of the fossil fuel and depletion of natural carbon sinks [4], [5]. The energy for future power generation should meet the criteria of sustainability, recyclability, reliability, cleanliness, cost-effectiveness, and flexibility [33]. From an environmental point of view, energy security is a must. The balance of the ecological system ought to be maintained and the zero-emission criteria have to be fulfilled strictly [34]. The concept of alternate sources of energy was conceived during the world oil crisis in the year 1970 [35]. Energy sources are divided mainly into three categories as given below:

1. The concentrated sources such as
    a. Coal
    b. Oil
    c. Gas
    d. Wood
    e. Nuclear

2. The intermediate category like hydro

3. The least concentrated such as
    a. Wind
    b. Solar
    c. Tidal
    d. Geothermal
    e. Wave

The less concentrated sources generally come under the renewable energy category. The future energy sector seems to rely upon these renewable resources and among them, hydrogen is considered to be a viable and sustainable energy carrier. One of the major advantages of using hydrogen gas is the methods to avail hydrogen fuel are ecological friendly. Hydrogen gas has been recognized as the future for power industries because of the environment-friendly nature of the combustion product, versatility, high energy content per unit mass [36]. It satisfies the need related to social, economic, and environmental issues.

The economic and technical development of the hydrogen economy was aimed at project hydrogen as an efficient fuel for the future. Hydrogen gas can be used in the internal combustion engine or a fuel-cell, fertilizer industries and petroleum industries. It has been reported an annual growth of 6 % in the sale of hydrogen gas especially in the refineries [37]. The idea of using hydrogen gas however, has been subsided with the drop in oil price in the international market and because of many other agendas. It is in the 1990s when the havoc of the greenhouse effect has triggered around the globe, the researchers and scientists restart thinking of hydrogen fuel. Hence the critical assessment of all possible energy sources to produce clean energy and their methods of production is envisaged. To fulfil the need for energy and maintain an ecological balance, scientists are paying their attention to a new and

renewable sources of energy. Recently, the hydrogen economy has come out as a trend in the field of power generation. The conversion of hydrogen gas for empowering modern civilization by various methods is a matter of concern. Hydrogen gas can be produced in many ways. Some of the methods will be discussed in the following subsections. Hydrogen is envisaged as the global fuel for safety, efficient, flexible, affordable, domestic resource. The high calorific value (HHV=141.9 $MJ.kg^{-1}$ and LHV=19.9 $MJ.kg^{-1}$) of hydrogen gas makes it a suitable candidate for power generation. It is almost two and a half times greater than that of gasoline [38]. The reaction by-product of the combustion reaction of hydrogen and oxygen yields only water establishing its environmentally benign nature [39]. These particular characteristics of hydrogen fuel also make it suitable for mobile applications. The storage and transportation of hydrogen gas have been recognized as the major hindrance to the hydrogen economy. This issue can be attributed to the low boiling point (20 K) and reduced compressibility of hydrogen gas [13], [14].

2.2 Hydrogen economy

Hydrogen economy is the term used for hydrogen fuel containing low carbon emission for different uses particularly in heating, automobile, seasonal storage of energy, *etc*. This term is firstly, introduced in General Motor (GM) Technical Centre in the year 1970 by John Bockris. Hydrogen is the most abundant of all elements in the universe. Hydrogen is estimated to make up to more than 90 % of all the atoms. Hydrogen on the Earth is chemically combined with other elements. The most common hydrogen-containing substance is water [40]. The other sources of hydrogen are in combination with carbon in the family of hydrocarbons. To separate hydrogen from the carbon in the hydrocarbons or from oxygen in water, energy must be supplied. This energy generally comes from the combustion of fossil fuels that are precursors for the production of greenhouse gases, acid rain, and global climate change which induce health hazards and environmental problems [41].

Hydrogen can be used as a fuel in future with many social, economic, and environmental benefits to its credit. It has the long-term potential to reduce the dependency on foreign oil and lower the carbon emissions from the transportation sector. During the last few decades, the idea of post-fossil fuel hydrogen-based economy started to gain momentum. Molecular H_2 has the highest energy content per unit weight among the known gaseous fuels (143 $GJ.ton^{-1}$) and is the only carbon-free fuel.

2.3 Methods of production

Hydrogen though abundant, is rarely found as a free element in the environment [42]. Extensive survey of literatures has revealed the various methods of production of hydrogen gas. Chaubey *et al.* reviewed the different emerging technologies for the production of hydrogen gas [43]. Some of the methods are (a) gasification of biogas, (b) water electrolysis, (c) splitting of water under the sun with the aid of catalysts [44], (d) partial combustion of hydrocarbons [45], (e) reforming hydrocarbons by steam [46], (f) the reaction of water with hydrides [47], (g) carbohydrate pyrolysis [48], (h) chemical reaction of metals in the presence of aqueous alkalis [49], *etc.* Each method has its own merits and demerits in terms of cost, conversion efficiency, method of production, *etc.* The slow conversion rate of hydrogen production through biological process is a limitation of this method [41]. Hydrogen production by partial combustion of hydrocarbons produces green-house gases. Water electrolysis is efficient in terms of conversion rate but the cost associated with this process has restricted its usability [50]. Production of hydrogen gas by chemical method has appeared to be a viable method in terms of cost, cleanliness, *etc.*

Hydrogen gas is extracted chemically by biomass reforming, coal gasification, partial reforming of natural gas water photolysis, *etc.* Almost 95 % of hydrogen gas has been obtained by coal gasification and steam reforming of water [51]. Production of hydrogen gas from biomass, which is clean and renewable, is a promising technology. It is reported that the production of hydrogen-rich syngas from biomass can be increased in the presence of Ni catalyst by adding MgO. The yield of hydrogen was reported as 1194.6 $ml.g^{-1}$ of biomass [52]. In the presence of Pt as a catalyst hydrogen gas is produced in the NaCl solution by using Ni-rich AZ91D Mg alloy. The evolution of hydrogen gas is reportedly increased with the increase in the temperature of the NaCl solution [53].

Photocatalytic splitting of water with the help of nano-sized TiO_2 is a low cost and environment-friendly technology to convert solar energy to hydrogen energy as reported [51]. Solar hydrogen can be produced by Zn/ZnO water splitting thermos-chemical cycle. It is reported that the formation of Zn nanoparticles and in-situ hydrolysis for hydrogen generation is a viable and economic method of production. The production of hydrogen gas from MgH_2 with concentration of 1M KCl in pure water has been investigated. It is suggested that a significant increase in the production of hydrogen gas is observed when Mg is milled for half an hour [54]. The hydrolysis reaction of Mg or MgH_2 with water yields hydrogen gas. But due

to the formation of passive layer of $Mg(OH)_2$, the reaction stops suddenly. It is reported that this problem can be eliminated if Mg is milled with salt particles [55]. The volume of hydrogen gas produced from low-grade Mg in the presence of NaCl solution and Pt coated Ti as catalyst pressed over the Mg, is reported as 302.3 $ml.min^{-1}$ for 1600 s. It has been also reported that around 7.5 times increase in the production of hydrogen is observed when the catalyst is grounded with the Mg samples [56].

X-ray diffraction, DTA, and EDX techniques are used to determine the chemical properties of the hydrogen generating materials. The dependency of the rate of the chemical reaction on the quantity and quality of the composite has been reported [57]. Aluminium is a promising metal for on-board hydrogen production. For portable energy source applications, a microprocessor fuel system has been developed with Al and water as reactants. There are two such types of systems. In the first type, water is directly introduced. On the other hand, water vapor enters in the second type. A maximum conversion of 78.6 % concerning Al is achieved in the second type [58]. Rapidly quenched Ni-Al alloy is a good source of hydrogen energy. The reaction depends on the parameters *viz.* size of the particles of Ni-Al alloy, concentrations of the NaOH solution, and temperature. It is reported that the reaction between Ni-Al alloy and aq. NaOH can be well fitted with the shrinking core model.

In the process of hydrogen generation, NaOH has been given a lot of importance. NaOH being a catalyst promoter to the production of hydrogen gas. In many applications like steam methane reforming, coal gasification, biomass gasification, *etc.* NaOH is an important ingredient. Metallic Al powder when reacts with tap water or deionized water produce hydrogen gas. In the reaction, metal oxide crystals like TiO_2, Cr_2O_3, Fe_2O_3, NiO, *etc.* act as a modifier. The effect of various sizes of TiO_2 on the reaction rate at ambient temperature is investigated. The metal oxide modifier produces hydrogen gas from Al and water reaction significantly at 25 $^{\circ}C$ [59]. The Al-water reaction to produce H_2 gas in presence of choline hydroxide (2-Hydroxy-N, N, N-trimetylethane-1-aminium) accelerates the reaction. The activation energy is reported as 45.92 $kJ.mol^{-1}$. Moreover choline hydroxide solution is less corrosive than NaOH [60]. Al-Li alloy is a good carrier for hydrogen energy. It is clean and environment friendly as well. An amount of 1155.03 ml of H_2 per gram of Al-Li alloy has been reported [61]. Milled Al-Bi-hydride in pure water and at room temperature can yield ample amount of hydrogen. The hydrolysis reactivity increases if Al-Bi-hydride salt is milled for 5 h. The yield of H_2 has been reported as 1050 $ml.g^{-1}$ in 5 min [62]. The effect of different parameters like Al-water ratio,

reaction temperature, particle size *etc.* has been investigated thoroughly. It is reported that when Al is activated by Li, the Al-water reaction can be carried out with tap water at room temperature. Depending on the operating conditions, an amount of 200-600 $ml.min^{-1}.g^{-1}$ of Al is reported [63].

Although these techniques are matured and have the lowest costs, they cannot act as a long term strategy for the hydrogen economy because the raw materials used are all based on fossil fuels, which are neither sustainable nor clean. Reforming biomass, an abundant and renewable source may be considered as a sustainable way to produce hydrogen but its carbondioxide (CO_2) neutrality is still a controversial issue. Furthermore, this technique is seriously restricted by the low hydrogen yield and energy content of biomass. Moreover, additional energy will be required for the conversion of syngas into hydrogen through water–gas shift reaction. The high cost for growing, harvesting, and transporting biomass is another disadvantage for biomass utilization. Water photolysis, an advanced chemical technology regarded to be very promising, is still under development and some technical difficulties make it far from industrial applications. Considering these facts, the production of hydrogen gas from aluminium-water reaction in the alkaline medium is a viable technique.

The thermal property and electrical conductivity of aluminium and its alloys are quite encouraging. The high energy density 29 $MJ.kg^{-1}$ and low density 2700 $kg.m^{-3}$ of aluminium metal make it a good carrier of energy. Moreover, aluminium can also be recycled establishing the approach of a sustainable source of energy. The low weight of aluminium and its alloys ease the fabrication of a lightweight portable energy conversion system. Aluminium and its alloys are used for the Al-water reaction in the presence of alkalis for hydrogen production [64]. In some other works Al metals are activated by the different mechanical processes to facilitate the rapid production of hydrogen gas. Mechanical activation of Al can be achieved by grinding and metallic alloying with Ga. Mechanical alloying of only 2-5 % of Ga and In with Al can result in better activation of Al as reported by Slocum [65]. Xu *et al.* have demonstrated activation of Al metal with liquid Ga, In, and Se to carry out the Al-water reaction without any interruption in the production of hydrogen gas [66]. Hence, some works have been published regarding the activation of Al with some Al-alloys and composites, but they are not sustainable. These alloys and composites got dissociated in the ambient condition.

The reaction by-product of Al and water reaction *i.e.*, $Al(OH)_3$ is used to produce some Al salts which find application ranging from water treatment ($Al_2(SO_4)_3$) to pharmaceutical industries. The production of hydrogen gas from Al water reaction does not necessarily require Al of high purity, unlike aluminium/air batteries. Al available from beer cane, scraps are good source to produce hydrogen gas of very high purity. The devices where hydrogen gas of very high purity is required can be obtained by this method of production [67]. The production of hydrogen gas from commercially available Al and water has not been studied in depth. This process is easy, cheap, and safe as well. The reaction between Al and water is found to be ceased after a certain period. The reason can be attributed to the formation of a passive oxide layer of aluminium hydroxide over the aluminium surface, which hinders the direct contact of water molecules with the metal surface. There are several ways by which this preventive layer of oxide film can be removed. The layer can be destroyed by controlling (a) alkali concentration, (b) reaction temperature, (c) aluminium morphology, (d) the properties of the aluminium raw material, and (e) magnetic stirring. One such technique is the use of alkaline NaOH solution. The OH^- ions present in the NaOH solution dissolve the oxide layer and facilitate the intervention of water molecules to carry forward the reaction yielding hydrogen gas [49], [58], [67]. But, as the reaction continues for long, the amount of OH^- ions diminishes and at a certain point of time, the production of hydrogen gas gets saturated. Now a day, some other techniques are also adopted to activate the aluminium surfaces. Mechanical alloying of aluminium with different elements [64], [68] and ball milling with salt and some oxides are some of the effective techniques [57]–[61], [69]. The surface modification of aluminium can promote it to react with water even at room temperature to produce hydrogen [62]–[65]. There is fewer literature available stating the reaction of pure aluminium with water at high temperature or steam. Literature containing any information regarding the reaction of pure water and pure aluminium is almost negligible [66]–[68], [70], [71].

2.3.1 Activation of aluminium

The rate of production of hydrogen gas can be enhanced by using activated aluminium powder. It is reported that the aluminium particles activated by mechanical means can be a good source of hydrogen gas. The alloys of Al with various metal *e.g.*, In, Ga, Sn, Bi, *etc.* are good agent for water-aluminium reaction for the production of hydrogen gas as reported [64], [72], [73]. Aluminium particles are also mechanically treated to obtain fresh surfaces of aluminium to facilitate the water - Al reaction. The cut piece Al and ball-milled aluminium particles have

fresh surfaces with an extended surface area. The effect of freshly prepared aluminium surface on the production of hydrogen gas has also been investigated thoroughly [70], [72], [74]. In some researches salt particles are used with the Al particles during the processing to obtain better surfaces for the reaction [70], [74]. In this method Al and salt particles are amalgamated with different Al-salt ratios. The crystalline salt particles are broken down during the milling process and the sharp edges of salt particles cut the Al particles into a large number of pieces. Thereby, it increases the specific surface area and makes it feasible for the water molecule to react extensively during the reaction process. Hence, the kinetics of hydrolysis is also increased. Maximum rate of 75 $ml.min^{-1}.g^{-1}$ of Al of production of hydrogen has been reported for Al particles milled with salt particles [70].

Fan *et al.* [75] reported the hydrolysis effectiveness of Al metal alloyed with other metals. It is stated that the ball milling of Al with Zn, Ca, Ga, Bi, Mg, In, and Sn is much more productive than making alloys of these metals by the process of melting. The hydrolysis property of the alloy of Bi and Sn with Al metal is quite good than the alloys of Zn, Ca, and Ga. The reaction rate is much faster for Al-Bi alloys than Al-Sn alloy. The introduction of Zn and Ga metal with the alloy of Al-Bi increase the rate of production of hydrogen gas. On the other hand, other metals like Sn, In, Mg deaccelerate the hydrolysis of Al alloy. The production of hydrogen gas in the presence of aq. NaOH is a good approach taking slight care of the corrosive nature of NaOH solution. The reaction rate is fairly slow in this reaction as reported [72], [76]. Soler *et al.* tested KOH in the reaction between Al and water to produce hydrogen gas as a catalyst. Theoretically, there is no consumption of KOH occurs except for Al and water. The KOH is converted into potassium aluminate during the reaction process, which undergoes dissociation to return to alkali. However, a minimal amount of KOH is reacted with CO_2 in contact with air, causing the diminishing of KOH and suppressing the reaction rate. Comparative study of the effectiveness between NaOH and KOH in the production of hydrogen gas by the Al-water reaction is carried out by Porciuncula C. *et al.* [38]. It was reported that the reaction proceeds at a faster rate in case of NaOH than KOH. The activation energy for the reaction acted by KOH is higher than the reaction assisted by NaOH. A higher rate of reaction for KOH is reported by Soler *et al.* though, the proper explanation is not presented [77].

The reaction of Al in the alkaline environment is exothermic and thereby, producing heat and hydrogen gas at an optimal temperature of (70-80) ^{o}C as reported [77]. Another approach has been adopted to overcome the issue related to the slowing down of the hydrolysis kinetics of

Al-water reaction by the use of Hg and Zn amalgam. It is found that the reaction kinetics accelerates a better way while Zn amalgam is used as the catalyst rather than using Hg as a catalyst. The activation energies are reported as 43.4 $kJ.mol^{-1}$ and 74.8 $kJ.mol^{-1}$ for Zn amalgam and Hg coated Al respectively [68].

2.4 The size of Al pellets

The size of the Al pellets determines the rate of the reaction. Al pellets with lower surface areas are found to be more profound in the liberation of hydrogen gas [52], [53]. It was reported that 60-80 % of hydrogen gas can be obtained by using 6 µm size of Al particles and also close to 100 % of yield is possible using water at 200 ^{o}C [78]. Another researcher has obtained 70-90 % of hydrogen gas by using Al powder of size 4-7 µm at 200-230^{0} C [79]. It is stated that the production of hydrogen gas can be increased by using water at a higher temperatures and smaller powder size of Al. It has been suggested that Al particle of size 3 µm can run a faster reaction up to 50 ^{o}C and at nearly vacuum condition, but it is astonishing fact that the production of hydrogen gas is nil at 75 ^{o}C and atmospheric pressure. The reaction of Al particle of micron size with water vapor, (230 ^{o}C) is carried out by another researcher. The conclusion of the experiment is that 100 % yield of hydrogen gas can be achieved at elevated temperature and micron-sized Al particles with a rapid rate of production [79]. The research carried out by Elitzur S. *et al.* showed that the hydrogen production rate depends on the specific surface area (m^2. g^{-1}) of the Al particles.

2.5 The chemistry of Al-water reaction

In-situ production of hydrogen gas has been attracted by many scientists. It expels the storage and transportation issues related to hydrogen gas. Al is a potential metal to yield an ample amount of hydrogen gas. The production of hydrogen gas by the corrosion reaction of aluminium metal is a viable technique of hydrogen production. Aluminium based material is reluctant to corrosion due to the oxide layer formed over the surface. Hence, NaOH is used in the aluminium-water reaction as a reaction promoter. The proper mechanism of hydrolysis of water in the reaction between Al-water has not been understood yet [67], [80], [81]. However, it is revealed from various literatures that the reaction mechanism follows the route given by equation no. (2.1) up to 280 ^{o}C producing bayerite, $Al(OH)_3$ and liberate hydrogen gas [58], [82]. The passive oxide layer over the Al surface has been confirmed from the work done by Bunker *et al.* [68] in the secondary ion mass spectrometry. It was suggested that a dense layer

of hydroxide ions inhibits the direct contact of water molecules with the Al surface. The chemical equation involved in the reaction between Al and water in the presence of aq. NaOH solution is [67], [80], [81].

$$2Al + 6H_2O + 2NaOH \xrightarrow{yield} 2NaAl(OH)_4 + 3H_2 \qquad (2.1)$$

$$NaAl(OH)_4 \xrightarrow{yield} NaOH + Al(OH)_3 \qquad (2.2)$$

Equation nos. (2.1) and (2.2) yields

$$2Al + 6H_2O \xrightarrow{yield} 2Al(OH)_3 + 3H_2 \qquad (2.3)$$

It is implicated that the cavitation effect comes into play to destroy the protective oxide layer of bayerite. Nie *et al.* [83] has proposed a multi-stage mechanism for the reaction. Initially, an incubation period followed by the first reaction, and in the end, the reaction slows down. In the incubation period, the protective oxide layer is hydrated. After which the penetration of water molecules takes place to react with the Al surface, hence giving rapid production of hydrogen gas. They have stated that at the final stage of the reaction mechanism the precipitation of the bayerite, $Al(OH)_3$ occurs. A similar type of result has been found in other publications too [84]. The authors have emphasized two main parameters that control the production of hydrogen gas *viz.* pH and the amount of aluminium hydroxide ion in the solution. Activation energies of 62 $kJ.mol^{-1}$ and 53 $kJ.mol^{-1}$ are reported from their experimental findings for boehmite and bayerite respectively. The activation energy in the range of (53-100) $kJ.mol^{-1}$, particularly below 100 $^{\circ}C$, has been reported in some literatures [59], [60]. The generation of hydrogen gas at low temperature is favourable because it does not require a sophisticated state-of-the-art reactor to control the reaction procedure. There is (54-56) % loss of energy has incurred in the production of hydrogen gas as reported. Therefore, it is anticipated that the high-temperature production of hydrogen gas can compensate for the loss incurred. High-temperature production of hydrogen gas also minimizes the need for additives, nano powders and increases the reaction kinetics at the same time.

NaOH in this reaction is regenerated after the completion of the reaction. It acts as the catalyst in the reaction reducing the activation energy by altering the transition state of the reaction to produce the hydrogen gas. The Al-water reaction is dependent on the initial temperature and concentration of the aq. NaOH solution. From the various literature survey, it has been

observed that with the rise in temperature and concentration the rate of the reaction increases. The reaction follows a first-order kinetics. The activation energy for Al-water reaction has been reported as in the range of 42.5-68.4 $kJ.mol^{-1}$ [69], [76], [85]. The activation energies for 1M, 2M, and 3M concentration of NaOH are given by 67.77 $kJ.mol^{-1}$, 64.79 $kJ.mol^{-1}$, and 57.45 $kJ.mol^{-1}$ as reported by another researcher [38]. It is reported that 1 g of Al when reacts completely with water under ambient condition in the presence of aq. NaOH yields 1360 ml of hydrogen gas [78], [86]. The OH^- ions present in NaOH solution dissolve the aluminium oxide layer and facilitate the production of hydrogen gas [86]. However, the rate is very slow (100-280 $ml.min^{-1}g^{-1}$) at ambient conditions as reported. But, with the rise in temperature and concentrations of aq. NaOH solution, the rate further increases [87].

The Al-water reaction depends on the size of the Al particles. The reaction rate is faster for smaller particles. As the reaction is characterized by surface chemistry. Therefore, the specific surface area plays an important role in this reaction. The reaction kinetics is controlled by the Arrhenius equation. The mechanism of the reaction has been best illustrated by the shrinking core model. According to this model, the water molecules firstly come in contact with the Al particles. As the suitable condition has arrived the hydrolysis of water starts. The reaction ceases after some time because of the formation of a protective oxide layer over the Al surface. Ultrasonic agitation, magnetic stirrer are some mechanical techniques by which the protective layer can be destroyed and the production of hydrogen gas can be resumed. The water molecule proceeds to the core of the Al particle after the initiation at the surface. The barrier of the oxide layer diminishes as the reaction temperature increases. Normally, the reaction of Al and water in presence of aq. NaOH solution is carried out under atmospheric pressure and below boiling point of water [57], [62], [77], [88]–[90]. The reaction rate and yield of hydrogen gas in the low temperature are very less due to the inhibitive nature of the protective oxide layer. The addition of alkaline solutions that contains hydroxide ions, remove the protective layer and causing the intervention of water molecules to the Al surface.

In some literatures, it is observed that salt particles are also used for the same purpose. Al alloyed with reactive metals also promotes the hydrogen yield. The reaction promoted by Ga and trace amount of In and Sn improves the reaction rate [91]. Lithium-based activator is used in the reaction between Al and water to self-sustain the reaction at room temperature and 100 % yield of hydrogen has been reported in some cases. The reaction rate is possible to control by controlling the water temperature, size of the Al particles, altering the process of activation

of metal and changing the ratio of metal and water [82]. Nanoparticles of Al are also reacted with water to investigate the yield of hydrogen. The reaction is found to be faster. But the problem of oxidation associated with the nanoparticles and the high cost cannot be overlooked. Therefore, the Al nanoparticles are not feasible for in-situ productions of hydrogen gas. Yavor Y. *et al.* reported the ultrasonic agitation of the Al particles in the reaction between aluminium and water. This method of recovering the Al surface from the protective oxide layer to continue the reaction can reduce the use of activated Al particles or the use of the corrosive acidic or alkaline solution.

2.5.1 Outcomes of various works

A systematic investigation correlating the kinetics of hydrogen gas production to various process parameters like the composition of Al, size, volume, morphology, reaction temperatures, the concentration of the alkaline medium, *etc.*, is required to establish for any progress in the large scale hydrogen production for practical applications. Teng *et al.* [86] reported that the generation of hydrogen gas strongly depends on the surface area of the by-product layer $Al(OH)_3$ (bayerite). Hydrogen generation is more rapid when the by-product layer is present. In fig. 2.1 the effect of residual on the production of hydrogen is presented. The effect of two different types of $Al(OH)_3$ powders stirred for 24 hours (top and bottom) and as-received $Al(OH)_3$ powders on hydrogen generation is shown in fig. 2.2. The as-received powder of 5 μm has some effect on hydrogen generation. The stirred $Al(OH)_3$ is divided into two parts 'top' and 'bottom' and their effect is observed. The 'top' part exerts a prominent effect on hydrogen generation.

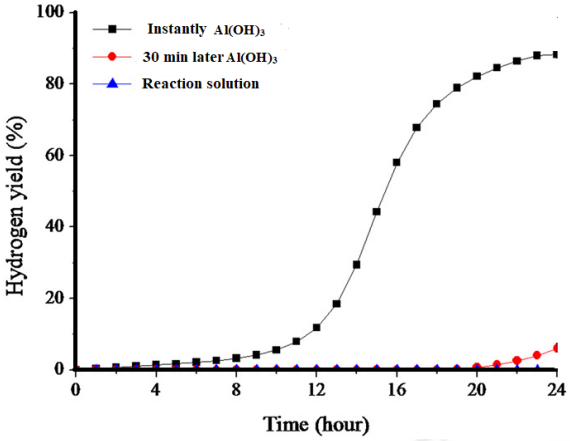

Fig. 2.1 Effect of the filtered reaction solution and two different $Al(OH)_3$ powder on hydrogen generation [86]

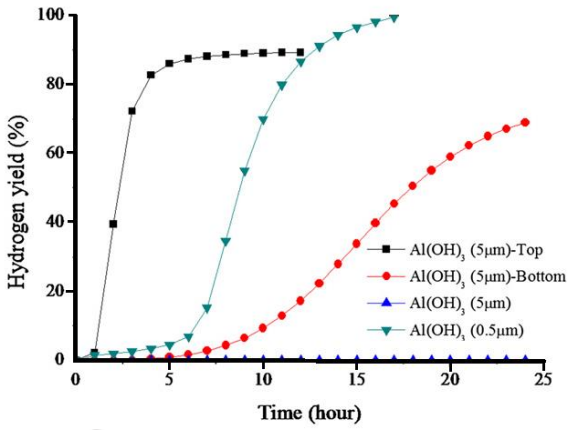

Fig. 2.2 Effect of different sized commercial $Al(OH)_3$ powder on hydrogen generation during Al/water reaction [86]

Gai *et al.* [39] reported that small-sized Al powder can be employed directly to generate hydrogen without any activation or modification. They used a shrinking core model [39], [85] to analyse the reaction process. Al-water reaction is controlled by the surface chemical mechanism at the initial stage. Later, it is controlled by the diffusion of the H_2O molecule through the by-product layer. The activation energy for the reaction increased from 64.2 $kJ.mol^{-1}$ to 88.7 $kJ.mol^{-1}$ with increasing the Al particle size from 98.38 nm to 24.94 μm. X-ray analysis, shown in fig. 2.3 revealed that the reaction by-products are bayerite, a boehmite, or a mixture of them. The reaction by-product is found to be strongly dependent on the reaction temperature.

Mahmoodi and Alinejad [74] have studied the generation of hydrogen by freshly prepared Al particles. The experiments are carried out by using fresh surfaces of Al by milling Al particles with salt. It is observed that hydrogen gas generation has got enhanced. In this, the salt acts like a nano-miller during milling and prevents oxidation of Al surfaces by developing a protective layer over the Al surface.

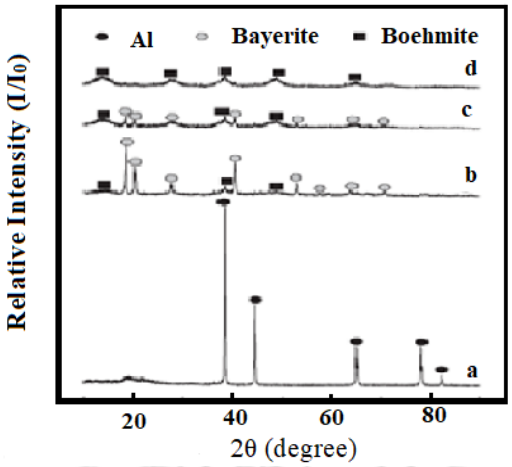

Fig. 2.3 X-ray patterns for (a) as –received 98.38 nm Al powder, (b),(c) and (d) that in (a) after reaction with water at 20 °C for 82.12 h, 40 °C for 5.05 h and 60 °C for 1.88 h, respectively [39]

Gai *et al.*, have studied the reaction of Al powder with water under ambient conditions using six different sizes of Al particles of an average size of 98.38 nm. Both nano and micro-sized Al powders can react with water and generate hydrogen under ambient pressure at mild temperatures. Al nano-particles almost completely reacts with water at 20 ºC. Most of the micrometre-sized Al powders react with water at a temperature of > 40 ºC. The maximum hydrogen-generation rate (~ 80 cc $H_2.min^{-1}. g^{-1}$ of Al) of 98.38 nm Al powder at 50 ºC and 60 ºC can be compared to that (> 100 cc $H_2.min^{-1}. g^{-1}$ of Al) of Al in alkaline solution. They used a setup shown in fig.2.4.

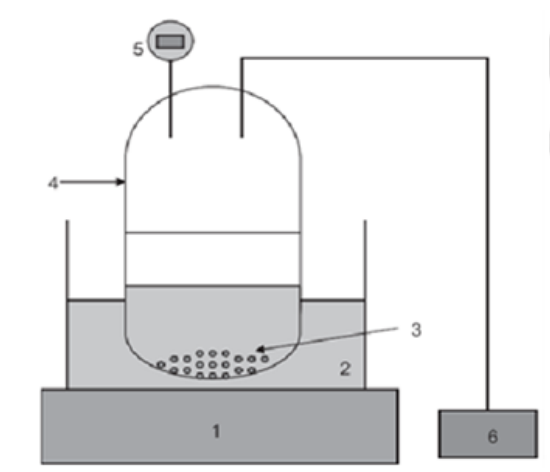

Fig. 2.4 Schematic diagram of hydrogen generation set-up: (1) thermostat, (2) water bath, (3) reactants (water and Al powder), (4) reactor, (5) pressure gauge, and (6) vacuum pump [39]

Several authors have used the Shrinking core model to analyze the reaction kinetics between Al and alkaline water system [76], [77], [92]. Solar L. *et al.* have considered the Al-water reaction as a solid-liquid heterogeneous reaction with spherical shape for the solid and assuming an isothermal reaction. The following rate equation is given by

$$1 - (1 - \alpha)^{\frac{1}{3}} = kt \qquad (2.4)$$

where, k- surface chemical rate constant,

When the mass transfer of the by-product is the rate-controlling step the rate equation is given by

$$1 - \left(\frac{2}{3}\right)\alpha - (1 - \alpha)^{\frac{2}{3}} = k't \qquad (2.5)$$

where, k'= mass transfer rate constant.

A curve is plotted using equation nos. (2.4) and (2.5) and obtained the following curves.

The slopes of the curves will give the values of k and k'.

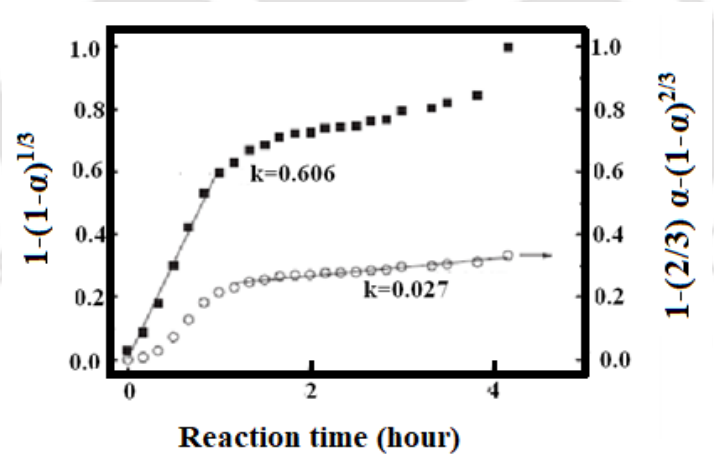

Fig. 2.5 Fitting of the experimental data by shrinking core model controlled by the surface chemical reaction (♦) and the H_2O diffusion through by-product layer (o) for the reaction of 98.38 nm Al powder with water at 40 °C, where the initial pressure in the reactor is 1 bar [77]

The authors have carried out a set of experiments at different temperatures and different particle sizes. The rate of the reaction increased with an increase in temperature. The activation energy is calculated using Arrhenius equation as shown below:

$$k = Ae^{-E_{a/RT}} \qquad (2.6)$$

where, A- pre-exponential factor, E_a - Activation energy

A curve between ln(k) and 1/T is plotted. The slope of the curve will give the value of activation energy and the intercept will give the value of the pre-exponential factor. It is shown in the fig.2.6.

Deng and co-workers [93] have surveyed the state-of-the-art hydrogen generation materials for portable applications. The reaction of Al with water produces around 3.7-4.8 wt. % hydrogen with the generation of neutral by-products

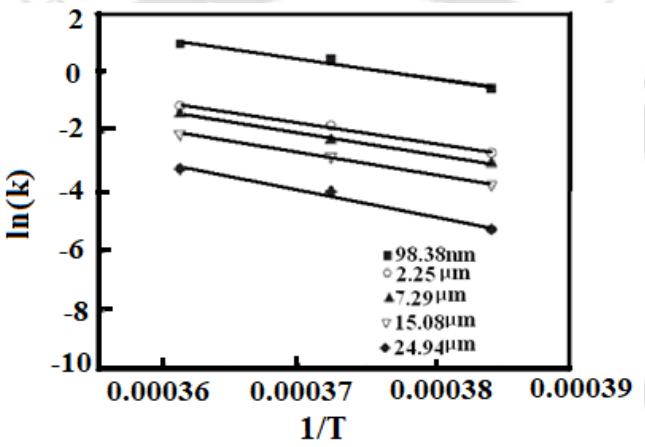

Fig. 2.6 Arrhenius plots for the reaction of different particle sized Al powders with water

2.5.2 Life cycle assessment (LCA)

The environmental impact, measured by evaluating the hydrogen life cycle as fuel, varies depending on the source of hydrogen, the process, and the complexity of the productive chain. Dante *et al*. [94] investigated the environmental impact by evaluating the hydrogen life cycle. They proposed some features to be considered for analyzing the LCA. There are some proposed methods for LCA. The LCA phases are:

- The purpose of using hydrogen.
- Environmental effect of the selected life cycle of hydrogen.
- Classification based on the process of hydrogen extraction.
- The emission of CO_2 is an indicator of the viability of the process.
- The life cycle is selected based on the indicator.

They have concluded that the LCA varies with the different processing methods of hydrogen production and the in-situ production of hydrogen from a renewable source is very effective.

2.6 Hydrogen as a fuel for internal combustion engine (ICE)

Soberanis and Fernandez [95] reviewed the technical adaptations for IC engines to operate with gas/hydrogen mixtures. They have stated that the emission of unburned hydrocarbons is the by-product of lubricating oil. The use of hydrogen in the IC engines with slight modifications can give rise to many advantages over fuel cell systems. Due to the wide flammability limit of hydrogen gas, the spark ignition (SI) engine can work with hydrogen with very little throttling as well as combustion with a variety of equivalent ratios. An IC engine works better with hydrogen in a lean mixture. The theoretical combustion reaction of hydrogen with oxygen is given by:

$$2H_2 + O_2 \rightarrow 2H_2O \qquad (2.7)$$

Backfire or pre-ignition is a series of obstacles in the hydrogen engine as reported [96]. It occurs mainly due to the combustion of the air-fuel mixture in the intake manifold and if the mixture comes in contact with some thermal sources. The auto-ignition occurs when some unburned mixtures enter into the combustion chamber and come in the hot spots either before spark or after spark. This leads to knocking in the engine. The authors have reported on high-pressure injection of the hydrogen into the cylinder by modifying in the existing IC engines [81]. Gasoline electronic injectors that have been developed so far cannot be used for hydrogen fuel. A large volume of hydrogen has to be injected due to its lower energy density. No-lubricant property of hydrogen may also cause surface damage to the fuel injector. The high-pressure gas injection can also be causing gas leakage. However, CNG electronic injectors may be used.

A comprehensive overview of H_2ICE was reported by Verhelst and Wallner [97] and discussed the fundamentals of the combustion of hydrogen, details regarding different mixture formation strategies, their emission characteristics, *etc.* Measures to convert existing vehicles to a dedicated hydrogen engine, and a state-of-the-art on increasing power output and efficiency while controlling emissions and modelling are discussed in detail. To avoid the engine knocking due to high flame speed and wide range of ignition limits they have modified the spark plug and ignition system exists with the existing IC engines.

2.6.1 Engine performance analysis

Das L.M. [98] investigated the engine performance on different fuel injection mood. Five different fuel injection modes are reported in literature are:

- Carburetion
- Continuous manifold injection (CMI)
- Timed manifold injection (TMI)
- Low-pressure direct cylinder injection (LPDI)
- High-pressure direct cylinder injection (HPDI)

Carburetion is not a suitable injection system because of the uncontrolled mixing of air and causing backfire as reported in the literatures. The comparison study between CMI and TMI also reveals that CMI is not as efficient as TMI. Since hydrogen is a gaseous fuel, CMI is not vastly different from carburetion. The testing of LPDI is also not fruitful due to some practical considerations. The mixing time of air and fuel is very short in this mode. Above all, the TMI mode of fuel injection has resulted satisfactorily. Figure 2.7 given below demonstrated the variation of Indicated thermal efficiency (ITE) and the equivalent ratio for TMI and CMI.

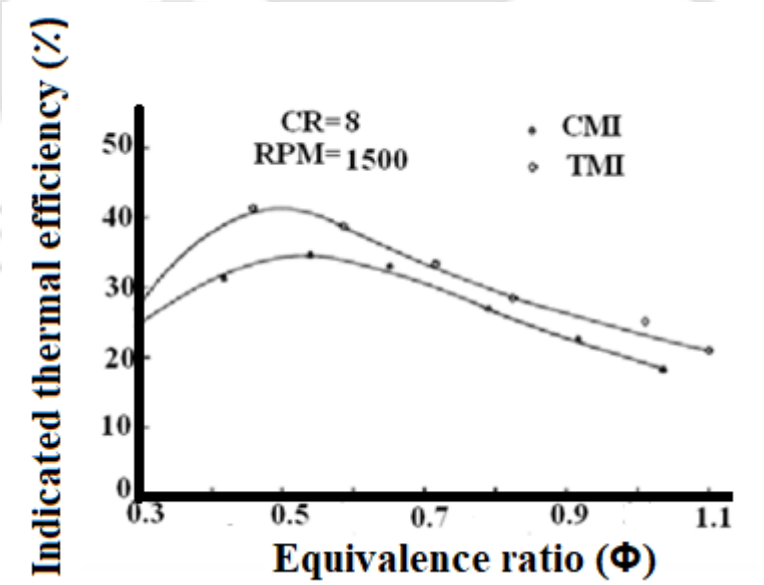

Fig. 2.7 Variation of ITE with respect to the equivalence ratio for both fuelling modes such as CMI and TMI [98]

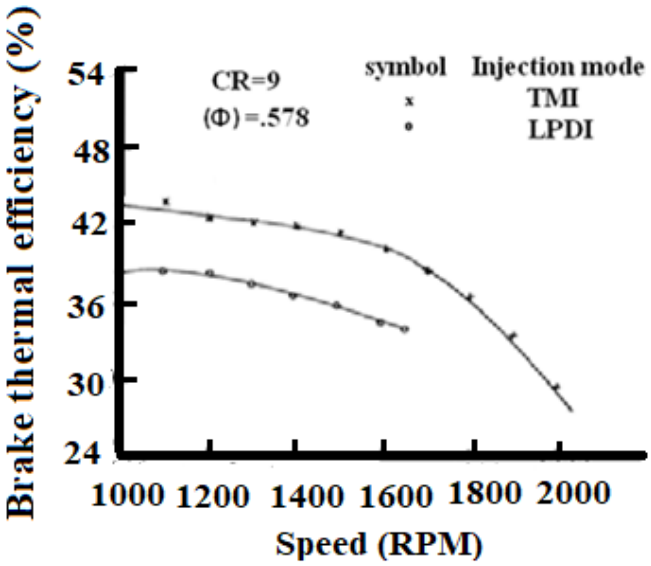

Fig. 2.8 BTE w.r.t. speed at constant equivalence ratio for both the TMI and LPDI operation [98]

A TMI system can be used as the alternative to load control method by throttling process. This system reduces the chance of combustible mixture in the manifold leading to less probability of abnormal combustion. The system injects fuel just after the beginning of the intake stroke. It also provides pre-cooling effect and lessens the chance of pre-ignition at hot spots. TMI also quench and dilute some residual combustible materials near the TDC. A hydrogen-fuelled engine with a TMI system can be useful for both CI and SI engines [99]. Hydrogen fuelled engine incorporated with TMI behaves like a diesel engine with nearly the same brake thermal efficiency.

2.7 Machine Learning Techniques

Integration of AI, Big Data (BD), and Advanced Digital Technologies (ADT) with the Energy Management System (EMS) can substantially improve the efficient use of the renewable sources of energy. The combined systems of AI and energy are named as Smart Energy Management Systems (SEMS). AI, BD, and ADT have the great impact in the foreseeable future [100]. In the context of SEMS, AI can be utilised to energy generation forecasting, [17] demand forecasting, demand side management [101], optimized energy storage operations, energy theft detection, and predictive maintenance and control *etc*. AI models can be used to all types of renewable energy like wind energy, solar energy, ocean energy, bio energy geothermal energy, hydrogen energy, and hybrid energy [102]. Fuzzy logic (FL), Genetic algorithm (GA), ANN, Wavelet Neural Network (WNN), Support Vector Machine (SVM), Decision Trees, Hybrid, and Ensemble are some of the AI techniques. Hybrid ML is relatively

simple, faster and more accurate. Training of these models require ample data, thus BD technique is required.

2.7.1 Intelligent Algorithms

The intelligent algorithms can provide the best output autonomously by interlinking the various input variables. The EMS has to depend on some fixed mathematical formulae for its operating process, if algorithms are not applied on them. The AIs have the adaptive capability to work together with multiple intelligent algorithms. Some of these algorithms are trained, tested, and validated based on BD techniques. ANN, ML, and Deep Learning are falling in this category [100]. Among the various intelligent algorithms, the percentage user of Neural Network, Fuzzy Logic, Bayesian Network, Heuristics, Support Vector Machine, and Q-Learning are 33 %, 34 %, 6 %, 3 %, 18 %, and 6 % respectively [100]. Hence, Fuzzy Logic is a very popular method of optimization technique preceded by Neural Network.

2.7.2 Fuzzy Logic (FL)

It is a branch of decision making that enables to understand and expose the reality in the real world that everything is matter of degree. FL is a computing paradigm that helps in data manipulation and representation [103]. It can be regarded as the extension of Binary theory which does not use crisp definition and distinction [104]. It is first proposed by L. Zadeh in 1965. There are two types Fuzzy Interface systems namely Mamdani, and Sugeno [105]. The advantage of Mamdani Fuzzy is its intuitiveness and suitable for human interpretation. Mamdani Fuzzy reasoning is used for language control systems in which data is captured from experienced workers [106]. FL includes five working methods *viz.* (a) Fuzzify inputs, (b) Apply Fuzzy operator, (c) Apply implication methods, (d) Aggregate all outputs, and (e) Output Defuzzify [105].

(a) Fuzzify inputs: Here the Fuzzy Inference System input the precise value and map to 0-1 through Fuzzy membership value.

(b) Apply Fuzzy operator: In this step each input variable is fuzzified to obtain the output and then a logical operator is used to find the weight of each Fuzzy rule.

(c) Apply implication methods: This method obtains the Fuzzy set by using Min or Prod method.

(d) Aggregate all outputs: The results of Fuzzy logic are based on the conclusions of all the Fuzzy rule. Hence, for each rule the implication method is used. Therefore, multiple number of Fuzzy set is obtained and the final Fuzzy set is synthesised based on the aggregate of each set.

(e) Output Defuzzify: Finally, Defuzzifying of the synthesised Fuzzy set is done to get the accurate value. Deblurring methods include centroid, bisector, median of maximum, maximum of maximum and maximum of minimum.

FL uses the following steps to operate: (a) Fuzzy rule, (b) Universe partitioning, (c) Creating relationship between input and output membership functions, and (d) Rules combination [107]. This technique is vastly utilised to predict the probable threats more efficiently. It works on the linguistic terms to generate the Fuzzy rule that connects the input variables logically to the output variables of the system. The data obtained from the experiments are placed in logical order to establish a mathematical model. Adaptive Neuro-Fuzzy Inference System (ANFIS) is a hybrid system which combines both neural network with fuzzy logic. ANN has the ability of self-diagnosing, which helps fuzzy systems to auto-correct a system [108]. In ANFIS membership functions are updated using a hybrid optimization method (backpropagation and least squares estimation) [109]. In many experiments it is observed that the experiments take several hours to complete. Due to which it is not possible to conduct a large number of experiments. Hence, by using small numbers of data the prediction cannot be done with a high accuracy to establish a mathematical model. In kinetic study also the traditional methods of simulation is not efficient to predict the behaviour of the kinetics of the reaction with high precision [110].

The introduction of Machine Learning and Deep Learning techniques of data science in the recent years have been emerged in as a useful tool to predict the engineering problems with high accuracy. The different Machine Learning methods [111] *viz.* AI, the ANN, the FL, the RBFNN, the PSO, the GA, *etc.* provide the useful tool to interpolate any practical engineering problems. ANN modelling is found to be an effective technique to solve complicated problems with higher satisfaction. It is a very user friendly and systematic tool to classify the faults in a system, grouping, and recognition of the flow pattern [112]. It establishes the mathematical relationship between the input-output parameters from a given set of data and particularly beneficial for non-linear problems. The ability to control and predict the futuristic solution to the problem makes it more familiar amongst the researchers. To predict the production of

hydrogen gas and reaction kinetics, some researchers have used ANN technique [88], [90]. The ANN model sets the logical relationship between input-output parameters. The most commonly used ANN method is the back propagation technique in which the data are trained and the possible errors between the actual data and ANN data are found out. It then back propagates to optimize the error between each successive layers and stop when error percentage comes to a set value [4].

2.7.3 Multiple Linear Regression (MLR) Model

Multiple linear regression (MLR) modelling is a machine learning technique that establishes the relationship between several independent parameters and dependent parameters using data obtained from experiments. MLR technique was used very effectively in many engineering applications. Xu *et al.* have predicted the surface integrity during machining of titanium alloys with cutting parameters as the input variables [113]. Ciulla and D`amico used the MLR technique for forecasting building energy performance [114]. Meerasri and Sothormvit used the drying temperature, time, and sample coating to predict the moisture content in pineapple cubes by MLR technique [115]. Dutta and Robi developed an MLR technique to predict the creep curve of nuclear pressure tubes [116]. The model was developed by taking stress, temperature, and time as the input parameters and creep strain as the output parameter. From these studies, it appears that the MLR technique can effectively be used for predicting the hydrogen generation curve in a reactor involving a reaction between Al and aq. NaOH under various conditions.

2.7.4 Artificial Neural Network (ANN)

In the human brain the neurons are the sensory parts of the body. It detects the stimuli, send to brain for processing and send back the signals to do the action. Thus, the neurons are interconnected and operates in a back propagation way. ANN is also the mathematical relationship of the various neurons that are interconnected, called machine learning language [111]. The history of ANN is several decades back. In the early age of 1940s ANN has been used for various engineering problems [117]. ANN was elaborated in the beginning by authors Rumelhart *et al.* in the year 1986 and Hecht-Nielsen in 1990. Feed Forward Back Propagation Network Modelling (BPNN) is familiar among the researchers. ANN consists of three layers *viz.* input layer, single/multi middle layer called as hidden layer and output layer. However, for most engineering applications single hidden layer is used. Independent variables compose

the input layer, while the output layer is the dependent variable. The dependent and independent variables are interconnected with some nodes called as neurons. These neurons have the ability to save data and subsequently process the data within the network. The data obtained as input function are processed based on the transfer functions (*tansig*, *logsig*, *purelin*, *etc.*) and send to the next layer. The output of the hidden layer neurons is the input for the output layer and send it to the output layer with different weightage.

The ANN modelling is very fast and accurate at the same time, unlike other physics based simulation techniques. The individual layers and the neurons are connected with some weight functions (W_{ij}). Each neuron is activated by biases (θ_j) in every layer of the network architecture. The mathematical relationship between the input and output parameters are processed in the hidden layer. The more the number of neurons the more complex is the network. The more the number of neurons in the network can reduce the simulation error up-to a great extent and it leads to a generalisation of the architecture. The optimum numbers of neurons, epoch and transfer function are obtained by hit and trial method [118]. The BPNN is consisted of two passes. The input data signals in the input layer are fed in forward pass for processing. Depending on the transfer function and weight of the neurons the signal is sent to the output layer. The output signals of the network processed by the neurons are compared with the actual values. The error between the actual and predicted values are analysed and propagate back to the input layer through the hidden layer. The weight and bias are modified during back propagation to improve the error. This iterative process is known as the training of the data of the experiments.

An epoch in ANN is defined as a single step to modify the weight functions of every training data sets. To modify the weight and thereby, reduce the error between the real experimental output vector and the predicted data a number of epochs are required. The total number of epochs needed to get a precise model in ANN is set as convergence rate. To optimize the error of the network by the adjustment of the weights, suitable optimization techniques are used. There are various back propagation methods available *viz.* Levenberg-Marquardt (trainlm), gradient descent with momentum (traingdm), sealed conjugate gradient (trainscg), resilient (trainrp), Bayesian regulation (trainbr), gradient descent (traingdm), *etc.* These methods are used to solve and predict the pattern of different engineering problems. Among these various methods Levenberg-Marquardt is used widely [110], [119], [120]. The particular ANN architecture is selected when the training data are trained successfully with optimize error.

Now, the same ANN model is tested with another sets of data points which were not used to train the network. An over-fitting of data is obtained when the difference of error during training and later on testing is very large. A well fitted data sets can be attributed to the close error during training and testing of data that leads to an effective architecture and it can be selected. The selected architecture is further confirmed to be accurate with another sets of data which are not used previously. This process of selecting the architecture is called as validation. After successfully obtained the ANN model, it can be used to obtain the output parameters for some unknown conditions.

2.7.5 Radial Basis Function Neural Network (RBFNN)

The radial basis function neural network (RBFNN) is an effective machine learning tool to establish the polynomial relationship between the various input-output parameters. RBFNN has been used in wide areas of research as revealed from the study of different literatures. The imbalance in the classification of data in a population is addressed by this method [121]. In civil engineering problems like landslides, and soil erosion RBFNN is successfully applied [122]. The security safety system is formulated based on a generalized radial basis function [123]. In the agricultural field, RBFNN is applied to predict the disease involving tomato leaves [124]. Alsaffar *et al.* [125] introduced the RBFNN and Backpropagation multilayer perceptron (BPMLP) to predict hydrogen produced by methane dry reforming. The PSO and the RBFNN optimization techniques are employed for the estimation of catalytic conversion of hydrogen gas through water gas shift reaction.

2.7.6 Least Square Fit (LSF) Method

Wang *et al.* [126] applied the least square fit method to measure the energy storage in lithium-ion batteries. Tawalbeh *et al.* [127] reported the use of optimization techniques to maximize the production of hydrogen and efficient storage devices. The development of an integrated energy system coupled with hydrogen is modelled by data-driven AI&ML tools [128]. The least-square fit method may be considered as a special case of the maximum likelihood approach [129]. In this method the actual raw data points are plotted and a line of standard is drawn manually to reduce the error between the actual and the predicted data. The square of the errors of the different parameters in a constitutive equation is minimized by performing partial differentiation and equalizing it to zero. A ‘goodness of fit’ polynomial of a higher order curve is fitted to derive an equation of the form given below [130]

$$f(p) = q_0 + q_1 p + q_2 p^2 + \cdots \ldots \ldots \ldots q_n p^n \qquad (2.8)$$

The constants $q_1, q_2, \ldots \ldots q_n$ are so adjusted that the raw data are modified to obtain the best fit of the polynomial.

2.8 Hydrogen fuelled furnace

A furnace is a thermodynamically closed system, the prime aim of which is to heat a raw material to a very high temperature to change some of its physio-chemical properties. In many industries like steel making industry, non-ferrous industry, ceramic and glass industry, and calcination in cement factories furnace is an essential component. A furnace is expected to use the heat input up to the full scale *i.e.*, the efficiency should be very high with minimum loss of energy. The furnace refractory materials are maintained well from erosion and corrosion during the sintering of materials. According to a report, published in 2017, 36 % of the global energy consumption is utilized by the industries [131]. Steelmaking, glass and ceramic, metallurgical are some of the energy-intensive industries. The operating temperature of the furnaces used ranges from (1000-1500) $^{\circ}$C [132]. The specific energy consumption of these furnaces varying from 2.4 to 14 MJ.kg^{-1} of finished product according to a survey [109]–[117], [119]. However, the specific energy consumption alters to a great extent based on the working temperature, nature of the finished product, fuel and oxidizer, *etc.* The primary sources of heat in a furnace are as given below:

- Fossil fuel (coal, diesel, *etc.*)
- Electrical energy
- Chemical energy

There are many types of furnaces available *viz.* Coke oven, Rotary kiln, Multiple hearth furnace, Fluid bed roaster, Batch -type, and Sintering tube furnace. Fossil fuel has been traditionally used in the iron making and sintering process to remove carbon dioxide. Though the reduction of carbon dioxide by using fossil fuel has good efficiency, the combustion of fossil fuel creates lots of hazards for the environment. Electrical energy is also used in the sintering furnace for power requirements. But the use of these energies can be limited by developing hydrogen gas-fuelled furnace for the sintering process.

Researchers throughout the globe are investigating the various parameters of hydrogen-fuelled furnaces. The results are being optimized to effectively use hydrogen gas for furnace, which simultaneously releases the dependency either on fossil fuel or electricity. Their works also

incorporate the state-of-the-art of the mechanism for the injection of hydrogen-rich fuel in the sintering bed of a sintering furnace. The use of hydrogen for combustion in a closed chamber like the furnace always accompanied with severe problems. As the world has experienced the havoc created by the explosion of hydrogen gas in different parts of the world. Hydrogen gas is much more dangerous in a confined place rather than in an open space. It is stated that the sintering performance is enriched by injecting more amount of hydrogen fuel and allow it to combust for a longer time within the permitted range. The permitted values are 0.6-0.8 % and for 8 minutes as mentioned [133]. It is further elucidated that the early introduction of hydrogen gas into the sintering furnace has the potential to improve the sintering quality better than injecting at a later phase. The required timing is 5-13 minutes.

2.8.1 Steelmaking industries and CO_2 emission

Global carbon emission has become a critical issue from the last few decades and the concomitant effect in the depletion of the ozone layer and associated ailment cannot be ruled out. According to the reviewers, the steel industry is the major contributor to the global increase in the level of carbon dioxide [120]–[124]. The continuous dissolving of the natural carbon sink is also a serious matter of concern. A policy is adopted to reduce the carbon emission per unit of GDP by 60-65 % as compared to 2005. But, in reality, it is predicted that by the year 2030, the carbon emission level will attain at the climax and therefore, the emission is needed to be cut down. Steel is manufactured from iron ore which includes different stages to obtain the final product. The whole process is conducted at several degrees of temperatures. Fine iron ores are agglomerated and make a lump before proceeding to the smelting of liquid iron. The initial process of sintering of iron ore is a high enthalpy process and requires tremendous temperature [134]. This stage uses 10 % of the total energy and liberates 10 % CO_2 of the total by burning fossil fuel. Steelmaking industries use the third-highest level of fossil fuel as reported. Hence, it is obvious that the application of fossil fuel has to be depleted to lessens the emission of not only carbon dioxide but also some other toxics. Therefore, in the present-day hydrogen gas has been acknowledged as the principal carrier of energy in various sectors. In steelmaking industries too, it has got importance for both the sintering process and the blast furnace process. Hydrogen gas can diminish the liberation of CO_2 as the by-product of the combustion of hydrogen gas is water [135].

The combustion of liquid fuel in a furnace by spraying the fuel is studied for different fuels. The flame is divided into horizontal and vertical type. The horizontal flame is applied in some

compacted heating device [136]. Hydrogen jet flame has been investigated and the integral expression defining its trajectory is put forwarded [137]. The horizontal flame is effected by the buoyancy and the dimension of the burner impacts the flame temperature. Kim *et al.* [137] investigated the range of radial expansion of the hydrogen flame in the surrounding and the effect of buoyancy on the hydrogen jet while it is released from the high-pressure vessel. The nature of dispersion of the hydrogen flame into the atmosphere is necessitated to be acknowledged in the process of controlling the threat possessed by it. The Gaussian diffusion model is invalid to analyze the dispersion characteristics of hydrogen gas as the gas outflow and the succeeding dispersion follows an unsteady 3D pattern. Hydrogen gas escapes from a high-pressure tank, immediately forms a jet and the atmospheric air is entrapped into it. The air-hydrogen mixture gets diluted and the buoyancy comes into play its role as soon as the hydrogen gas gets lighter. The buoyancy force bends the hydrogen jet upward. The hydrogen jet which comes out of the high-pressure storage tank is a choked jet. Once the choked jet passes on to the sub-sonic jet, the prediction of the dispersal behavior of the hydrogen flame becomes more complicated.

2.9 Storage

Hydrogen gas has many uses *viz.* Cooking food, affordable electricity, driving a car, powering factories, aviation industries, *etc.* Hence, it points towards a new dawn of useful and sustainable, efficient source of energy, which can mitigate the energy crisis in the present situation. However, hydrogen storage is another important constituent for the development of the hydrogen economy. Although hydrogen has a high gravimetric energy density, its volumetric energy density is very low due to its low density. In addition, hydrogen is a flammable gas with an ignition energy of only 0.02 mJ. That means even a static electricity discharge or an agitation of compressed or liquid hydrogen may generate sufficient energy to cause its ignition. Thus, the technological development for compact and safe hydrogen storage has been a challenging task. To store more hydrogen for a given volume, conventional methods include high-pressure compression and low-temperature liquefaction. Although these two technologies are matured in today's industries, their applications to hydrogen storage are not safe and there are still many technical problems to be resolved. The energy conversion of hydrogen gas by this process is much lower as compared to the tanks containing diesel and gasoline [99].

Researchers have tried to develop metal hydrides to store hydrogen gas and got success up to a certain level [138], [139]. But fails to act as a hydrogen reservoir for a prolonged time. Hydrogen gas has the potential to be used as the source of energy for static as well as dynamic applications with averting adverse effects on the atmosphere. Those nations who are not having sufficient natural resources to produce their fuel and have to depend on other countries, hydrogen gas can be helpful for them to meet the power requirement. The main obstacle in the growing hydrogen economy is the issue related to the storing. Hydrogen gas can be stored as follows: a) pressurize gas, b) cryogenic liquid, c) solid fuel as chemical or physical combination with other materials, such as metal hydrides, complex hydrides and carbon materials or on-board application by methanol reforming [140].

Hydrogen gas is stored by transforming its physical state into liquid or gaseous state in pressurised tank or cryogenic tank. The process by which hydrogen gas has been stored till date is not very favourable from application point of view and for safety purpose. This is because of low boiling point (-252.87 $^{\circ}$C) and low gaseous density (0.08988 g. L^{-1} at 1atm) of hydrogen. To maintain liquid hydrogen at cryogenic temperature an arrangement of refrigeration unit is required [141], which added extra cost to the system and make it a more complicated design at the expense of 40 % energy loss due to the increase in weight of the system [142]. However, the storage of the hydrogen gas at very high pressure is not advisable due to the chance of leakage. The storage of hydrogen gas either in liquid or gaseous form is always vulnerable to catch fire. So, safety is not assured in either stationary or mobile application. Hydrogen production by steam reforming of methanol requires an extra steam reformer to extract hydrogen from the carbon, which requires additional space and add weight to the system [140].

The environmental and economic aspects are considered to make a futuristic model for hydrogen storage by the US Department of Energy (DOE) [143]. The minimum storage capacity of the system has been decided to be 6.5 wt. % and 65 g. L^{-1} of hydrogen gas available, within the decomposition temperature range of 60-120 $^{\circ}$C for commercial applications. The proposed system has been critically analyzed for its material toxicity property and the cost-effectiveness. The study of various publications has revealed that the carbon nanotubes, carbon fibres, and activated carbon are ideal candidates to store hydrogen by the process of low-temperature absorption of chemical compounds or by adsorption of a gas by carbon elements. However, the results obtained for the hydrogen storing capacity of carbon nanomaterials are not very encouraging. Data show the storing capacity of the carbon material between 0.2 to 10

wt. % [136], [137]. Though in today's scenario the carbon material has been developed a lot in storing hydrogen gas, still it is not sufficient to run an automobile engine [144]. Some researchers have tried hydrides of Mg to store and carry hydrogen gas. These hydrides can increase their temperature or decrease the external pressure during the need for hydrogen gas discharge.

A good metal hydride should have the following characteristics *viz.* high hydrogen contain capacity per unit mass, low dissociation temperature, fair dissociation pressure, lower value of heat of formation so that hydrogen extraction is easy, the dissipation energy for the formation of metal hydrides is kept low, reversibility, less amount of energy waste during the charging and discharging of hydrogen gas, high rate of conversion, high inertness towards oxygen and air for better reliability, recyclability, and well factor of safety. Many works suggest the use of various metal hydrides such as $LaNi_5$, TiFe, $TiMn_2$ for hydrogen storage. However, according to the criteria set by US Department of Energy, they are not able to meet the requirement for practical application. The hydrogen keeping capacity is only 2 wt. % as reported.

A series of Mg based hydrides have been acknowledged as the potential and promising hydrides for hydrogen storage with 7.6 wt. % of capacity. Extensive research is conducted to reduce their dissociation temperature, increase durability, and safety. The hydrogen conversion rate is increased by allowing some catalysts to react with the hydrides. The ball milling is also done which is accompanied by defects and enhance surface areas [145]. A thorough investigation of sodium borohydride and ammonia borane is carried out in this regard by other scientists. It is aimed at fabricating a system which releases hydrogen gas at a moderate rate at ambient condition [33], [146].The high cost of metal hydrides and the requirement of high temperature for the release of hydrogen gas impede its wide utilization [99], [147]. Nakayama *et al.* reported the storage of hydrogen gas by using clathrate hydrate. A conceptual model of in-situ storage of hydrogen gas has been proposed [148]. Clathrate hydrates have a crystal structure with cage-like constructions. They consist of the water molecule and the foreign molecule engulfed inside the cage structure. The rhombohedral structure of hydrogen hydrate has been discovered in the year 1993 [149]. This particular structure has cavities of lesser size and the guest particles are entrained in the lattice. Thereby, making it possible for the clathrate hydrate to store hydrogen gas. Recently, certain chemical reactions of reactive metals accompanied by hydrogen evolution have received increasing interest in the field of hydrogen energy because of their potential applications in both hydrogen production and storage. In these

reactions, the hydrogen sources such as water and hydrocarbons are usually used as one of the reactants, from which hydrogen will be extracted with the help of metals of high activity. This is an innovative application of an old technology as hydrogen evolution through the displacement reactions of metals was discovered several centuries ago and some of these reactions have already been studied thoroughly. In certain metal reactions, a violent hydrogen release occurs soon after the contact between reactants even under mild conditions.

On-demand hydrogen release using metals can eliminate the need for hydrogen storage. For those scenarios, hydrogen is indirectly stored in the form of its sources. Such systems can be more compact and much safer. Considering the stringent safety requirements for hydrogen storage, the production of hydrogen on-demand during the chemical reaction between aluminium and alkaline water can be developed as a viable, environment friendly, and cost effective technique. Development of a viable reactor for the production of hydrogen gas on-demand would to a great extent solve the present problem of oil price hike, especially for automobile applications. Several reactors have been designed for the on-demand supply of hydrogen by this chemical reaction, each design has its limitations though.

2.10 Precautions

Hydrogen gas is inflammable with high heat energy content and hence, the utmost care has to be taken while using in varied applications. The controlled use of hydrogen gas has more benefits than demerits. People are quoted frequently with the dangerous nature of hydrogen gas, *e.g.* hydrogen bomb [150]. The conventional and skill-full use of hydrogen gas has no connection with its havoc nature. Hydrogen flame radiates very less unless it falls in the direction of flame, there is little chance of getting burnt. It is observed that the heat radiated from petrol fired flame is of high order than a hydrogen flame, and thus brings a threat to the life and property. The primary risk linked with hydrogen gas flame is its low minimum ignition energy and low lean limit of flammability. Therefore, a small leakage of hydrogen gas in a closed chamber may pose menaces. The ignition energy of hydrogen is so less that the high velocity of leakage through the air can combust due to the air friction [151].

Hydrogen gas when contained in a tank at high pressure, special care should be taken so that there is no chance of leakage. The molecular diameter of hydrogen gas is very less than other fuel molecules. Thus, it is very difficult to retain hydrogen gas in storing devices. It is mentioned that hydrogen gas cannot be confined by using a high-pressure pipe, lined with poly-

tetra-fluoro-ethylene (Teflon) [152]. The leakage of hydrogen gas can lead to a massacre if it undergoes combustion in a confined room. The same can be avoided in an outdoor case. Hydrogen gas in a closed room can accumulate and become the hot spot of combustion, unlike at outdoor the gas diffuse away in the atmosphere [151]. There is one exception for the large escape of liquid hydrogen gas, in which the gas is denser than air till it boils off by capturing heat from the surroundings.

This is a well-known fact that hydrogen gas is odourless and colourless. It is very hard to detect the presence of hydrogen gas without having any means [153]. Hence, it is emphasised to have a state-of-the-art laboratory for testing hydrogen gas and safety considerations for any kind of emergency. A number of researchers have agreed with the safe use of hydrogen gas as a fuel for its better efficiency and environmentally benign nature than the fossil fuel [148]–[150]. The safety of the combustion of hydrogen gas can be realised with the proper engineering design of the reactor and scientific use of the gas with proper precautions. The safety considerations are not supposed to impede the hydrogen economy.

2.11 Cost analysis

The socio-economic benefit of academic research whether scientific or humanities is always a prior goal. The various scholarly articles aimed at the development of the society, science and technology, and economic strengthening of any nation. It is very important to define research work in terms of time and economic benefit. Statistical tools are very useful to describe the financial aspect of the project or research work. Some of the tools are the Break-Even Analysis, the Net present value Method, the Return On Investment, the Payback Period Method, the Internal Rate of Return Method, *etc.* The proper distribution of capital is the most crucial in the modern financial management system.

2.12 Summary of literature survey

The different methods of production of hydrogen gas have their own merits and demerits. Hydrogen gas produced by the hydrolysis process is costly to be used extensively. Steam reforming of water to produce hydrogen uses fossil fuel, which is not environment friendly. The conversion rate of hydrogen gas by the biological process is very slow. This impedes the use of this process. The hydrogen production from metal hydrides requires high temperatures. The storage of hydrogen is found to be inefficient. Moreover, hydrogen gas has very low ignition energy (0.02 mJ), and hence vulnerable to explosion. Considering all these aspects

hydrogen production from Al and alkaline water reaction is found to be a viable, cost-effective and environment friendly technique. Machine leaning algorithms can be successfully implemented to predict the evolution of hydrogen and kinetics of the reaction mechanism. The mathematical model of the rate equation for the production of hydrogen energy by chemical method can be established with the help of machine learning tool. In-situ hydrogen can be used in the industrial furnaces as a better replacement of fossil fuel and electricity for practical applications.

2.13 Gaps in the literature review

The following points are to be addressed from the review of the literatures:

1. An extensive systematic study of the kinetics of the reaction between aluminium and the alkaline solution is required to be carried out. The experiments have to be carried out at a higher concentration of NaOH.
2. Correlation between reaction rate and temperature, concentration, size & shape of aluminium, composition, *etc.* has not been established. The optimum condition for the concentration of NaOH solution and temperature has not been defined.
3. There is not any effective technology to store hydrogen gas for a prolonged time.
4. On-board production of hydrogen gas is yet to be addressed.
5. The production of hydrogen gas depends not only on temperature and pressure but also some other factors that affect its production. Factors like the size of Al pellets, shape, morphology, type of water, the volume of water, *etc.*
6. The proper design of a reactor for the production of hydrogen for the sintering furnace application is yet to be developed.
7. Research related to the use of machine learning based computational technique has not been established to predict the evolution of hydrogen gas for real time applications.
8. Investigation of combustion of hydrogen produced by chemical methods for sintering tube furnace application (efficiency *etc.*) not yet carried out.

Chapter-3

Materials and Method

3.1 Introduction

Generation of hydrogen gas by various methods have been highlighted in chapter 2. From the literature survey it appears that the reaction of aluminium and aq. NaOH solution is a viable environment friendly technique for the generation of pure hydrogen gas. A hydrogen generator was developed to carry out the experiments and generate hydrogen production data by the chemical reaction. These data were used for modelling the reaction kinetics. For evaluation of the applicability of this technique, a hydrogen fuelled sintering tube furnace was fabricated and the thermal efficiency of the furnace was investigated. The procedures followed for this investigation are described in detail in the subsequent sections.

3.2 Preparation of aluminium sample

3.2.1 Raw materials

Scrap aluminium in the form of hollow sections as part of the window and door panels having thickness 1.0 mm were used as the raw material. As-received Al sections were first cleaned with acetylene to remove grease and dust particles. These were cut into small pieces using hand shearing machine.

3.2.2 Sodium hydroxide solution

Commercially available sodium hydroxide pellets of 97 % purity were procured from the local market. The NaOH pellets were dissolved in distilled water to obtain the aqueous NaOH solution of required molarity. The reactions at high temperatures are conducted by dissolving NaOH in water with the required temperature.

3.3 Design and Fabrication of the Chemical Reactor

A reactor is a closed device in which reactants are allowed to react at the particular reaction condition. Safety of the reactor is very important since the gas which is evolved during the reaction is hydrogen gas. A reactor was fabricated for carrying out the chemical reaction

between Al and aq. NaOH solution for the generation of H_2 gas. Enough safety precautions were taken to prevent any H_2 gas leakage during the experiments. The features of the reactor include provision for (a) inserting the reactants in to the reaction chamber, (b) H_2 gas out let, (c) removal of the solid reaction products after the completion of the experiment, (d) insertion of thermometer to measure the reaction temperatures, (e) stirrer to remove the passive layer of $Al(OH)_3$ formed on the surface of the Al pellets, and (f) water bath for maintaining the temperature of the reactor. Figure 3.1 illustrates schematically the setup used for carrying out the kinetic experiments. The reactor consists of a 250 ml filtration flask kept in a water bath which is maintained at a constant temperature. The stirring of the reactor is facilitated using a magnetic stirrer placed in contact with the water bath. The temperature inside the reactor is measured at regular periods using an industrial mercury thermometer (specification -10 ^{o}C to 110 ^{o}C) which was kept dipped in the reactor solution. The hydrogen gas generated in the reactor is transferred to the bottom of an inverted water column using a flexible pneumatic tube, which was placed inside a water bath exposed to air. The inverted column is made of a poly-methylmethacrylate (PMMA) tube of 4.5 cm ID and 100 cm length. A graduated scale with zero reading at the top is attached to the inverted tube to measure the water level in the tube. The photograph of the setup is presented in fig. 3.2

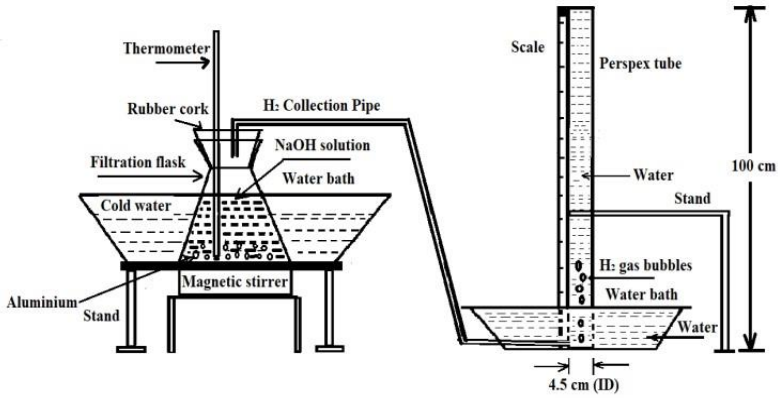

Fig. 3.1 Schematic diagram of the experimental setup for hydrogen gas generation

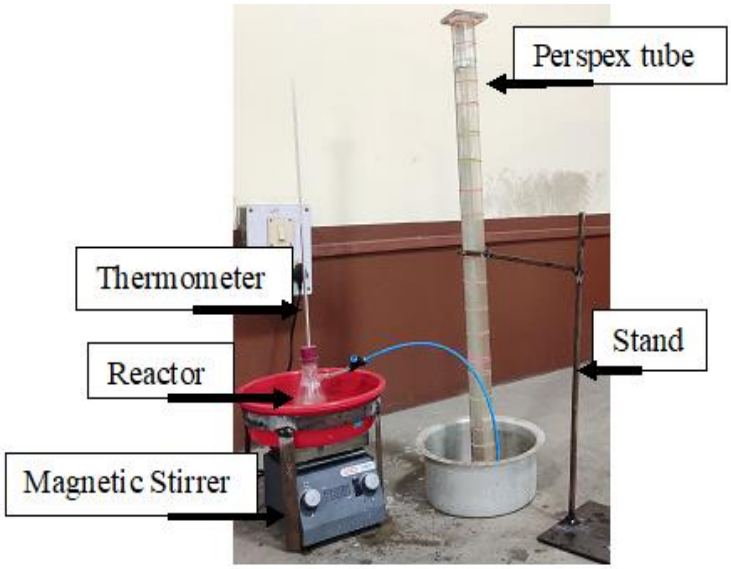

Fig. 3.2 Photograph of the H_2 generation set up

3.4 Experimental Procedures

The hydrogen generation rate during chemical reaction between Al pellets and aq. NaOH solution in the reactor was investigated. The experiments are carried out by varying the parameters *viz.*, the concentration of NaOH solution, temperature, size of Al pellets, and the volume of water. The experimental matrix under which the reactions are carried out is presented in Table 3.1.

Table 3.1 Experimental Matrix for the hydrogen generation

Temperature (K)	Concentration (M)				
	1	2	3	4	5
303	✓	✓	✓	✓	✓
313	✓	✓ #*	✓	✓	✓
323	✓	✓	✓ #	✓ *	✓
333	✓	✓	✓	✓	✓

These data were used only for validating the ANN model using BPNN

* These data were used only for validating the ANN model using RBF and LSF

3.5 Modelling

3.5.1 Constitutive equation for hydrogen generation

Mathematical modelling by one-variable-at-a-time approach is incapable of establishing the impact of multiple variables interactions on the output. The Least Square Fit is a statistical tool that analyses the inter-relationship among multiple variables, which can be established by comparing the simulated and experimental data. The correlation between the variables is achieved by the minimization of the sum of the squares of the differences between the actual value and simulated value. In this study, the evolution of hydrogen gas (*V)* is considered as a function of water temperature *(T)*, NaOH concentration *(C)*, and reaction time *(t)*. *i.e.*, mathematically expressed by

$$V = f(T, C, t) \qquad (3.1)$$

It is found that the hydrogen generation profile is non-linear and hence equation no. (3.1) takes the form

$$V = G * C^{\alpha} * e^{\left(\frac{-E_a}{RT}\right)} * t^{\beta} \qquad (3.2)$$

Here, *G, α,* and *β* are constants. E_a and *R* are the activation energy and universal gas constant respectively. Equation no. (3.2) can be reduced to the linear form by taking a natural log.

$$lnV = lnG + \alpha lnC + \left(-\frac{E_a}{R}\right)\frac{1}{T} + \beta lnt \qquad (3.3)$$

The error E_i is defined as follows:

$$E_i = lnV - lnG - \alpha lnC + \left(\frac{E_a}{R}\right)\frac{1}{T} - \beta lnt \quad (3.4)$$

$$\sum_{i=1}^{N} E_i^2 = \sum [lnV - lnG - \alpha lnC + \left(\frac{E_a}{R}\right)\frac{1}{T} - \beta lnt]^2 \quad (3.5)$$

where, N is the number of data points

Taking partial derivative of $\sum_{i=1}^{N} E_i^2$ with respect to lnG and equate to zero we get,

$$\frac{\sum_{i=1}^{N} \partial E_i^2}{\partial lnG} = 0$$

$$2\sum_{i=1}^{N}\left[lnV - lnG - \alpha lnC + \left(\frac{E_a}{R}\right)\frac{1}{T} - \beta lnt\right](-1) = 0$$

$$\sum_{i=1}^{N} lnG + \sum_{i=1}^{N} \alpha lnC - \sum_{i=1}^{N}\left(\frac{E_a}{R}\right)\frac{1}{T} + \sum_{i=1}^{N} \beta lnt = \sum_{i=1}^{N} lnV \qquad (3.6)$$

Similarly, equation nos. (3.7), (3.8), and (3.9) are obtained and given below:

$$\sum_{i=1}^{N} lnGlnC + \sum_{i=1}^{N} \alpha(lnC)^2 - \sum_{i=1}^{N}\left(\frac{E_a lnC}{R}\right)\frac{1}{T} + \sum_{i=1}^{N} \beta lntlnC = \sum_{i=1}^{N} lnVlnC \qquad (3.7)$$

$$\sum_{i=1}^{N} \frac{lnG}{T} + \sum_{i=1}^{N} \frac{\alpha lnC}{T} - \sum_{i=1}^{N}\left(\frac{E_a}{R}\right)\frac{1}{T^2} + \sum_{i=1}^{N} \frac{\beta lnt}{T} = \sum_{i=1}^{N} \frac{lnV}{T} \qquad (3.8)$$

$$\sum_{i=1}^{N} lnGlnt + \sum_{i=1}^{N} \alpha lnClnt - \sum_{i=1}^{N}\left(\frac{E_a lnt}{R}\right)\frac{1}{T} + \sum_{i=1}^{N} \beta(lnt)^2 = \sum_{i=1}^{N} lnVlnt \qquad (3.9)$$

Equation nos. (3.6-3.9) form a set of linear equations which may be represented by a matrix of order four. The matrix is given below:

$$\begin{pmatrix} N & \sum_{i=1}^{N} lnC & -\sum_{i=1}^{N} \frac{1}{T} & \sum_{i=1}^{N} lnt \\ \sum_{i=1}^{N} lnC & \sum_{i=1}^{N} (lnC)^2 & -\sum_{i=1}^{N} \frac{lnC}{T} & \sum_{i=1}^{N} lnClnt \\ \sum_{i=1}^{N} \frac{1}{T} & \sum_{i=1}^{N} \frac{lnC}{T} & -\sum_{i=1}^{N} \frac{1}{T^2} & \sum_{i=1}^{N} \frac{lnt}{T} \\ \sum_{i=1}^{N} lnt & \sum_{i=1}^{N} lnClnt & -\sum_{i=1}^{N} \frac{lnt}{T} & \sum_{i=1}^{N} (lnt)^2 \end{pmatrix} \begin{pmatrix} lnG \\ \alpha \\ \frac{E_a}{R} \\ \beta \end{pmatrix} = \begin{pmatrix} \sum_{i=1}^{N} lnV \\ \sum_{i=1}^{N} lnVlnC \\ \sum_{i=1}^{N} \frac{lnV}{T} \\ \sum_{i=1}^{N} lnVlnt \end{pmatrix} \qquad (3.10)$$

The above matrix *i.e.*, equation no. (3.10) takes the form given by

$$[A][X] = [B]$$

$$[X] = [A]^{-1}[B] \qquad (3.11)$$

The elements of $[A]$ and $[B]$ are obtained by carrying out the experiments of hydrogen production from the Al-H_2O reaction. The four unknown parameters of the constitutive

equation no. (3.2) *viz.* G, α, E_a, and β are determined by solving equation no. (3.11). The corresponding values are shown in Table 4.6 below (section 4.2.3).

The values thus obtained are substituted in equation no. (3.2) to predict the H_2 production under various conditions of *T, C,* and *t*. A correlation was established between the actual data and predicted data. Equation no. (3.2) is validated with two unknown conditions as indicated in Table 3.1 with a (*) sign.

3.5.2 Multiple Linear Regression (MLR)

Multiple Linear Regression (MLR) is a data driven curve fitting multivariable mathematical technique to obtain a relationship between the input and output variables for any process. The principle behind the application of MLR is the minimization of the sum of the squares of the differences between the experimental and predicted value. In this study the volume of hydrogen gas generated per gram of Al (V in mol. g^{-1}) is expressed as a function of reaction temperature (T) in K, concentration of aq. NaOH (C) in mole and time (t) in minute. *i.e.*, of the form

$$V = f(T, C, t) \tag{3.12}$$

Equation no. (3.12) can be explicitly written as [154]

$$V = GT^{\alpha}C^{\beta}t^{\gamma} \tag{3.13}$$

where, G, α, β, and γ are the constants. Taking logarithms, equation no. (3.13) assumes the form of a linear equation as

$$\log(V) = \log(G) + \alpha \log(T) + \beta \log(C) + \gamma \log(t) \tag{3.14}$$

The data obtained from the actual experiments are used to determine the values of G, α, β, and γ. The regression constants were obtained using the function 'REGRESS' in MATLAB® 2020b (Math Works Inc.). The time dependent volume of gas generated by the reaction is obtained by substituting the values of the constants in equation no. (3.13).

3.5.3 Artificial Neural Network (ANN) modelling

Machine learning tool such as ANN is used to predict the evolution of hydrogen gas for industrial utilization and establish the kinetics of the reaction between Al-H_2O. ANN is a data driven modelling technique where the output is obtained even if the physical relationship between the input-output variables are not known. In the present study, limited experiments

were performed to generate sufficient data for the ANN modelling. Twenty sets of experiments of hydrogen generation from aluminium-aq. NaOH solution reaction, as indicated in Table 3.1, were carried out for this purpose. Out of these, two experiments *viz.* 2M/313 K and 3M/323 K were not used for modelling purposes. The data obtained from these two experiments were used only for validation of the developed ANN model. From the remaining 18 experiments a total of 613 input-output data sets were extracted for the modelling. These data were segregated into three groups: (a) 337 data sets (55 %) for training purposes; (b) 185 (30 %) for testing; and (c) 91 (15 %) for validation of the ANN architecture. The values of temperature, concentration, time, and the volume of hydrogen gas evolved are mapped to lie between 0.1 and 0.9. A number of trial training experiments were carried out by varying the number of neurons in the hidden layer, target error goal transfer functions at input-hidden layer and hidden-output layer. The transfer functions used were *tansig*, *logsig*, and *purelin*. The best ANN architecture and the processing function were achieved by training the neural network using the input-output data sets for the training and testing.

The mathematical model for the ANN is based on the equation no. (3.1). The modelling is done by multi-layer perceptron feed forward back propagation method. The three neurons represent the temperature, concentration, and time in the input layer. The architecture has been shown in fig. 3.3 below. The output layer consists of the dependent parameter *viz.* volume of hydrogen gas generated. The simulation of training, testing and validation is carried out in MATLAB® 2020b (Make: Math Works Inc.). The *trainlm* function is used to attune the weights and bias according to the Levenberg-Marquardt optimization algorithm. This *trainlm* method is a very efficient method to solve non-linear problems. Training and testing of the network architecture were carried out using the 337 and 185 data sets respectively. During the training period, only one hidden layer was used. A number of trial experiments were carried out by (i) varying the number of neurons in the hidden layers from 5 to 35, (ii) using different transfer functions viz. *tansig, logsig, and purelin* combinations, (iii) keeping minimum deviation error between the predicted and the experimental values, and (iv) varying the error goal between 0.0001 and 0.00001. During the training and testing, the best network architecture was chosen based on the statistical analysis of the experimental and network data. The statistical parameters are described in the subsequent paragraphs.

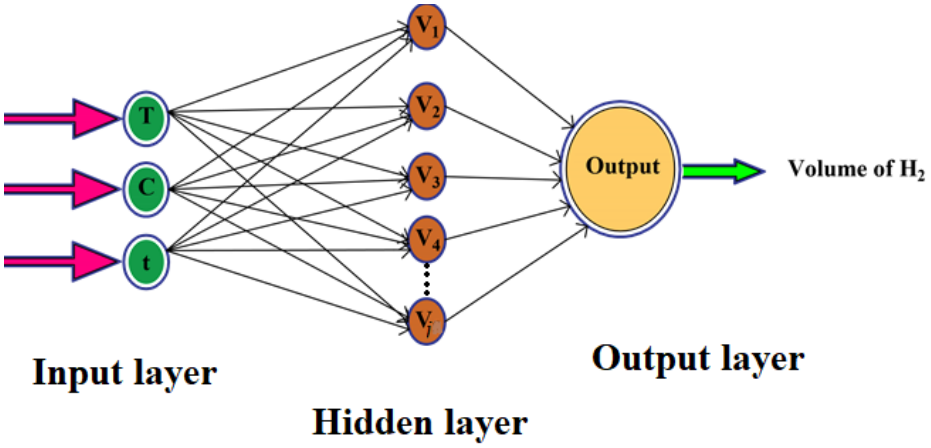

Fig.3.3 Architecture of the Artificial Neural Network

3.5.4 Statistical Analysis

The error between the actual and the predicted values during the training process is minimized by the network by adjusting the weights. The performance of the network is measured by using root-mean square functional error which is given as follows [120].

$$RMS_{error}^{f} = \sqrt{\frac{\sum(V_e - V_p)^2}{NV_e{}^2}} \qquad (3.15)$$

where, V_e is the experimental value, V_p is the predicted value, and N is the number of data points. The training error and the testing error are determined separately. The effective error of the training and testing data are calculated using the following equation:

$$Effective\ error = max\ [RMS_{error}^{f}\ of\ traing\ data - RMS_{error}^{f}\ of\ testing\ data] \quad (3.16)$$

The over fitting of data for the network is when the testing error is substantially larger than the training error. The network is assumed to be well fitted when the error between the testing and training data is significantly less. The details of the results obtained during testing and training of data has been presented in "Appendix III." The best architecture network during the numerical trial experiments was chosen depending on the following conditions: (a) minimum functional RMS error between training and testing data, (b) 98 % of the predicted data falls within a deviation error of ± 5 % of experimental values, and (c) at least 95 % of the predicted data falls within a deviation error of ± 2 % of the experimental values. The prediction ability of the trained network is verified by using Statistical tools such as coefficient of correlation (R_{cc}), average absolute relative error (AARE), and average root mean square (RMS) error. These are given as follows:

$$R_{cc} = \frac{\sum_{i=1}^{N}(V_e - \overline{V_e})(V_p - \overline{V_p})}{\sqrt{\sum_{i=1}^{N}(V_e - \overline{V_e})^2 \sum_{i=1}^{N}(V_p - \overline{V_p})^2}} \quad (3.17)$$

$$AARE = \frac{1}{N}\sum_{i=1}^{N}\left|\frac{V_e - V_p}{V_e}\right| * 100 \quad (3.18)$$

$$RMS\ (error) = \sqrt{\frac{1}{N\sum_{i=1}^{N}\left(V_e - V_p\right)^2}} \quad (3.19)$$

where, V_e is the experimental value and V_p is the predicted value, $\overline{V_e}$ and $\overline{V_p}$ are the average values of V_e and V_p respectively and N is the number of data points used in the network.

3.5.5 Sensitivity Analysis

The importance of input parameters *viz.* temperature, concentration, and time on the volume of production of hydrogen gas is predicted by using the best weight matrix of ANN and Garson's algorithm [155]. A novel method of partitioning the weights of neural network to determine the influence of each input parameter on the output was proposed by Garson and is given by

$$C_j = \frac{\sum_{p=1}^{p=nb}((|w_{jp}^{ab}| \div \sum_{q=1}^{na}|w_{qp}^{ab}|) \times |w_{pr}^{bc}|)}{\sum_{q=1}^{q=na}\{\sum_{p=1}^{p=nb}((|w_{jp}^{ab}| \div \sum_{q=1}^{na}|w_{qp}^{ab}|) \times |w_{pr}^{bc}|)\}} \quad (3.20)$$

where, C_j is the relative importance of the j^{th} input parameter on the output parameter, na and nb are the number of input and hidden neurons respectively, w is the connection weight. The subscripts *a, b,* and *c* designate to input, hidden and output layers respectively. The subscripts *p, q,* and *r* represent the input, hidden, and output neurons respectively. After the artificial neural network is frozen, the model is validated with 91 data points, which are not used in training and testing the architecture. The neural network is also used to simulate the output for experimental conditions which is not carried out.

3.5.6 Radial basis function neural network (RBFNN)

ANN is the latest and most important intelligence computational paradigm that processes information of a network by simulation technique of neuron network that resemblances human brain. One of the most important advantages of the ANN technique is the ability to compute non-linear relationships thereby, reducing the tediousness and complexity of the conceptual

model [157]–[158]. Radial Basis Function Neural Network (RBFNN) uses the RBF function as a kernel function and has a feed-forward structure. The RBFNN sets a relationship among the several input-output parameters through function normalization, noise detection, classification, *etc.* As shown in fig. 3.3 the three layers' architecture consists of (a) the first layer which is known as the input, (b) the middle layer is called the hidden layer, and (c) the third layer is known as the output. The hidden layer is composed of radial basis function neurons and may be one or more. These layers are connected like a multi-layer perceptron (MLP) model. However, the collector and activation function are replaced with each other. The activators of the hidden layer neurons follow the radial basis function or Gaussian function whereas, the output layer function is linear [159]. Distinct advantages of using RBFNN for computational work in comparison to others include faster learning algorithms and nonappearance of local minima problems [160], [161].

The Gaussian function $\zeta_j(x)$ for the hidden layer is represented as given below [158]:

$$\zeta_j(x) = exp\left[-\frac{\|x-c_j\|}{\delta^2}\right] \qquad (3.21)$$

where, $c_j and\ \delta$ are the centre and spread of the j^{th} RBF node respectively.

The output V of the network is calculated by using the weighted sum of the hidden layers' output. The weight (w_j) is obtained by using ordinary least squares.

$$V = \sum_{j=1}^{n} w_j \zeta_j \qquad (3.22)$$

Training of data can be performed by two steps method such as (i) setting the centre by clustering the training data (337 data in this case), and (ii) estimation of weight vector by the ordinary least square method. In the present RBFNN model, 337 data points (55 % of total data) are used to train the model. Meanwhile, RBFNN is suitable for interpolation rather than extrapolation [162]–[164]. MATLAB®2020b software provides NEWRB function for the selection of the best neural network. The function defines an approximate RBFNN which automatically determines the neurons in the hidden layer. During the execution of the function, the neurons will be added till the target error square sum is attained or the maximum number of neurons in the hidden layer is reached. The prediction excellence of the RBFNN is assessed by the statistical tool namely correlation coefficient (R_{cc}) and absolute average relative error

percentage (AARE %). Figure 3.3 depicts the architecture of the RBFNN. Temperature *(T)*, concentration *(C)*, and time *(t)* are the input parameters denoted by the circles in fig. 3.3. The middle layer is the hidden neuron (*v*), and the third layer is the output layer which is the volume of H_2 liberated (*V*).

3.6 Study of thermal efficiency of H_2 fuelled sintering tube furnace

3.6.1 Experimental Setup and Sintering Furnace

The experimental setup for investigating the performance of the sintering furnace using hydrogen fuel is shown schematically in fig. 3.4 and the photograph of the test rig is presented in fig. 3.5. The setup consists of the following: (i) a hydrogen reactor fitted with valve V_1, (ii) an air compressor for supplying the air at required pressure through valve V_2, (iii) two rotameters for measurement of hydrogen flow rate (specification is 0-10 liter per minute) and air flow rate (specification is 0-30 liter per minute), (iv) a burner on a stand for combustion of the fuel-air mixture, (v) a sintering tube furnace, (vi) tube connections, (vii) thermocouples (T_1, T_2, T_3, T_4, T_5, and T_6), and (viii) data acquisition system (DAQ) for record of temperature. The reactor is made of stainless steel having 10 liter capacity. The lid of the reactor can be opened to introduce the reactants, *i.e.*, NaOH solution and Al pellets into the reactor chamber. The fuel-air ratio is adjusted by controlling the flow of these gases by opening the outlet valve from the reactor and regulating the pressure in the compressor.

Hydrogen gas generated by the chemical reaction is transferred through rotameter and tube fittings to the burner where it gets mixed with the air from the compressor in the required fuel-air ratio. The details regarding the sintering furnace, the thermocouple positions, and the chimney are shown in fig. 3.6. Figure 3.7 depicts the photograph of the furnace. The furnace consists of two concentric stainless steel cylinders. The outer cylinder is 260 mm ID, 6 mm thick, and 500 mm long whereas, the inner cylinder is 60 mm ID, 4 mm thick, and 1000 mm long. Henceforth, the combustion chamber referred to is the annular space between the inner and outer cylinder. Both ends of the outer cylinder were welded to 260 mm OD and 60 mm ID and 2 mm thick flanges using TIG welding. The inner tube was inserted through the 60 mm hole of the flange and sealed using high-temperature ceramic wool impregnated with sodium silicate and allowed to harden. This ensured a proper leak-proof combustion chamber. A provision for inserting the burner through which the flame due to the combustion of hydrogen-air mixture at the required ratio is inserted into the annular space between the outer cylinder

and inner tube. The hot gas mixture passes through the combustion chamber and heats the inner tube which in turn heats the atmosphere inside the inner tube by conduction and convection respectively. The exhaust gas from the combustion chamber after the heat transfer escapes through the chimney provided at a distance of 470 mm as shown in fig. 3.6. In this teat rig a steel jar of volume 10 litre was used as a reactor instead of filtration flask to obtain higher amount of gas. The test rig consists of the following: (i) sintering furnace, (ii) a reactor, (iii) a data acquisition (DAQ) system, (iv) two rotameters for flow measurement of hydrogen gas and air, (v) thermocouples, and (vi) pneumatic pipe.

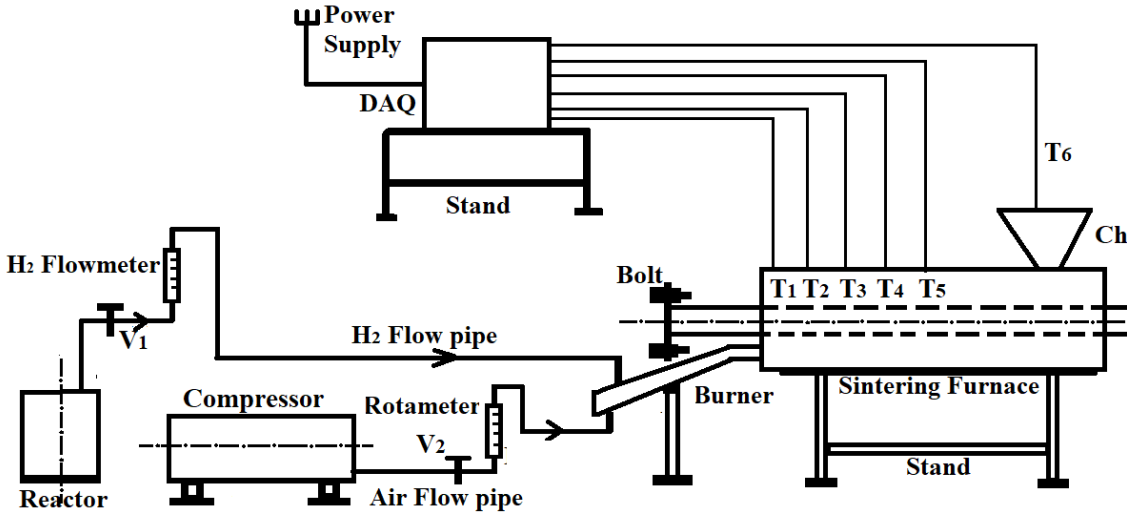

Fig.3.4 Schematic of the experimental setup of the sintering tube furnace

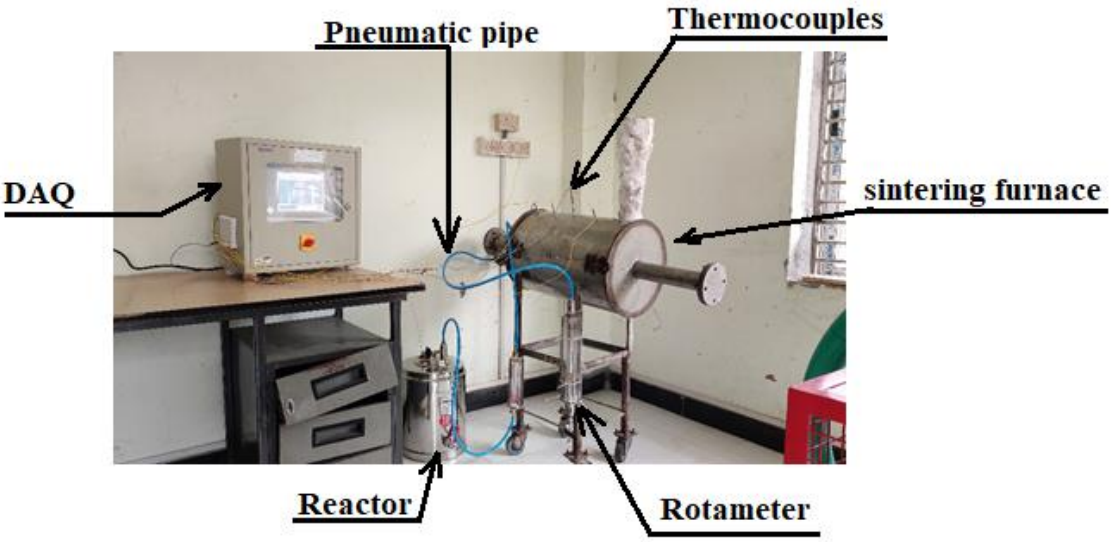

Fig. 3.5 Photograph of the sintering furnace test rig

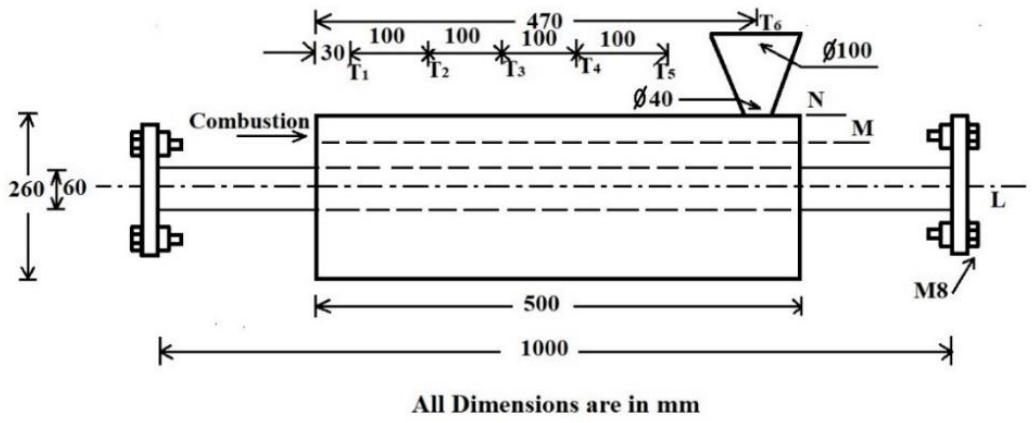

Fig.3.6 Schematic diagram of the sintering tube furnace with thermocouples position and chimney

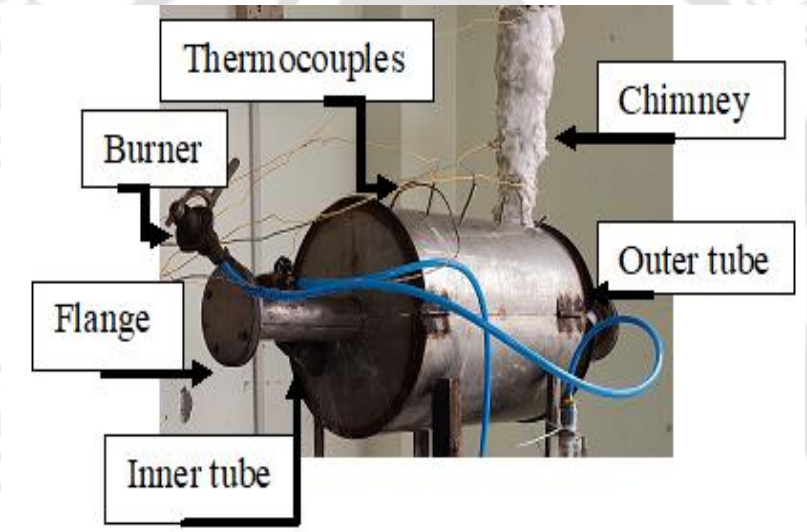

Fig. 3.7 Photograph of the sintering tube furnace with thermocouples position and chimney

Five thermocouples T_1 to T_5 were used to measure the temperature profile at distances 30 mm, 130 mm, 230 mm, 330 mm, and 430 mm from the gas inlet of the outer cylinder of the combustion chamber as depicted in fig. 3.6. During the flow of the hot gas mixture through the annular space, the temperature profiles along three lines were measured using these thermocouples placed at same distances from the gas inlet end. These are: (i) along the centre line of the inner tube, shown by line L (ii) centre line of the annular space between the two cylinders, shown by line M, and (iii) the outside surface of the outer cylinder, shown by line N. In addition, the temperature at the gas outlet was measured using the thermocouple T_6 placed at the top of the chimney. Separate experiments were carried out at the same conditions

of hydrogen gas generation and fuel-air ratio to measure the temperature profiles along these lines. The temperature of the variation along the radial direction of the combustion chamber near the inlet side was also measured.

3.6.2 Experimental procedures for determination of thermal efficiency of the furnace

The experimental procedure consists of two parts: (i) determination of the hydrogen generation rate due to the chemical reaction between aluminium and aq. NaOH solution and (ii) determination of the thermal efficiency of the sintering tube furnace due to the heat generated by the combustion of hydrogen produced by the above chemical method in the presence of air. In the former, experiments were carried out by reacting aq. NaOH solution with Al pellets at various combinations of temperature and concentration of the aq. NaOH and determined the condition of maximum hydrogen yield. While in the latter, keeping the same condition of maximality of H_2 production, the combustion of hydrogen was carried out at different fuel-air ratios and the efficiency of the furnace for these conditions was determined.

The fuel-air mixture at a definite proportion is combusted in the burner. The burner with the flame is then introduced at the inlet of the furnace and is allowed to flow parallel through annular space. The experiments were carried out at 7 different fuel-air ratios as mentioned in Table 3.2. The time-dependent temperature was recorded using the DAQ, from the instance the flame was introduced into the combustion chamber. Initially, the temperature profile along the three lines as mentioned in section 3.6.1 was taken. However, since later it was evident that the temperature along line M was representing the average temperature, the readings for Sl. nos. 5-7 in Table 3.2 were taken only along this line.

Stoichiometric fuel-air ratio (FAR_{stoic}) based on mass for H_2 and air is 1:34 [165][166]

Calculation of actual fuel-air ratio (FAR_{ac}) based on mass [167]

The volume flow rate for H_2 and air has been expressed in terms of mass flow rate ($kg.min^{-1}$) as described below. The fuel-air equivalent ratio (λ) is defined as the ratio of the actual fuel-air ratio (FAR_{ac}) to the stoichiometric fuel-air ratio (FAR_{stoic}).

For a volume flow rate of 10 lpm, taking the density of air as 1.225 $kg.m^{-3}$,

The mass flow rate of air $= \frac{10}{1000} \times 1.225 = 0.0125 \text{ kg. min}^{-1}$

For the volume flow rate of H_2 as 2.8 lpm, taking the density of hydrogen as 0.086 kg.m^{-3},

Table 3.2 Experiments carried out in the furnace

Expt. No.	Air flow rate (lpm)	H_2 flow rate (lpm)	Locations of the thermocouples along [*ref.* fig. 3.4]		
			Line L	Line M	Line N
1.	5	4	✓	✓	✓
2.	5	2.8	✓	✓	✓
3.	8	4	✓	✓	✓
4.	8	2.8	✓	✓	✓
5.	10	2.8	-	✓	-
6.	12	2.8	-	✓	-
7.	15	2.8	-	✓	-

The mass flow rate of H_2 = 0.0002 kg.min^{-1}.

Therefore, $$FAR_{ac} = 1:60 \qquad (3.23)$$

Hence, $$Equivalence\ ratio\ (\lambda) = \frac{FAR_{ac}}{FAR_{stoic}} = 0.57 \qquad (3.24)$$

Hydrogen fuel is more efficient for a lean mixture ($\lambda < 1$) than a rich mixture [96]. Similarly, the FAR_{ac} and the λ value have been estimated for the conditions of mass flow rates of H_2 and air as shown in Table 3.2.

The percentage thermal efficiency of the furnace is calculated for every set of experiments using the following equation:

$$\eta = \left[\frac{\text{Inlet temperature} - \text{Outlet temperature}}{\text{Inlet temperature}}\right] \times 100 \qquad (3.25)$$

The maximum thermal efficiency of the furnace for the flow rates of H_2 and air as mentioned in Table 3.2 is determined. The results of the experiments obtained are presented and discussed in detail in chapter 4.

3.7 Cost analysis

3.7.1 Break-Even Analysis (B/E analysis)

It is the most useful financial tool to be applicable in making investment decisions in Cost-Volume-Profit (CVP) analysis. It acts as a powerful technique in profit planning and control. The break-even analysis establishes a relationship between revenues and cost with respect to sales quantity. It allows knowing the level of sales at which point the revenues and cost coincide and that point is termed as Break-Even Point (BEP). At BEP total cost is equal to total revenues making it as no-profit, no-loss zone. Towards the right, it is profit zone and in left it is a loss zone. One assumption of this analysis is that the sum of variable cost (V.C.) and fixed cost (F.C.) always equals to total cost (T.C.). Two approaches exist to evaluate the BEP.

A. The formula approach
B. The chart approach

Both methods are employed here to tally the results.

3.7.2 Payback period

The Return On Investment (ROI) for any business is necessary for the growth and sustainability of the business. The ROI is expected to incur as early as possible. This is the amount of investment which when get back, the profit will follow. Hence, the estimation of the time of return is very essential. Payback period determines the time preferably in years for the ROI. Simple mathematics is employed to estimate the payback period as given below:

$$Payback\ period = \frac{Intial\ investment}{Cash\ flow\ per\ year} \qquad (3.26)$$

3.7.3 Depreciation accounting

The life of products decline with time. In financial systems depreciation accounting plays a vital role in deciding the life of an object. It may be defined as the value proposition decreases of a good for a particular time. Normally, it is calculated on per annum basis. A fix rate of depreciation per time is assigned to the products and the estimation is carried out to find the value of the product after a particular period. This is necessary to have an idea of replenish of the product.

3.7.4 Cost comparison of cooking using Electricity, LPG, and H_2 gas

The cost comparison of using the different modes of energy sources for household cooking purposes has been carried out. The modes of energy include in the present study are (a) electricity, (b) LPG, and (c) H_2 energy. 1 kg of water is heated from room temperature to 100 ^{o}C at 1atm by using the above mentioned sources of energy. The amount of energy consumed has been estimated and the cost was calculated for all the three modes of heating. Later, the costs are compared.

Chapter-4

Results and Discussion

The experimental procedures for the production of hydrogen gas from aluminium-water reaction in the presence of aq. NaOH solution adopted for the present study and the development of mathematical models for the reaction kinetics have been discussed in the previous chapter. This chapter presents the experimental results obtained, analysis of the results and discussions. Results of the modelling studies for the time dependent hydrogen generation experiments at different conditions *viz.*, constitutive modelling, MLR, BPNN and RBFNN have been presented and discussed in detail in subsequent sections.

4.1 Experimental results

4.1.1 Hydrogen yield

The hydrogen generation from Al-water reaction in the presence of aq. NaOH solution have been determined under different process conditions. The effect of temperature, the concentration of aq. NaOH solution, size of Al pellets, and volume of NaOH solution on the evolution of H_2 gas are studied. The stoichiometric yield of hydrogen gas is 1360 millilitres per gram of Al ($ml.g^{-1}Al$) [86]. The cumulative production of hydrogen gas at 5M/333 K after completion of reaction is found to be 1322 $ml.g^{-1}Al$ which is ~ 97 % of the theoretical yield. The relatively lower yield of H_2 gas than the stoichiometric yield obtained from the experiments can be attributed to the presence of a thin layer of aluminium oxide on the surface of the Al pellets and the possibility of presence of small amount of air in the reactor at the start of the reaction.

4.1.2 Mean hydrogen production at different temperatures and concentrations

Experiments for the conditions as mentioned in Table 3.1 were performed four times for repeatability. Since the amount of H_2 gas released were varying during each test, outliers were removed and the average of either two or three close readings were considered and plotted. Figures 4.1(a) – (d) depict the time dependent average hydrogen production at different conditions of temperatures and concentrations. All the curves depict initial faster rate of H_2 gas production. However, hydrogen gas release rate gradually decreases with time and almost gets

saturated. Table 4.1 presents the test conditions along with the time required to achieve 90 % of the total average yield of H_2 gas and the time taken to complete the reaction.

Table 4.1 Details of the average H_2 gas production from Al-H_2O reaction

Sl. No.	Test conditions	90% of the total average yield with maximum deviation (mol)	Time required to reach 90% yield (min.)	Overall average yield of H_2 (mol)	Time required to obtain overall yield (min.)	Overall average rate of production of H_2 ($mol.min^{-1}$)
1.	1M/303 K	$0.045^{\pm 11}$	360	0.05	940	5.3×10^{-5}
2.	2M/303 K	$0.046^{\pm 11}$	240	0.051	800	6.4×10^{-5}
3.	3M/303 K	$0.048^{\pm 11}$	168	0.053	300	1.8×10^{-4}
4.	4M/303 K	$0.048^{\pm 11}$	150	0.053	255	2.1×10^{-4}
5.	5M/303 K	$0.048^{\pm 10}$	111	0.053	190	2.8×10^{-4}
6.	1M/313 K	$0.043^{\pm 10}$	300	0.048	920	5.2×10^{-5}
7.	2M/313 K	$0.046^{\pm 10}$	234	0.051	780	6.5×10^{-5}
8.	3M/313 K	$0.045^{\pm 11}$	120	0.05	255	1.9×10^{-4}
9.	4M/313 K	$0.046^{\pm 11}$	105	0.051	190	2.7×10^{-4}
10.	5M/313 K	$0.047^{\pm 9}$	60	0.052	135	3.9×10^{-4}
11.	1M/323 K	$0.044^{\pm 12}$	240	0.049	840	5.8×10^{-5}
12.	2M/323 K	$0.045^{\pm 10}$	198	0.05	720	6.9×10^{-5}
13.	3M/323 K	$0.045^{\pm 11}$	35	0.05	90	5.6×10^{-4}
14.	4M/323 K	$0.046^{\pm 7}$	32	0.051	60	8.5×10^{-4}
15.	5M/323 K	$0.045^{\pm 6}$	22	0.05	50	1×10^{-3}
16.	1M/333K	$0.043^{\pm 10}$	190	0.048	840	5.7×10^{-5}
17.	2M/333 K	$0.045^{\pm 9}$	165	0.05	660	7.6×10^{-5}
18.	3M/333 K	$0.045^{\pm 6}$	33	0.05	75	6.7×10^{-4}
19.	4M/333 K	$0.045^{\pm 5}$	25	0.05	48	1×10^{-3}
20.	5M/333 K	$0.054^{\pm 5}$	31	0.06	45	1.3×10^{-3}

Figure 4.1 (a) reveals for the test condition 1M/303 K, $0.045^{\pm 11}$ mol *i.e.*, around 90 % of the total average yield of hydrogen in time 360 minute. The rate of evolution at this condition is indicated as 5.3×10^{-5} $mol.min^{-1}$ from Table 4.1. Similarly, fig. 4.1 (b)-(d) indicate the

average rate of production of H_2 gas as 6.5×10^{-5} mol.min^{-1}, 8.5×10^{-4} mol.min^{-1}, and 1.3×10^{-3} mol.min^{-1} for the test condition 2M/313 K, 4M/323 K, and 5M/333 K, respectively. The average rate of production of H_2 gas has been increased as the temperatures and concentrations are increased. In the present study, ± 12 % variation from the mean production of H_2 is considered satisfactory and hence, the average values of the results obtained have been accepted for the present analysis and modelling.

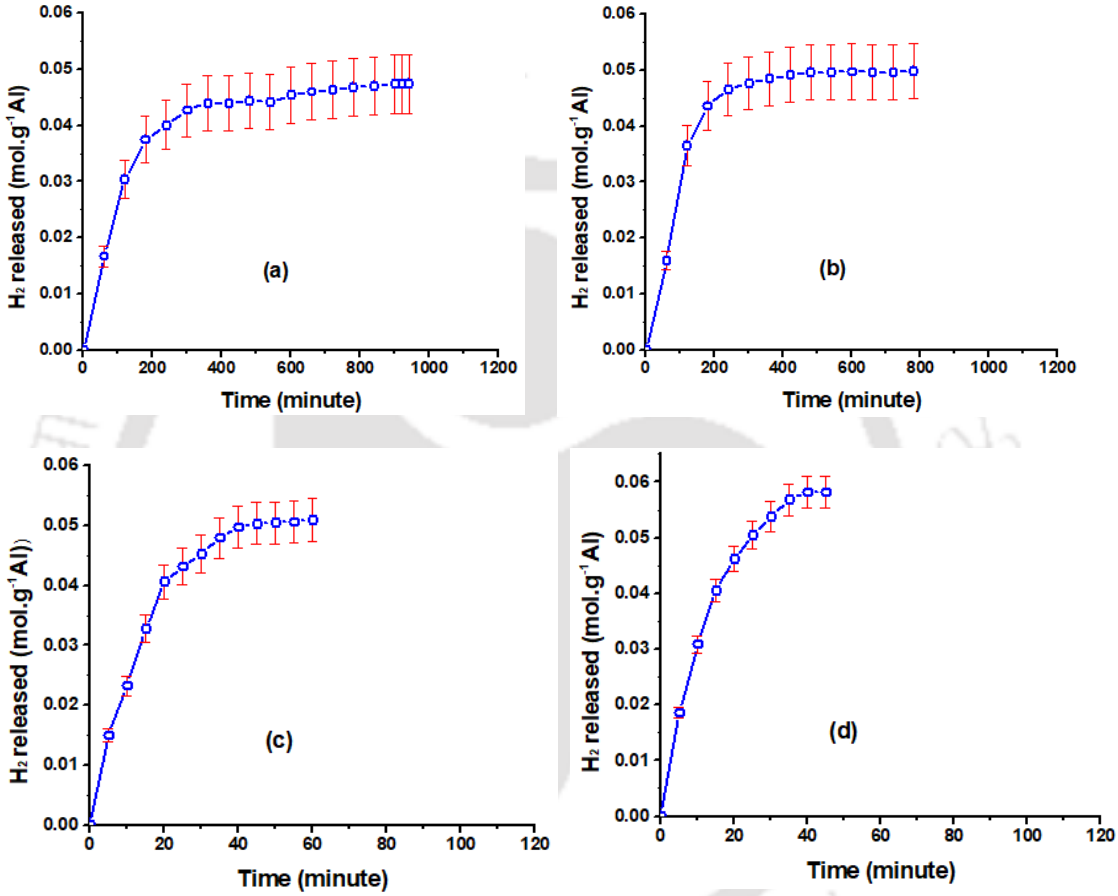

Fig. 4.1 Mean production of H_2 gas at (a) 1M/303 K, (b) 2M/313 K, (c) 4M/323 K, and (d) 5M/333 K

4.1.3 Hydrogen generation at different temperatures

The experiments were carried out with different concentrations of aq. NaOH solution with 1 gram of Al at various temperatures indicated in Table 3.1. The percentage yield of hydrogen gas at NaOH concentration of 4M and different temperatures are shown in Table 4.2. Figure 4.2 reveals that the overall yield of H_2 at different temperatures and 4M aq. NaOH varies between 80.32 % - 88.33 % of the theoretical value [64], [86]. *i.e.*, the H_2 gas yield at 333 K is 8 % higher compared to that at 303 K. The variation of H_2 yield with process temperature is attributed to either one or more of processing incapability, inadequacy in set-up design, the

nonexistence of an ideal work environment, inaccuracy in the measurement of the volume of H_2 released, and unassigned causes [168].

Table 4.2 Hydrogen yield at 4M aq. NaOH solution at different temperatures

Temperature (K)	H_2 yield per gram of Al (%)	Total production time (min)
303	80.32	255
313	83.33	190
323	85.00	60
333	88.33	48

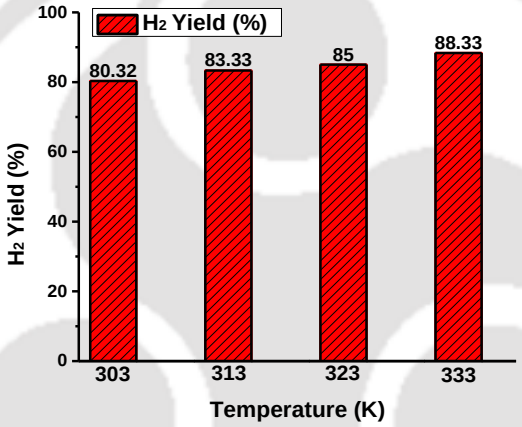

Fig. 4.2 H_2 yield at concentration 4M and for different initial water temperatures

The cumulative hydrogen production curves are plotted in figs. 4.3 (a)-(e) at different temperatures and concentrations. It is evident that the overall hydrogen production is dependent on the initial temperature of the aq. NaOH solution. The production of hydrogen gas at lower concentrations figs. 4.3 (a) - (c) is very slow. From fig. 4.4 it is revealed that the maximum yield of 97.23 % of the theoretical yield of hydrogen achieved at 5 M/333 K in 55 minutes. However, 90 % of this total maximum yield for the same condition is reached in 31 minute. For the test condition at 2M/313 K the time required for releasing maximum yield and 90 % of the maximum yield of hydrogen gas is 780 minute and 234 minute respectively. The results indicate longer time for achieving the maximum yield at lower temperatures. Although the rate of production is faster at the initial stage for the reactions at higher temperature, the total amount of hydrogen evolved is almost constant with ± 7.8 % variation between the test condition 1M/303 K and 1M/333 K. The same is obtained for the reaction 5M/303 K and

5M/333 K as ± 3.8 %.

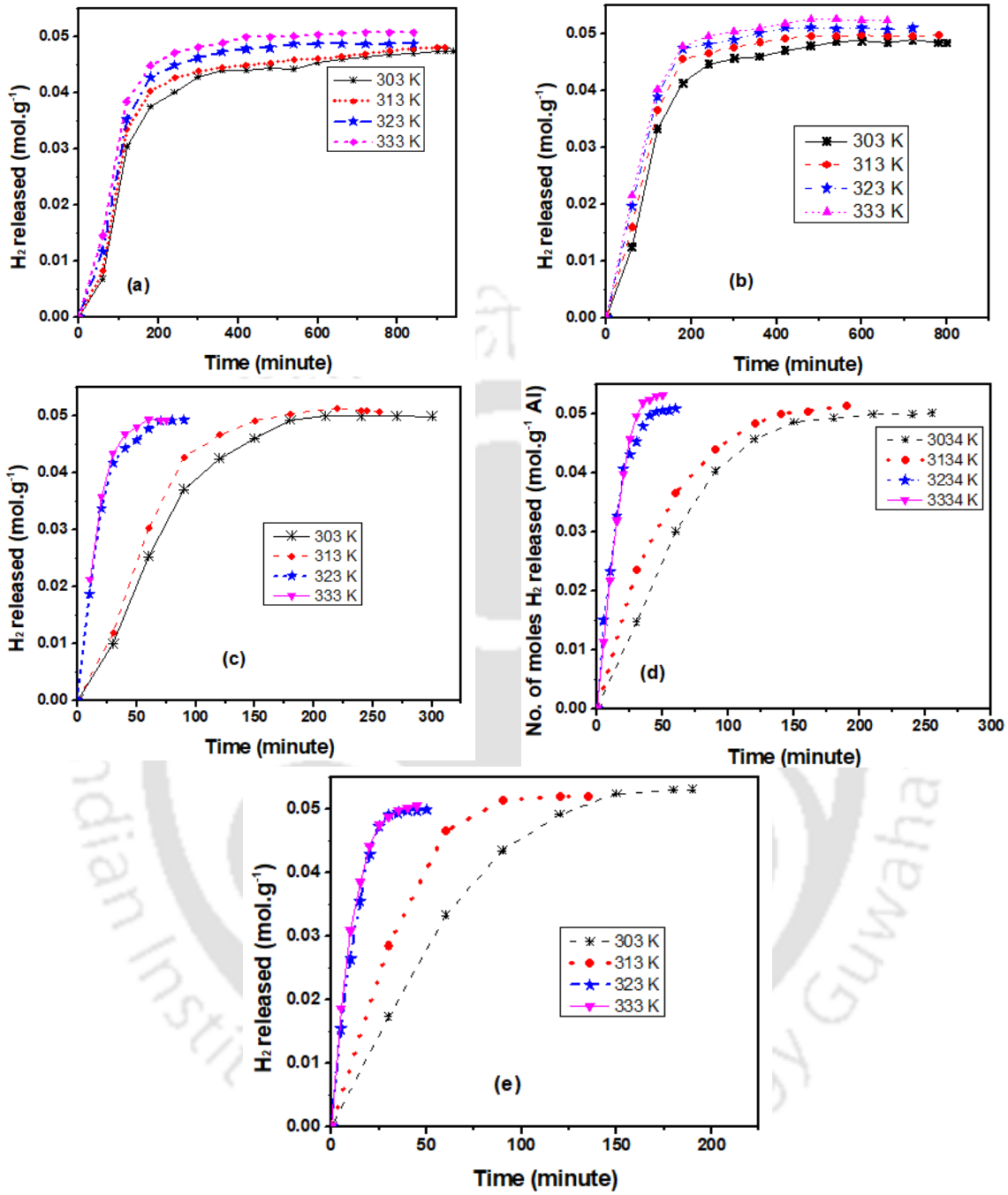

Fig. 4.3 H_2 production vs time at different temperatures and at aq. NaOH conc. (a) 1M, (b) 2M, (c) 3M, (d) 4M, and (e) 5M

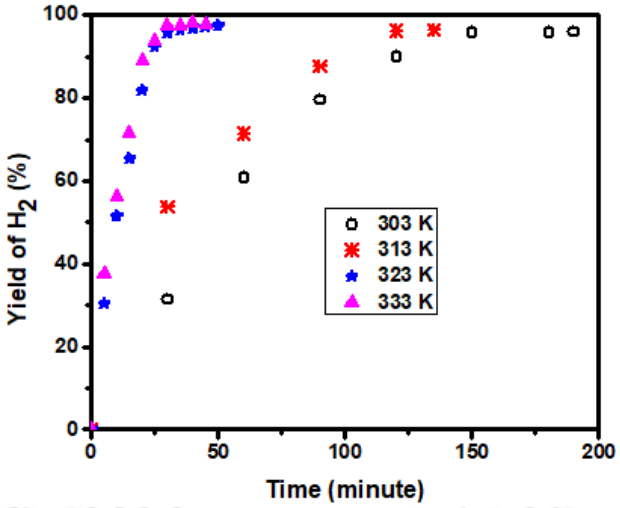

Fig. 4.4 Yield of H_2 vs time at different temperatures/5M

4.1.4 Hydrogen generation at different NaOH concentrations

The Al-water reaction system in the presence of aq. NaOH solution is dependent on the concentration of aq. NaOH solution. Figure 4.5 depicts the plot of the rate of production of hydrogen gas vs time at 323 K. The plot reveals very high increase in the rate of H_2 generation during the initial period. After achieving a maximum value, the rate tends to decrease with further increase in time. The maximum rate of production of hydrogen gas for 1M solution of aq. NaOH is 28.25 ml.min^{-1} which was achieved during a period of 10 minutes. The maximum rate of hydrogen generation increases to 52.03 ml.min^{-1} and 82 ml.min^{-1} within a period of 10 minutes and 5 minutes, respectively as the concentration is increased to 3M and 5M. The overall rate of production of H_2 gas for all the test conditions have been summarised in Table 4.1.

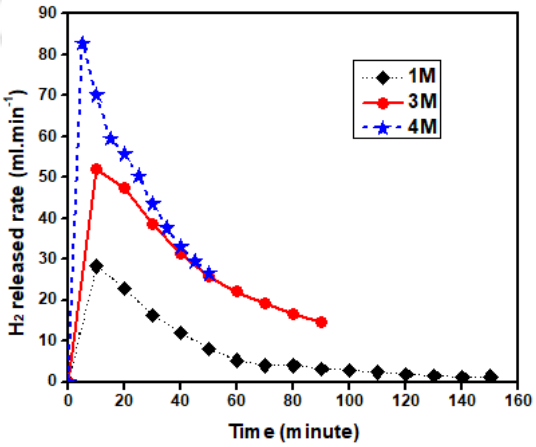

Fig. 4.5 H_2 release rate at 323 K

Figures 4.6 (a) - (d) indicate the evolution of H_2 gas for different concentration of aq. NaOH solution and at a particular temperature. The reaction rate is observed to be increased with the increase in the concentration of aq. NaOH solution. The rate of generation of H_2 initially, is monitored to be rapid for all the conditions. However, after attaining the maximum yield of H_2, the curves bent horizontally and the rate becomes very slow till the completion of the reaction.

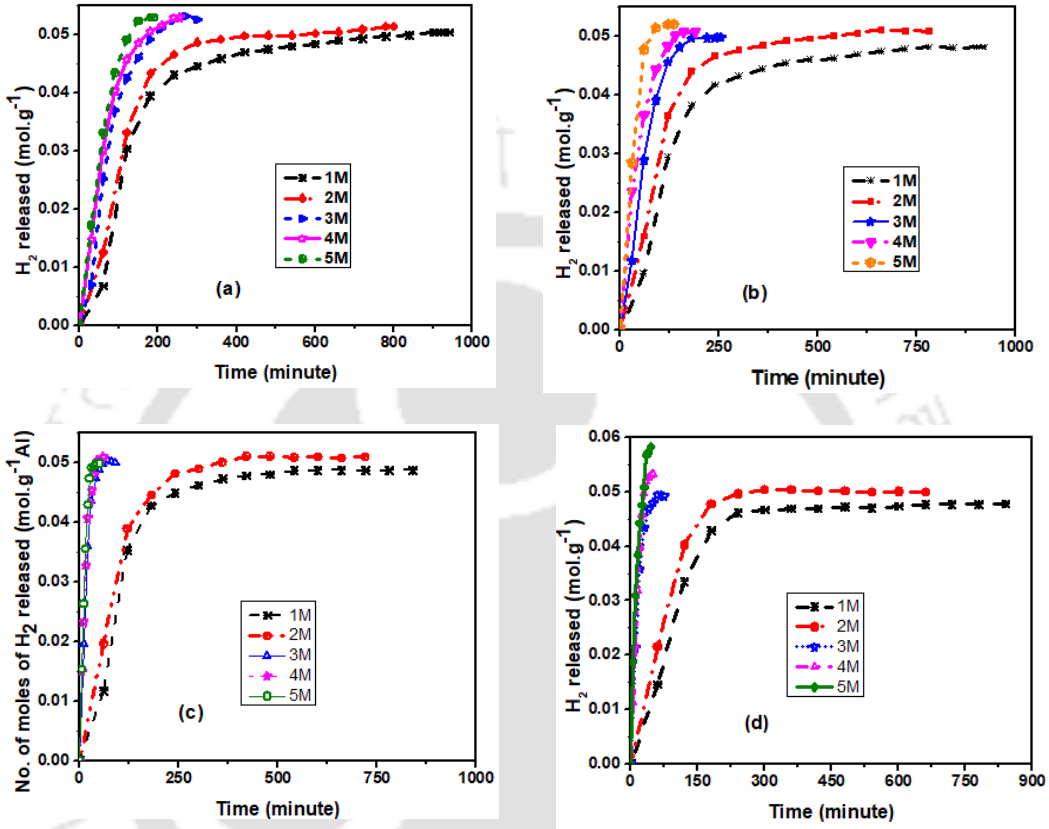

Fig. 4.6 H_2 production vs time for different concentrations of aq. NaOH at (a) 303K , (b) 313 K, (c) 323 K, and (d) 333 K

The maximum H_2 gas evolved at 303 K with NaOH concentrations of 1M, 3M, and 5M are 0.048 mol. g^{-1} Al, 0.051 mol. g^{-1} Al, and 0.052 mol. g^{-1} Al, respectively. The same are also determined for the temperatures at 313 K, 323 K, and 333 K. Figure 4.6 (b) reveals the yield of H_2 as 0.049 mol. g^{-1}, 0.052 mol. g^{-1} Al, and 0.053 mol. g^{-1} Al. The yield of H_2 for the concentration of 1M, 3M, and 5M at 333 K as evident from fig. 4.6 (d) are 0.052 mol. g^{-1} Al, 0.053 mol. g^{-1} Al, and 0.0582 mol. g^{-1} Al, respectively. The maximum yield of H_2 obtained as 97 % of the stoichiometric yield at 5M/333 K. It is revealed from the above discussions that with the rise in the concentration of aq. NaOH solution the reaction rate is faster and the yield of hydrogen gas is higher as well. The reason can be attributed to the amount of OH^- ions present in the reaction at the beginning are more [40], [60]. The ions dissolve the protective aluminium hydroxide layer on the Al surface. The reaction site in case of Al-water reaction is

the surface of the Al pellet. Thus, by eliminating the surface protective layer facilitates the reaction to occur without any hurdle. However, after some time the reaction attains a saturation level and the reaction slows down. This is due to the consumption of the OH^- ions during the reaction process and cannot further improve the surface of the Al pellets.

4.1.5 Effect of volume of water on hydrogen generation

The experiments are carried out firstly, with 100 ml of NaOH and secondly, with 200 ml of NaOH solution. The size of aluminium pellets used for both experiments is (25x25x1) mm and NaOH solution was prepared in distilled water. The overall yield of hydrogen gas is not affected by the volume of aq. NaOH solution significantly as indicated in figs. 4.7 (a) and (b). However, the initial rate of H_2 generation is affected by the volume of NaOH solution in the reactor. As depicted in fig. 4.7 (a) for 200 ml of solution, the initial rate of H_2 generation is 0.003 $mol.min^{-1}$ compared to 0.002 $mol.min^{-1}$ at 100 ml. The same has been observed in fig. 4.7 (b) to be 0.005 $mol.min^{-1}$ for 200 ml compared to 0.003 $mol.min^{-1}$ at 100 ml. The initial faster rate of production of hydrogen gas with a higher volume of NaOH solution can be attributed to the higher collision frequency of large numbers of water molecules with the aluminium. However, as soon as the protective aluminium hydroxide layer is formed over Al pellets, the contact of water and Al is lost, and slower production rate results.

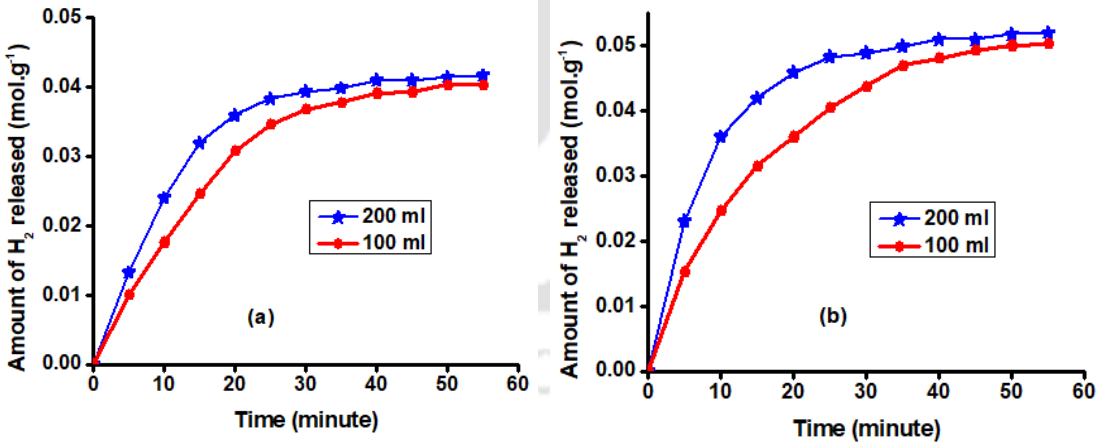

Fig. 4.7 Plot of H_2 gas released vs time at (a) 3M/333 K and (b) 5M/323 K for different volumes of solution in the reactor

4.1.6 Effects of the size of Al pellets

The effect of the size of Al pellets on the production of H_2 gas has been investigated. Two different sizes of Al pellets *viz*. dimensions L×B×H (in mm) of 25×25×1 (area 625 mm^2) and

25×37.5×1 (area 937.5 mm^2) are used in the reaction maintaining the same volume. The reactions are carried out at 4M/333 K and 5M/323 K. Figures 4.8 (a) and (b) show the hydrogen generation plot for the two different sizes of Al pellets. As revealed from fig. 4.8 (a), the rate of production of H_2 gas for smaller and bigger pellets are 0.003 $mol.g^{-1}.min^{-1}$ and 0.002 $mol.g^{-1}.min^{-1}$, respectively. Figure 4.8 (b) reveals the same as 0.004 $mol.g^{-1}.min^{-1}$ and 0.003 $mol.g^{-1}.min^{-1}$, respectively. The pellets with lower surface area per unit volume react with aq. NaOH at a much faster rate compared to the pellets with higher surface area per unit volume. This is mainly due to the higher contact area between the Al pellets and the aq. NaOH solution in the case of small-sized pellets [87]. The overall yield of hydrogen is found to be almost similar for both experiments. The slower rate of reaction for big-size particles can be attributed to higher incubation time for the water molecules to intervene in the Al pellets [169].

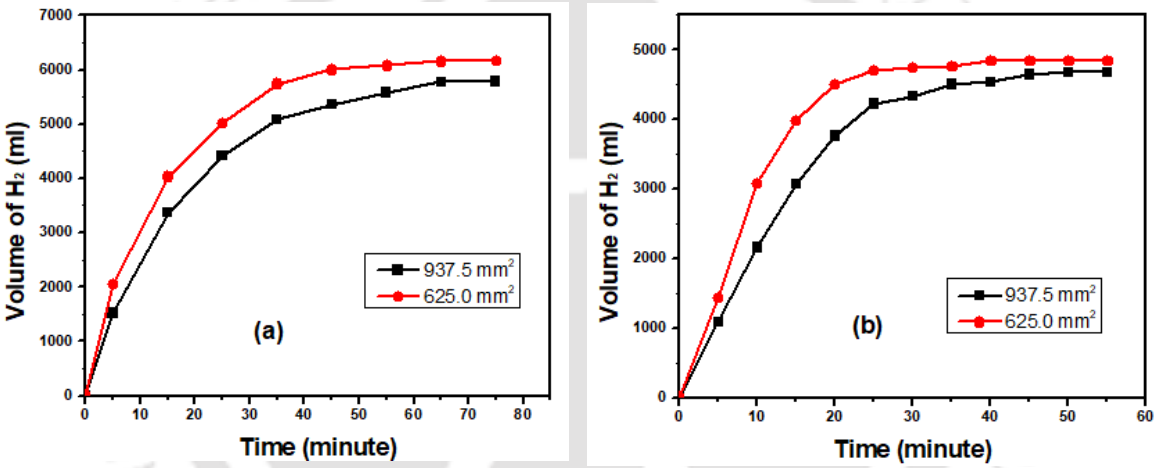

Fig. 4.8 H_2 gas released vs time for Al pellets with two different sizes at (a) 4 M/333 K and (b) 5M/323 K

4.1.7 Variation of hydrogen pressure

The overall pressure of the reaction follows the same trend as followed by the H_2 production curve. The reaction pressure increases with the increase in the concentration of aq. NaOH as well as the initial temperature of the reaction. Figures 4.9 (a) and (b) reveal that the pressure increases as the temperature of the reaction increases. Figure 4.9 (a) indicates that the pressure increases rapidly to 0.58 bar and 0.36 bar within a period of 5 minutes for the reaction temperature of 333 K and 323 K, respectively. Then after the reaction pressure increases with a decreasing rate and reaches an equilibrium in 25 minutes and 35 minutes, respectively. The maximum pressure attained are 1.01 bar and 0.82 bar, at 333 K and 323 K, respectively within a period of 65 minutes. Figure 4.9 (b) also depicts similar curves at 5 M concentration of aq.

NaOH with maximum pressure of 1.06 bar and 1.07 bar for temperatures of 323 K and 333 K, respectively within a period of 60 minutes.

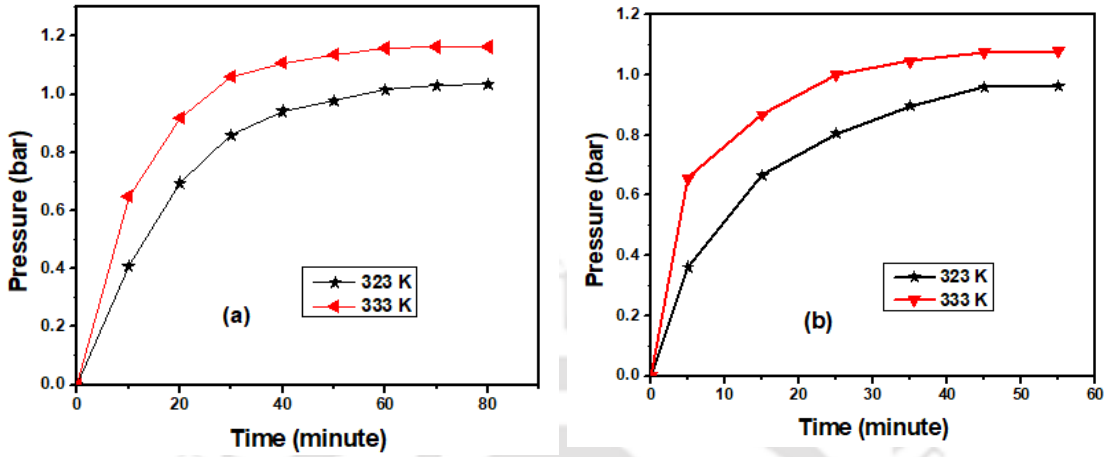

Fig. 4.9 Pressure vs time plot for aq. NaOH concentrations of (a) 4M and (b) 5M at different temperatures

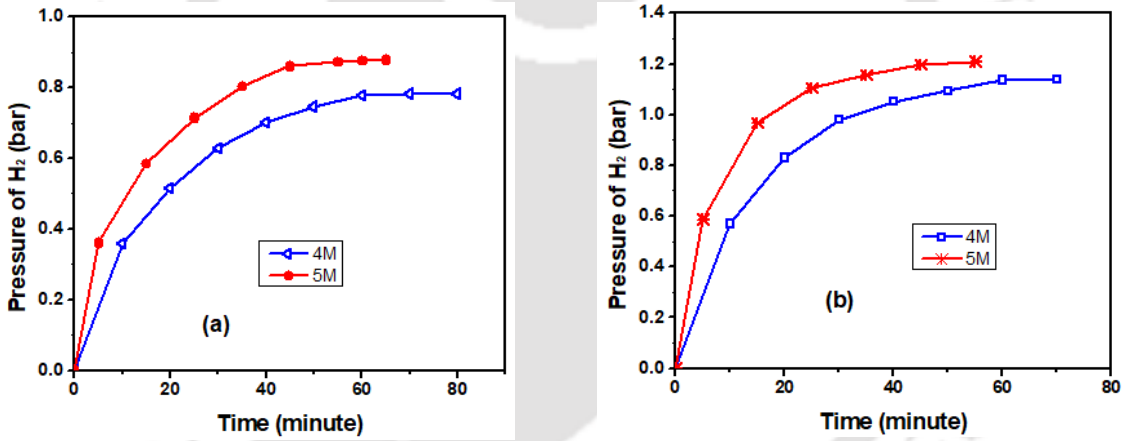

Fig. 4.10 Variation of pressure with time for different concentrations and at (a) 323 K, (b) 333 K

Figures 4.10 (a) and (b) indicate pressure vs time plot for temperatures of 323 K and 333 K at different concentrations of aq. NaOH, respectively. It is evident from figs. 4.10 (a) and (b) that the pressure rises as the concentration of aq. NaOH solution increases. The rate of production of H_2 gas at higher concentration is higher as discussed in the previous section 4.1.4. This can be attributed to the initial high pressure of the gas generated. Figure 4.10 (a) depicts maximum pressure of 0.88 bar and 0.78 bar at aq. NaOH concentrations of 5M and 4M, respectively within a time of 65 minutes and 80 minutes. The same is estimated from fig. 4.10 (b) and found to be 1.2 bar and 1.1 bar, respectively within a time of 55 minutes and 70 minutes.

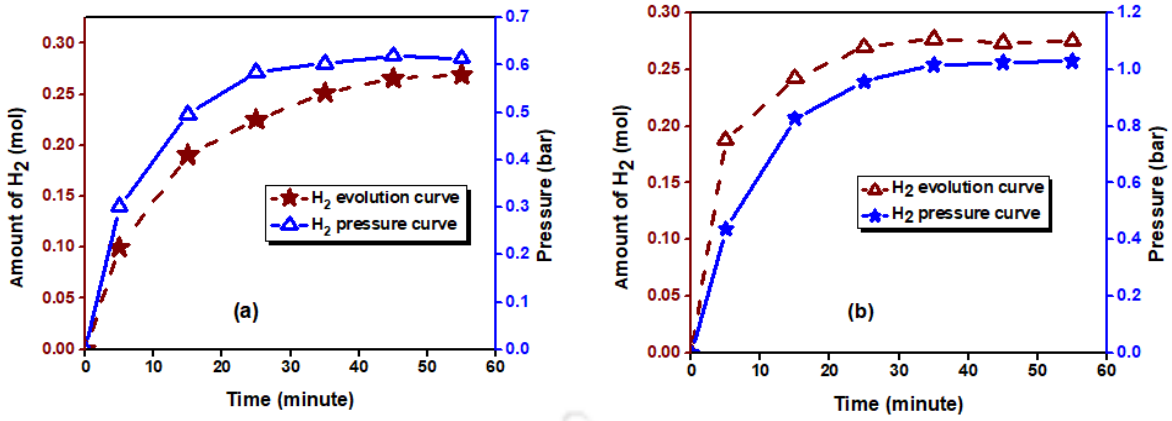

Fig. 4.11 Plot of H_2 evolved vs time for 5M solution at (a) 323 K and (b) 333 K

The pressure of the hydrogen gas during the reaction process increases as the amount of hydrogen gas increases. Initially, since the production of hydrogen gas is rapid, the pressure also develops rapidly as indicated in figs. 4.11 (a) and (b). Both the pressure curve and the H_2 evolution curve follow the same trend. A maximum amount of 0.26 mole of hydrogen gas corresponding to the maximum pressure of 0.61 bar in 55 min is observed in fig. 4.11 (a). Similarly, 0.28 mole of hydrogen gas have been obtained corresponding to the maximum pressure of 1.03 bar within the same time *i.e.*, 55 minutes as observed in fig. 4.11 (b).

4.1.8 Variation of pressure with the volume of NaOH

Figures 4.12 (a)-(f) depict the pressure variation during the evolution of H_2 gas with time for different volume of NaOH solution. The experiments are carried out at aq. NaOH solution of 3M, 4M, 5M and temperatures 323 K, 333 K. It is revealed from fig. 4.12 (a) the pressure rapidly increases to 0.34 bar in 10 minute in case of 200 ml solution whereas, during the same time interval pressure reaches to 0.17 bar for 100 ml solution. The pressure curves attain saturation after 50 minutes. The maximum pressure achieved for 200 ml and 100 ml solution are 0.65 bar and 0.63 bar at time 90 minute and 130 minute respectively. The gas pressure as indicated by fig. 4.12 (b) at an interval of 10 minutes are 0.50 bar and 0.28 bar for 200 ml and 100 ml solutions, respectively. Figure 4.12 (b) indicates the maximum pressures are 0.83 bar and 0.78 bar in 90 minute and 120 minute, respectively for 200 ml and 100 ml NaOH solution.

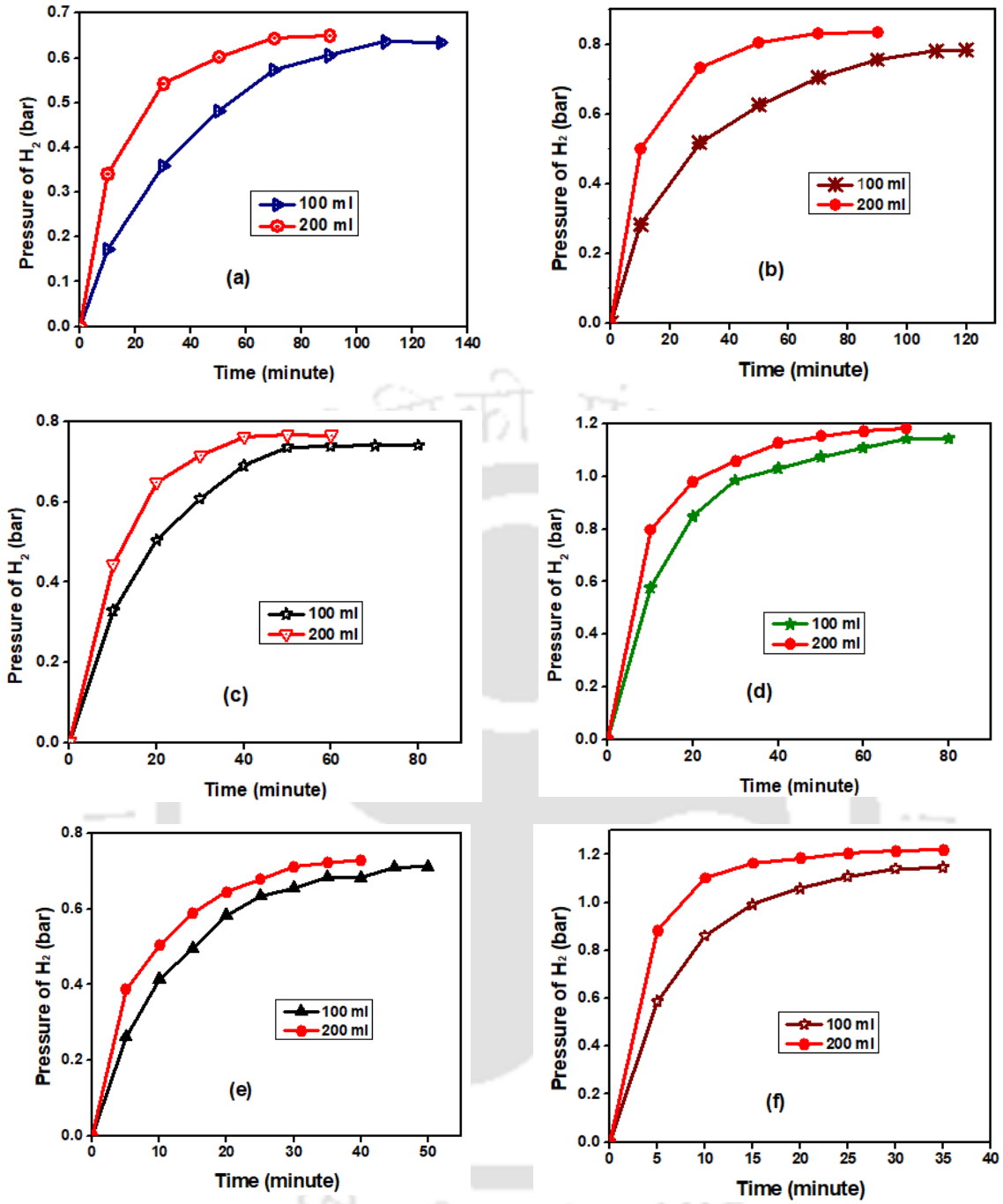

Fig. 4.12 Pressure vs time plot for different volume of NaOH solution at (a) 3M/323 K, (b) 3M/333 K, (c) 4M/323 K, (d) 4M/333 K, (e) 5M/323 K, and (f) 5M/333 K

It has been observed from fig. 4.12 (a)-(f) that pressure increases as the temperature and concentration increase. The fact of having higher pressure for higher volume of NaOH solution is attributed to the amount of hydroxide ion present is large for 200 ml of NaOH solution. Hydroxide ions destroy the barrier of the protective aluminum hydroxide layer and help in producing higher amount of hydrogen, consequently, the gas pressure is also high. As the reaction progresses, OH^- ions concentration decrease and the production of hydrogen gas reaches an equilibrium. As a result of that, hydrogen gas pressure is also stabilized.

4.1.9 Modeling of reaction kinetics

The kinetics of the chemical reaction between Al and aq. NaOH solution is important especially while developing a portable reactor. This is necessary since it provides insights into how fast reaction will proceed and how reaction conditions can be optimized for desired outcomes. The factors on which the kinetics of the reaction depends are: (a) concentration of the reactants, (b) reaction temperature, (c) presence of catalyst, if any and (d) the activation energy. The activation energy is defined as the minimum energy required for the chemical reaction to occur. In the present study aq. NaOH plays the role of a catalyst in the Al-water reaction and facilitates the reaction to occur. It is a known fact that as the concentration of aq. NaOH increases the activation energy drops so that the reaction can proceed easily. The rate equation relates the rate of the reaction to the concentrations of the reactants. Since the chemical reaction between Al and water is a first order reaction, the rate of the reaction is directly proportional to the concentration of aluminium. The constant of proportionality k is known as the rate constant. The rate constant can be expressed by the Arrhenius equation expressed by

$$k = A.e^{-E_{a/RT}} \qquad (4.1)$$

where, k is the rate constant in min^{-1}, A is the pre-exponential factor or collision frequency, R is the universal gas constant = 8.314 J K^{-1} mol^{-1} and T is the temperature (K).

The rate constants (k) at temperatures 303 K, 313 K, 323 K, and 333 K are found from the initial slope of the $ln[\frac{C_0}{C_t}]$ vs time (t) curve, shown in fig 4.13.

Determination of the rate constant (k)

The reaction between aluminium and water in the presence of aq. NaOH solution is given by equation no. (2.3) as discussed above and is given by

$$2Al + 6H_2O \xrightarrow{yields} 2Al(OH)_3 + 3H_2$$

As reported the volume of H_2 generated per gram of Al is 1360 cc. The initial volume of Al considered for the reaction is 0.37 cc.

At time t, let us assume *'x'* cc is the volume of H_2 generated which can be obtained from the experimental data sets. The volume of Al consumed to produce *'x'* cc of H_2 is estimated from the expression $\frac{0.37}{1360} \times x$ cc

For the first-order reaction, the differential rate equation is given by,

$$ln\left[\frac{C_t}{C_0}\right] = -kt \qquad (4.2)$$

$$\text{or,} \qquad ln\left[\frac{C_0}{C_t}\right] = kt \qquad (4.3)$$

where, C_0 is the initial volume of Al = 0.37 cc

C_t is the volume of unconsumed Al at time t = $0.37 - (consumed\ \text{Al})$

or, $= 0.37 - \frac{0.37}{1360}x$

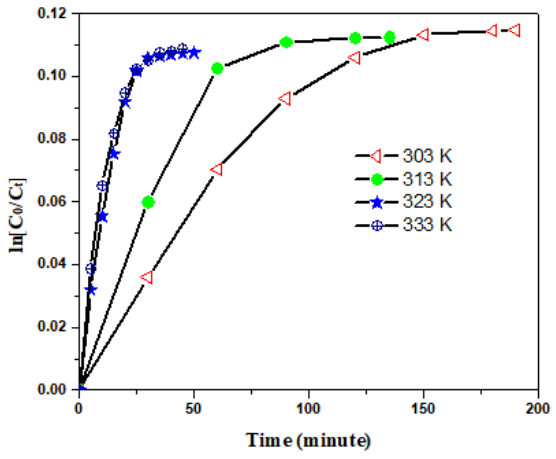

Fig. 4.13 Plot of $ln[\frac{C_0}{C_t}]$ vs t at different temperatures

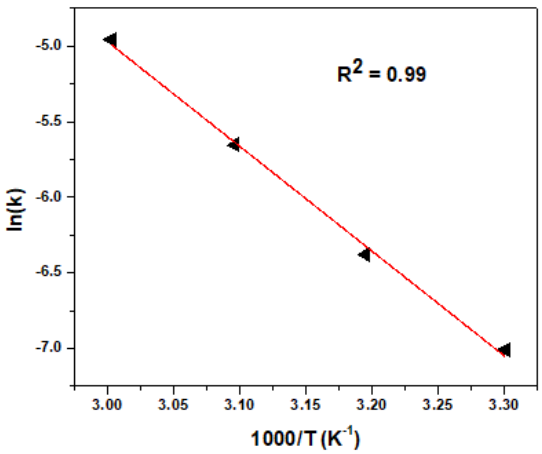

Fig. 4.14 ln(k) vs 1000/T plot

The activation energy of reaction is calculated from equation no. (4.1).

Taking logarithm on both sides

$$ln\,k = -\frac{E_a}{RT} + ln\,A \qquad (4.4)$$

$\frac{E_a}{R}$ is obtained from the slope of the line $ln\,k$ vs $1000/T$. From fig. 4.14 the value E_a is determined as 57.62 kJ.mol^{-1}. This value is very close to the value 53 kJ.mol^{-1} reported in the literature [84].

4.1.10 Activation energy for different sizes of Al pellets

The activation energy decreases as the size Al pellets decrease. Figure 4.15 illustrates the activation energy (E_a) vs area plot. In order to compare the activation energies for the different sizes of Al pellets the following pellets of sizes 925 mm^2, 1112.5 mm^2 and 3950 mm^2 were considered. From fig. 4.15 it is evaluated that the activation energy reduces from 78.21 kJ.mol^{-}

[1] to 57.62 kJ.mol^{-1} which is 26.33 % reduction as the area of Al pellets reduces from 3950 mm^2 to 925 mm^2 [7].

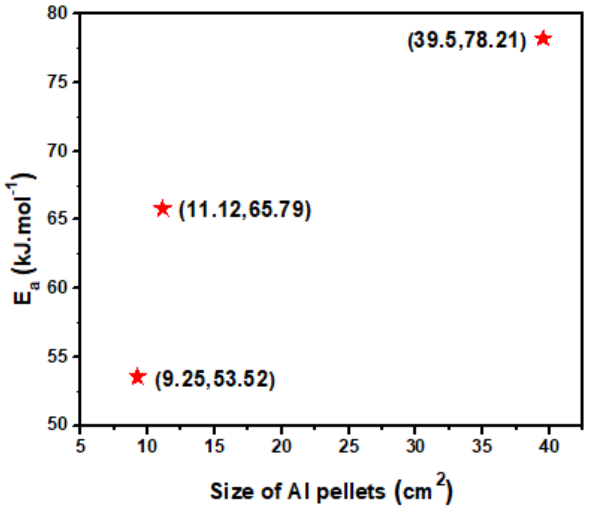

Fig. 4.15 Activation energy (E_a) vs size of Al pellets for Al-water reaction

4.2 Modelling by Machine Learning Techniques

4.2.1 Multiple Linear Regression Model

Multiple Linear Regression model is based on equation no. (3.13), *i.e.*, $V = GT^{\alpha}C^{\beta}t^{\gamma}$. The values of the constants G, α, β, and γ determined following the methodology mentioned in section 3.5.2 are 31.1906, 0.6304, 4.3717, and 0.4585, respectively. In order to authenticate the regression equation, the model was tested for the two conditions *viz*. (a) 5M/313 K, and (b) 3M/313 K as mentioned in Table 3.1. The data for these two conditions were not utilized during the regression model development. The H_2 gas evolved vs reaction time data simulated using the MLR equation is presented in fig. 4.16 along with the experimentally obtained curves. The values of R_{cc}, RMS error, and AARE % for the hydrogen generation curve as obtained by MLR at 5M/313 K are 0.84, 0.07, and 10.4 % respectively. The corresponding values at 3M/313 K are 0.89, 0.06, and 9.76 %. The values of R_{cc} and RMS error are acceptable. However, though the value of AARE % obtained during the simulation by the MLR technique is on the higher side, this can be accepted since AARE % error up to ~10 % is acceptable.

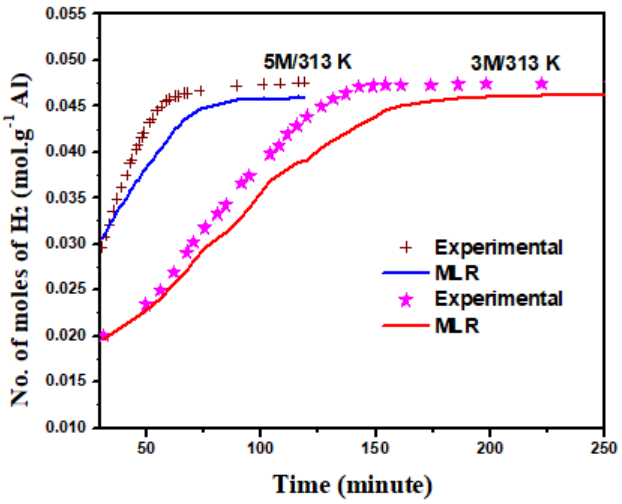

Fig. 4.16 Plots of MLR predicted and experimental cumulative volume generation of H_2 gas vs time for the two unknown conditions.

4.2.2 Feed forward back propagation neural network (BPNN)

BPNN architecture was arrived at by carrying out a number of experimental trials using the input-output data sets for training and testing simultaneously. This followed by validating network architecture using the validation data. Subsequently, the hydrogen generation data was simulated for the unknown conditions 2M/313 K and 3M/323 K. The results obtained are presented in the following sub-sections.

a) Training and Testing

The best neural architecture was arrived at by performing number of training and testing experiments simultaneously. The details regarding the training, testing and validation of the ANN architecture has been described in section 3.5.3. From the trial experiments, the best network architecture was obtained by using the *Tansig* transfer function at the input-hidden layer and *Purelin* at the hidden-output layer. The *tansig* function calculates the output by the expression.

$$Output\ of\ the\ neuron = \frac{e^{yz} - e^{-yz}}{e^{yz} + e^{-yz}} \qquad (4.5)$$

where, *z* is the net input to the neuron and *y* is a constant. *Purelin* function calculates output by the expression

$$Output\ of\ the\ neuron = yz \qquad (4.6)$$

The details regarding the best ANN architecture are shown in Table 4.3

Table 4.3 Details of the best ANN Architecture

No. of neurons in the input layer	3
No. of hidden layers	1
No. of neurons in the hidden layer	35
No. of neurons in the output layer	1
Processing function at the input hidden layer	*tansig*
Processing function at the hidden output layer	*purelin*
Error goal	0.00001

Figures 4.17 (a) and (b) show the plot of the experimental value of H_2 gas evolution vs ANN predicted values during the training and testing, respectively. A straight line is drawn from the origin at an angle of 45º to the horizontal axis. The points which lie on this straight line correspond to a perfect fit. Two lines corresponding to ± 5 % deviation error are also indicated in fig. Figure 4.17 (a) reveals that 333 points out of the 337 training data, which corresponds to 99.41 %, lie inside the ± 5 % error lines. The maximum deviation error of the ANN predicted data compared to the experimental data during the training process is 5.29 %. The correlation coefficient (R_{cc}), average absolute relative error (AARE) and RMS functional error during the training process are 0.99, 1.975, and 0.00014, respectively. The corresponding values during testing are 0.998, 1.377, and 0.00021 with a maximum deviation error of 6.27 %. During testing, 181 data points out of the 185 (*i.e.*, 97.8 %) is found to lie within the ± 5 % error lines.

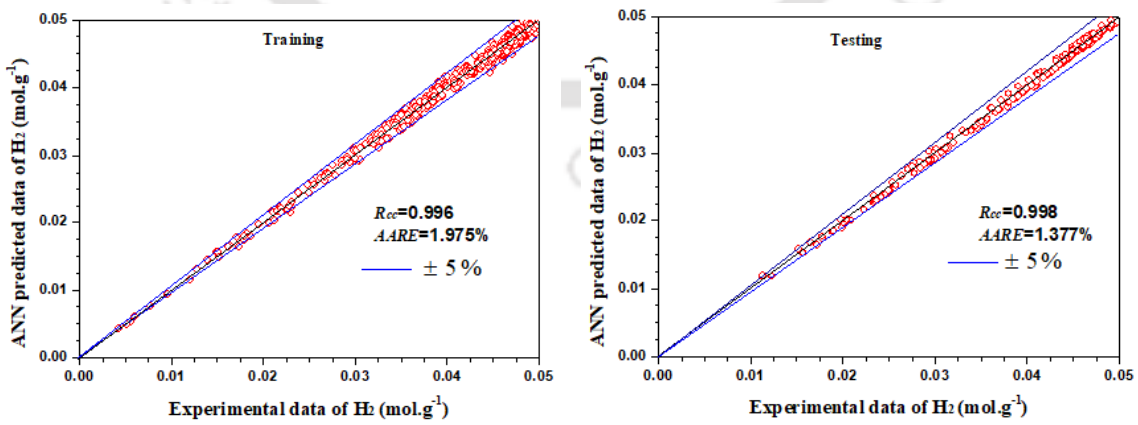

Fig. 4.17 The correlation between the experimental and ANN predicted data of the number of moles of hydrogen gas produced (a) after training and (b) after testing the neural network

Figures 4.18 (a) and (b) show the relative % error vs frequency count for the training and

testing, respectively. It is clear from the figures that the relative error is ± 6 % and ± 7 % for the training and testing, respectively. The relative % error indicates that 99.41 % of the simulated data lie within the ± 5 % error line for training and 97.8 % points lie within the ± 5 % error line for testing. Figures 4.19 (a) and (b) show the distribution of the ANN simulated data around the zero line (solid line in figures). The segregation of the data on both sides of the zero line indicates no systematic error in the ANN model. It also signifies the unbiased nature of the frozen ANN architecture. The main reason behind the principal error is the noise in the experimental data. However, it alone cannot be responsible fully for the predictive error of the model.

The relative importance of each of the input parameters to the output can be identified using the Garson algorithm given by equation no. (3.20). Figure 4.20 shows the relative importance of each of the input variables *viz.* temperature, concentration, and time on the production of hydrogen gas from Al water reaction in the presence of aq. NaOH solution. The share of the input variables ranges from 22.7 % to 37.5 %. The relative importance of 37.5 % indicates that the most influencing parameter for H_2 generation is the concentration of aq. NaOH solution. This is followed by temperature and time with relative importance of 29.7 % and 22.7 %, respectively.

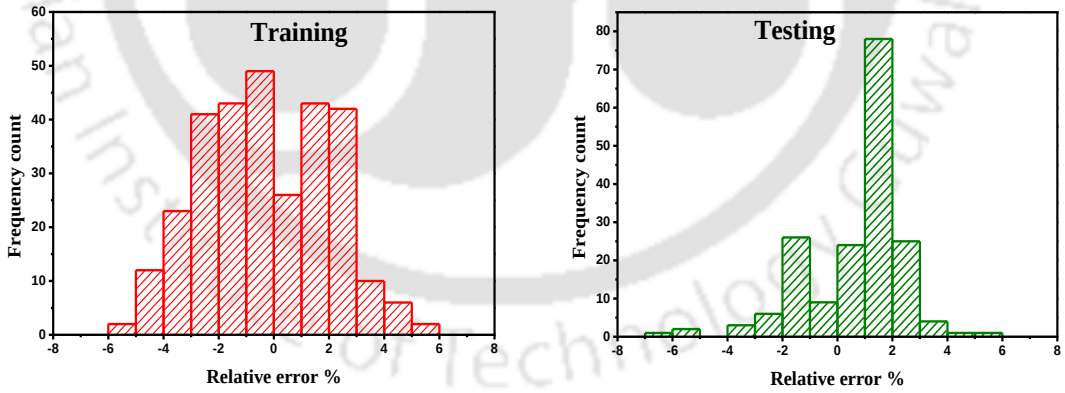

Fig. 4.18 The relative error between experimental and predicted data of the volume of hydrogen gas produced (a) after training and (b) after testing the neural network

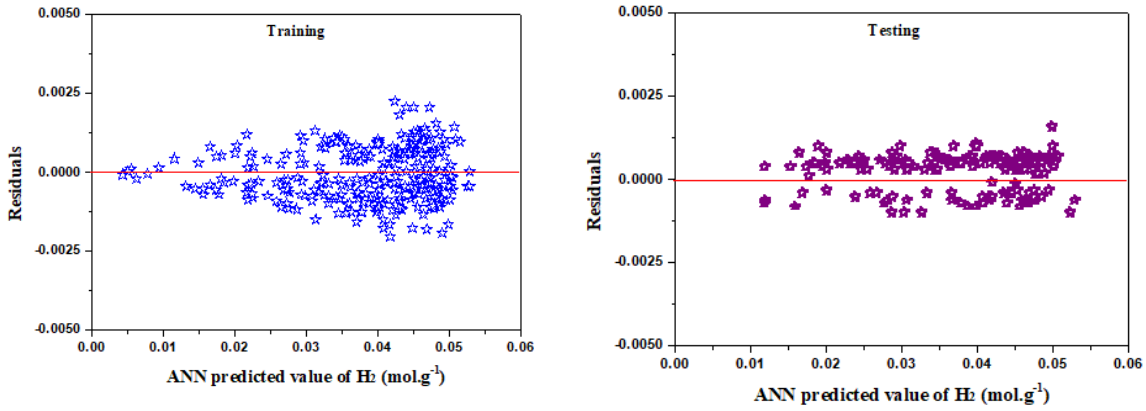

Fig. 4.19 Relation between residuals and ANN predicted data for (a) training and (b) testing of the neural network

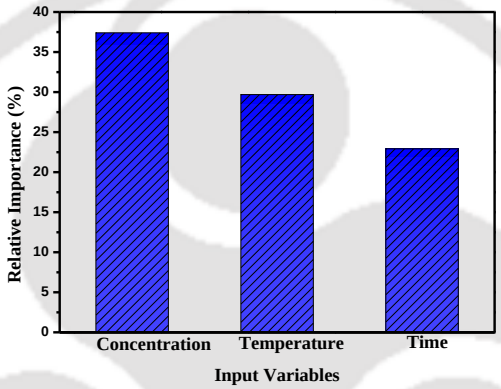

Fig. 4.20 The relative importance of the input parameters on the production of hydrogen gas to simulate the neural network using Garson's algorithm

b) Validation

The most suitable ANN architecture is frozen after successful training and testing. This architecture is used to validate the data which were not used during the training and testing phase. The curve between ANN predicted data and experimental data are plotted and shown in fig. 4.21 (a). Out of 91 data 89 data (97.8 %) lie within the $\pm$ 5 % line with a maximum deviation error of 4.44 %. The correlation coefficient (R_{cc}) and average absolute relative error (AARE) % are found to be 0.998 and 1.377 % respectively. Figure 4.21 (b) shows relative % error vs frequency count for the validation. It is clear from the figure that the relative % error varies from -4 % to +7 %. The residuals versus ANN predicted data are shown in fig. 4.21 (c). Having gained a confidence level of 95 % on the predictive capacity of the chosen ANN model, it is used to compare with the experimental data for the two unknown conditions *viz.* 2M/313 K and 3M/323 K.

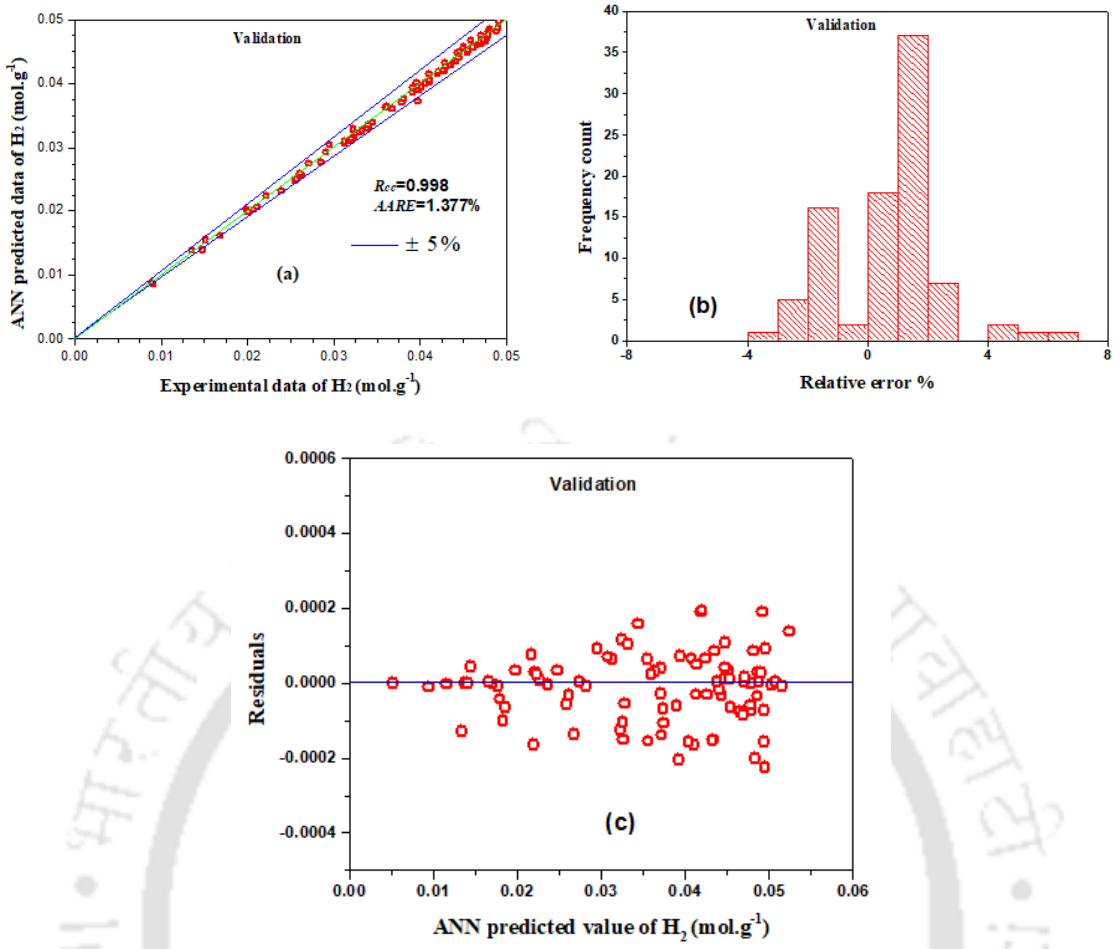

Fig. 4.21 (a) Correlation, (b) relative error between experimental and predicted data of hydrogen production, and (c) residuals versus ANN predicted data after validation

c) Simulation of H_2 generation by BPNN

The most suitable ANN architecture detailed in Table 4.3 is frozen. This frozen network is used to simulate the hydrogen generation for the conditions 2M/313 K and 3M/323 K. After the simulation the experiments were carried out for these two conditions to determine the time dependent H_2 gas generation by the chemical reaction. Figure 4.22 shows plot of cumulative H_2 released vs time during simulation for the above two conditions. It is indicating an almost perfect fit between the simulated data and original data. The values of the fitting parameters *viz*. R_{cc} and AARE % are shown in Table 4.4. From Table 4.4, it is observed that the values of R_{cc} and AARE vary in the range of 0.97-0.99 and 1.31-1.35 % respectively confirming the accurate predictability of the ANN architecture.

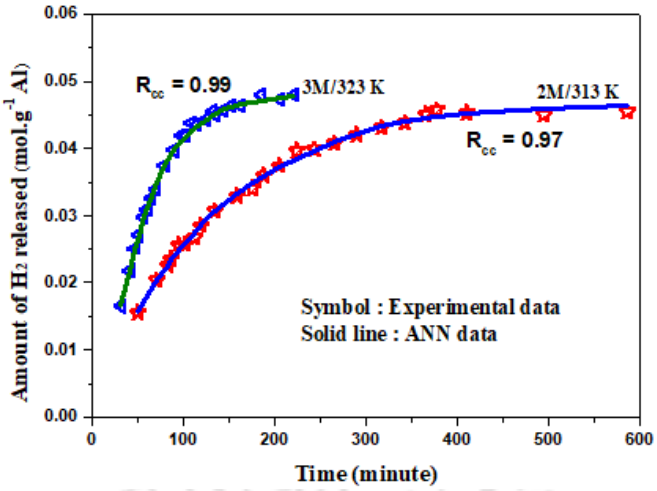

Fig. 4.22 Cumulative amount of H_2 released vs time during simulation

Table 4.4 Values of R_{cc}, and AARE % of the ANN predicted data correspond to the experimental data

Concentration (M)	Temperature (K)	R_{cc}	AARE (%)
3	323	0.99	1.31
2	313	0.97	1.35

To check the authenticity of the ANN architecture two sets of experiments were simulated and compared with the MLR simulation. The experimental conditions are 5M/323 K and 5M/303 K. Figure 4.23 shows the comparison among the curves obtained by experiment, ANN simulation, and MLR stimulation. It is clearly evident that the experimental curve and the ANN simulation are almost coinciding. However, the curve obtained by MLR simulation has deviated from the above two. The values of R_{cc} and AARE % between experimentally obtained graphs, the ANN, and the MLR predicted graphs for the above-mentioned experimental conditions are tabulated in Table 4.5. It is observed from Table 4.5 that the results predicted by the ANN model are almost the same as the experimental result with R_{cc} varying from 0.98-0.99. Whereas, the same is varying between 0.90-0.91 in the case of the MLR model. The results indicate that the ANN architecture is more accurate than the MLR model.

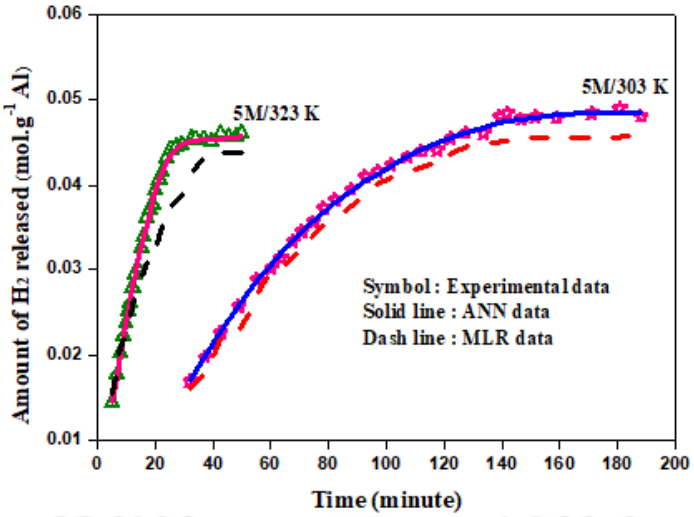

Fig. 4.23 Comparison of H_2 generation for experimental data, ANN simulation data, and MLR model

Table 4.5 Comparison of ANN and MLR model

Concentration (M)	Temperature (K)	ANN		MLR	
		R_{cc}	AARE %	R_{cc}	AARE %
5 M	323 K	0.99	1.37	0.90	0.08
5 M	303 K	0.98	1.33	0.91	0.06

4.2.3 Least square fit (LSF) method

The values of the constitutive parameters G, α, E_a, and β of equation no. 3.2, determined by the least square fit technique are listed in Table 4.6. Based on these values, hydrogen production was simulated for two unknown conditions of 2M/313 K, and 4M/323 K *i.e.*, these data were not used for determining the constitutive parameters.

Table 4.6 Values of unknown parameters for equation no. 3.2

G	α	E_a (kJ. mol^{-1})	β
30.3126	0.5439	57.1782	0.5014

The LSF predicted and experimentally obtained time-dependent data of H_2 liberation for the two unknown conditions are shown in figs. 4.24 (a) and (b). The simulated value of hydrogen generation is found to be slightly higher than the experimentally obtained values. The

correlation coefficient (R_{cc}) determined for the plots of predicted vs experimental values for 2M/313 K and 4M/323 K are 0.971 and 0.962, respectively. These values of the correlation coefficient indicate that the prediction of hydrogen gas by the LSF technique is reasonably satisfactory. Figures 4.25 (a) and (b) reveal the deviation of the predicted data from the mean line which is drawn at 45º to the horizontal axis. Figure 4.25 (a) implies that out of 28 data points 21 data points fall within ± 10 % line indicating 75 % points within the acceptance level of 90 %. The same is calculated in fig. (b) and found to be ~ 62 % of data points confined within the significance level of 90 %.

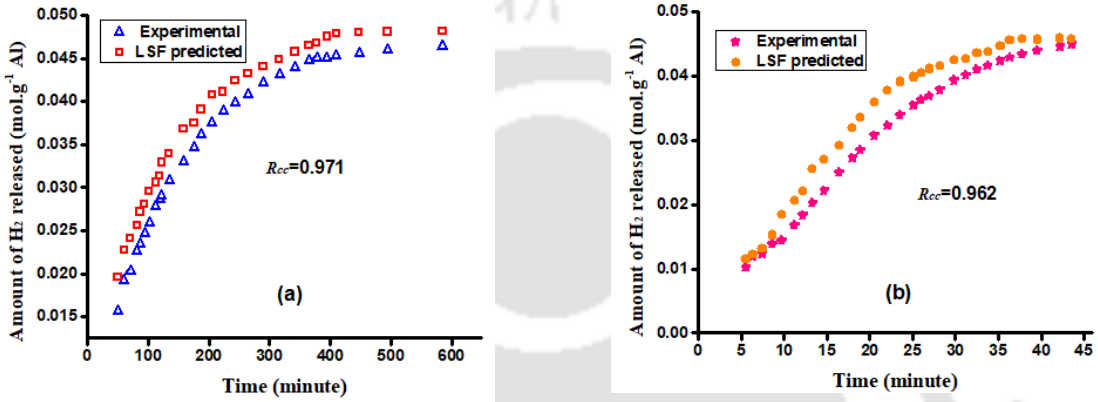

Fig. 4.24 Correlation between experimental data and LSF predicted value at (a) 2M/313 K, (b) 4M/323 K

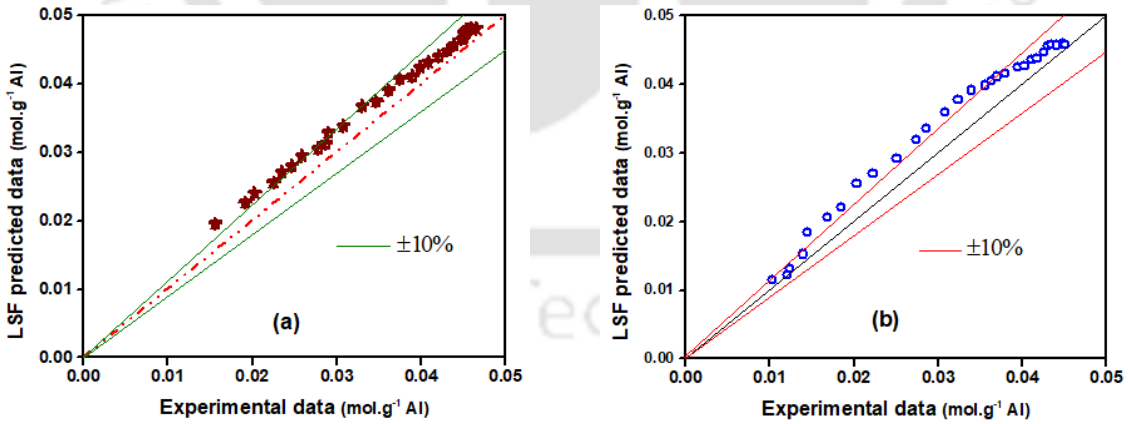

Fig. 4.25 The comparison between experimental data and LSF predicted data for the unknown conditions (a) 2M/313 K (b) 4M/323 K

4.2.4 Radial basis function neural network (RBFNN) technique

Modelling for the H_2 evolution during the chemical reaction was carried out as per the details mentioned in Table 3.1. Figures 4.26 (a) and (b) depict the correlation between the

experimental and RBFNN predicted data for the two unknown conditions: (a) 2M/313K and (b) 4M/323 K, respectively. A diagonal line at an angle of 45^0 is drawn as shown in fig. Another two lines representing ± 5 % deviation from the perfect fit line are also indicated in the figures. The data which fall on the 45^0 lines are considered to be a perfect fit whereas those data falling within the range of ± 5 % are considered to be highly acceptable. Figure 4.26 (a) indicates that only 2 out of the 34 data points for the 2M/313 K condition fall beyond a deviation error of ± 5 % *i.e.*, 94.1 % points are within the range of acceptance as shown. The coefficient of correlation R_{cc} and Absolute Average Relative Error % (AARE %) are found to be 0.991 and 1.91 % respectively. Similarly, from fig. 4.26 (b) it is revealed that for the 4M/323 K experimental condition only 3 out of 35 data points fall outside the ± 5 % deviation lines *i.e.*, 91.4% of data are within the range of acceptance. The corresponding values of R_{cc} and AARE % are found to be 0.99 and 1.49 % respectively, which also indicate very good simulation results. The above results indicate the high prediction capability of RBFNN for simulating the production of H_2 gas from the Al-H_2O reaction.

The plot of frequency count vs relative error % between the experimental data and RBFNN predicted data for the unknown condition of 4M/323 K is depicted in fig. 4.27. The overall relative error % varies from -4 % to +3 %. The standard deviation for the normal distribution of the data points is observed to be 0.889. Figures 4.28 (a) and (b) show the distribution of the residuals of the predicted data points around a central zero line for the experimental conditions of 2M/313 K and 4M/323 K, respectively. The uniform distribution of data around the zero line indicates the unbiasedness of the RBF neural network. The RBFNN predicted plot of the time-dependent hydrogen generation for the unknown conditions of (a) 4M/323 K and (b) 2M/313 K is plotted and compared with the data of H_2 obtained from subsequent experiments. It is shown in fig. 4.29 (a) and (b). The R_{cc} values of 0.999 and 0.991 indicate very good prediction capability by the RBFNN technique. The AARE % values are found to be 1.49 % and 1.91 % respectively.

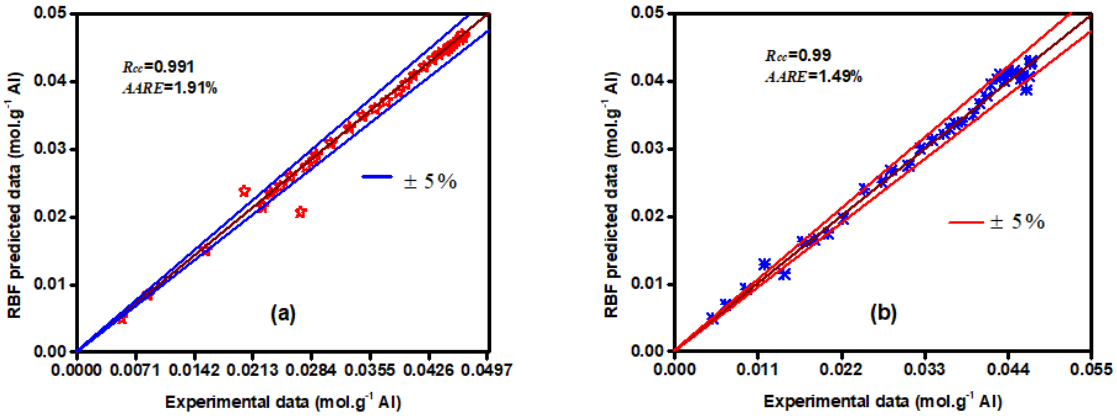

Fig. 4.26 The comparison between experimental data and RBFNN predicted data for the unknown conditions (a) 2M/313 K (b) 4M/323 K

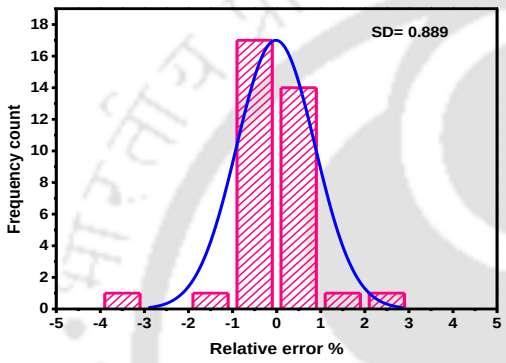

Fig. 4.27 Relative error between experimental data and RBFNN predicted data of H_2 production at 4M/323 K

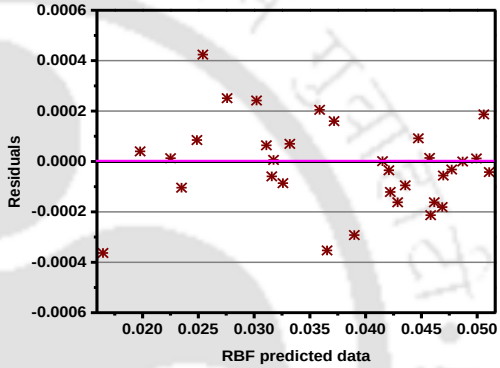

Fig. 4.28 (a) Plot between RBFNN predicted data and residuals at 2M/313 K

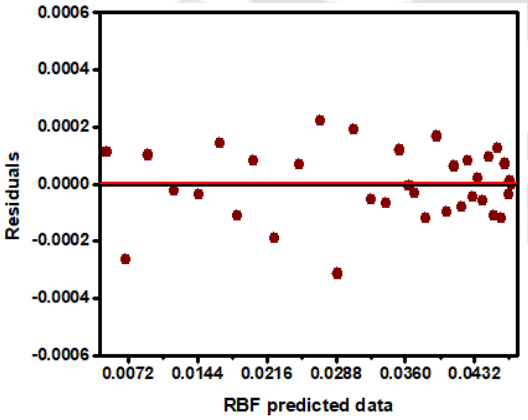

Fig. 4.28 (b) Plot between RBFNN predicted data and residuals at 4M/323K

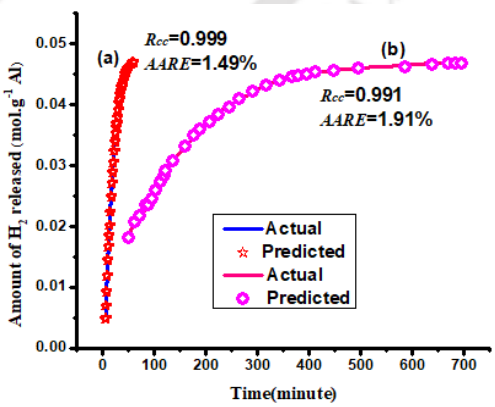

Fig. 4.29 Correlation between the experimental and RBFNN predicted data (a) 4M/323K and (b) 2M/313K

4.2.5 Comparison between Experimental, RBFNN and LSF

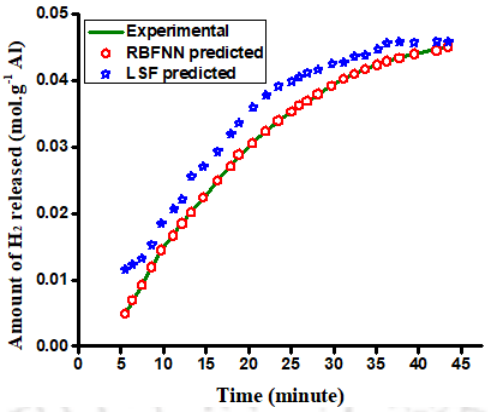

Fig. 4.30 Comparison plot among the experimental H_2 production data, RBFNN predicted, and LSF predicted data (4M/323 K)

The prediction accuracy of the two data-driven models *viz.* RBFNN and LSF for 4M/323 K are shown in fig. 4.30. The correlation coefficient (R_{cc}) for the experimental and RBFNN predicted data is given by 0.999 [fig. 4.29 plot (a)] and that of LSF is 0.962 [fig. 4.24 (b)]. The results indicate that the RBFNN model has better prediction capability in comparison to the LSF model.

4.3 Sintering tube furnace

4.3.1 Introduction

Hydrogen gas produced by the chemical reaction between Al and aq. NaOH solution is utilized on-board in a sintering tube furnace. The combustion of H_2 and air is carried out at different fuel-air ratios. The hot combustion product was used to heat a sintering furnace and the thermal efficiency of the furnace was determined for different fuel-air ratios. Since the maximum rate of hydrogen generation was achieved at 5M/333 K, this condition was used to generate the H_2 gas for the furnace efficiency study. In order to ascertain the viability of using H_2 gas for heating purpose, experiments were carried out using commercially available induction cooker, domestic kitchen stove using LPG as well as H_2 gas as fuel. The results of the comparative study for the time required for heating 1 kg of water using the above three energy sources as well as cost analysis are presented and discussed in the subsequent sections.

4.3.2 Temperature profile along the axial direction inside the sintering tube furnace

Hydrogen gas produced in the reactor and air supplied from the compressor is channelized to the gas burner where combustion of H_2 occurs. The hot combustion product is allowed to enter the inlet of the sintering furnace. The thermocouples T_1 to T_5 shown in fig. 3.3 measure the temperature of the hot gas at various locations which is recorded with the help of a DAQ. Thermocouple T_6 fixed over the chimney detects the exhaust gas temperature. The temperature vs time recorded by the thermocouples at different depths from the furnace surface, *i.e.*, along the lines L, M, and N in fig. 3.4 are depicted in figs. 4.31-4.33. The thermocouples T_1 to T_5 are attached to the surface of the furnace along line N whereas, they are placed inside the furnace along lines M and L as mentioned in section 3.6.1. The experiments are carried out with H_2 gas and air with flow rates of 0.0002 kg.min^{-1} and 0.012 kg.min^{-1}, respectively. The temperature profile obtained from thermocouples placed along the lines L and M as shown in fig. 4.31 and 4.32 can be distinguished from each other. However, as evident from fig. 4.33, the temperature profiles at the furnace surface (line N) are overlapping. It is necessary to maintain minimum loss across line N. The requirement for a sintering tube furnace is to have a minimum temperature gradient along the longitudinal axis of the furnace so that uniform heat is circulated inside the furnace chamber and at the same time have a large temperature gradient along the radial direction.

Figure 4.31 reveals that the gas temperature at the furnace entry (shown by T_1) remains almost constant at 543 K until around 9 minutes and then starts to increase at an average rate of around 6 K. min^{-1}. The temperature attains a maximum value of 603 K in 21 minutes and subsequently remains almost constant for the rest of the time. It is evident from fig. 4.32 that the temperature of T_1 at 17 minutes was 583 K and then started increasing at an average rate of around 5.2 K. min^{-1} to a maximum value of 635 K in the next 10 minutes. The outer surface temperature along the line N rises from ambient conditions to a maximum of 315 K as indicated by the thermocouples T_1 to T_5 in fig. 4.33.

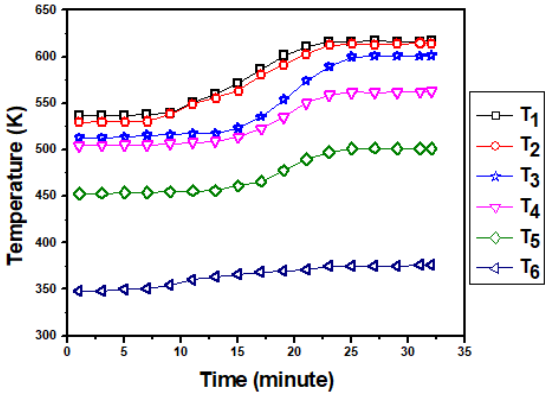

Fig. 4.31 Axial temperature distribution along the line L. The gas flow rate and airflow rate are 0.0002 kg/min and 0.012 kg/min respectively

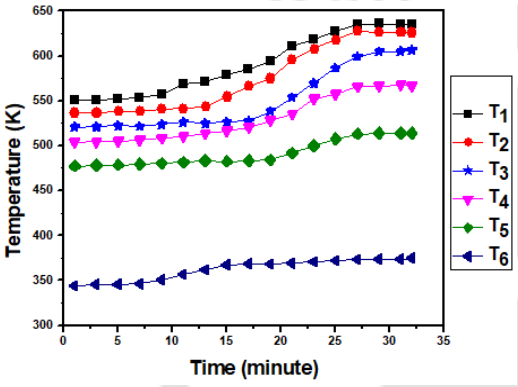

Fig. 4.32 Axial temperature distribution along the line M. The gas flow rate and airflow rate are 0.0002 kg/min and 0.012 kg/min respectively.

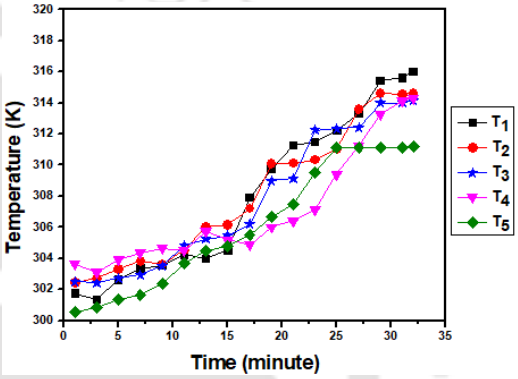

Fig. 4.33 Axial temperature distribution along the line N. The gas flow rate and airflow rate are 0.0002 kg/min and 0.012 kg/min respectively.

4.3.3 Radial temperature profile

Figure 4.34 reveals the radial temperature distribution at lines L, M, and N measured by the thermocouples placed at the same axial distance (thermocoupleT_3). The experimental condition is 0.0002 kg. min^{-1} of gas flow rate and 0.012 kg. min^{-1} of air flow rate. The experiment has been repeated three times with all the parameters kept constant. The temperatures measured were found to be varied within a range of ± 2 K for each repetition. The results of the radial temperature are summarised in Table 4.7 below.

Table 4.7 The average temperature obtained along the radial direction

Position of thermocouple	T_{max} (K)
Along line L	594
Along line M	606
Along line N	314

It is observed from Table 4.7 that the maximum temperature is obtained along line M. The reason is attributed to the fact that hot gas initially heated the annular region of the furnace by forced convection resulting in a higher heating rate. Furthermore, the inner pipe gets heated by convective heat transfer and conduction where the heating rate is comparatively lower than heating by forced convection. The heat loss to the surroundings is minimal due to the thermal insulation provided at the inside part of the outer cylinder. Hence, the remaining experiments to investigate the furnace efficiency at a fuel-air ratio (FAR_{ac}) of 1:60 are carried out by placing the thermocouples only along line M.

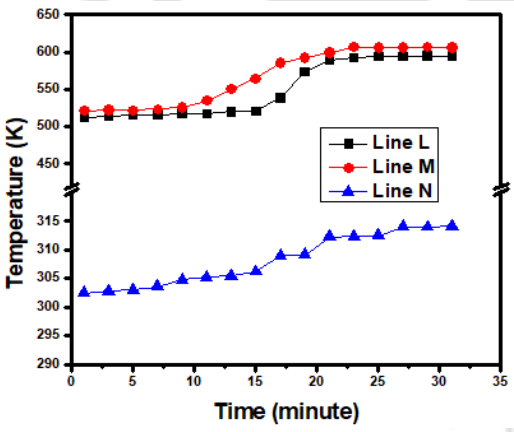

Fig. 4.34 Radial temperature distribution detected by T_3 along the lines L, M, and N for FAR_{ac} of 1:60

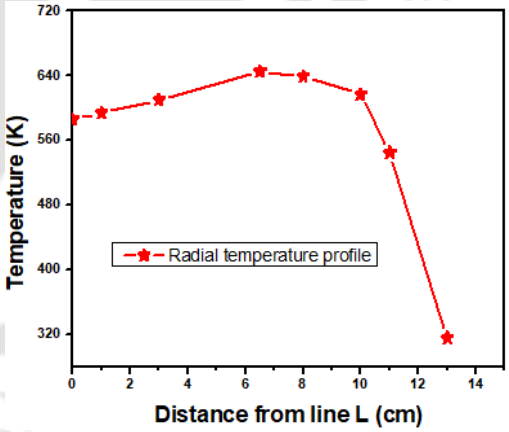

Fig. 4.35 Variation of temperature across the lines L and N at steady state measured by T_3

4.3.4 Radial temperature variation

For determining the steady-state radial temperature profile in the furnace, a separate experiment was carried out by placing an additional thermocouple at different radial distances from line L at the axial position of T_3. Figure 4.35 depicts the radial temperature distribution after achieving

the steady state condition. The temperature at the furnace centre line (*i.e.*, at line L) is 586 K and gradually increases towards line M. The maximum temperature of 646 K is obtained along line M. Thereafter, the temperature drops sharply towards the outer surface. The temperature gradient initially is slightly positive up to line M of the furnace which drops abruptly to the outer surface with a high gradient indicating very little amount of heat rejection to the surroundings thereby increasing the furnace efficiency.

4.3.5 Thermal efficiency

The thermal efficiency, using equation no. 3.25, of the hydrogen-fuelled furnace is calculated from the temperature data obtained for different FAR_{ac}. The efficiency obtained for different FAR_{ac} is tabulated in Table 4.8 and plotted in fig. 4.36. Maximum thermal efficiency of 76.22 % is obtained corresponds to FAR_{ac} =1:60 or in terms of flow rate, the best efficiency is obtained at 0.0002 kg. min^{-1} H_2 flow rate and 0.012 kg. min^{-1} air flow rate which corresponds to lean mixture $\lambda = 0.57$. At a lower value of λ (*i.e.* $\lambda < 0.57$), a shortage of fuel exists due to which excess air is present. Hence heat is lost by the unburnt part of the air resulting in lower energy density for combustion products. Further, the time of exposure of hot combustion products inside the furnace plays an important role in determining the thermal efficiency [170]. As this time is reduced due to the high air flow rate, the heat dissipation time reduces. Consequently, cooling increases and results in low thermal efficiency [171], [172]. The condition at $\lambda = 0.57$ corresponds to the stoichiometric H_2:O_2 ratio for combustion thereby providing a sufficient amount of air to burn the hydrogen completely. The heat generated is therefore effectively utilised inside the sintering tube furnace yielding high inlet gas temperature resulting in high thermal efficiency. The combustion of hydrogen is not completed at $\lambda > 0.57$ due to insufficient supply of air and consequently, the air temperature is not very high resulting in low thermal efficiency.

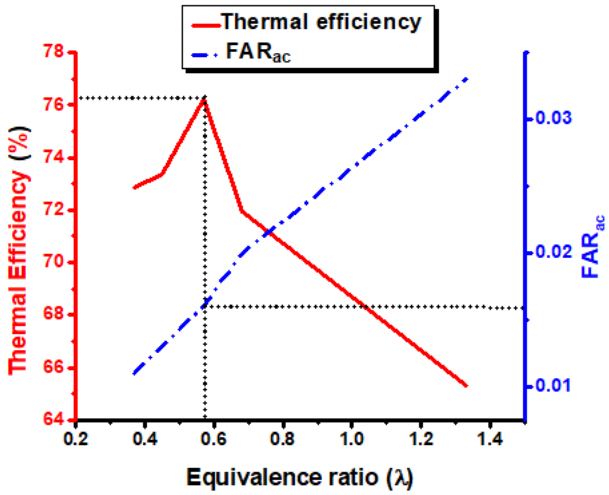

Fig 4.36 Plot of thermal efficiency vs λ and corresponding FAR_{ac} on the secondary axis

Table 4.8 Thermal efficiency of the furnace for various air flow rates and at the H_2 gas flow rate of 0.0002 kg. min^{-1}

Air flow rate (kg. min^{-1})	FAR_{ac}	λ	η (%)
0.006	1:30	1.13	65.30
0.010	1:50	0.68	71.92
0.012	1:60	0.57	76.22
0.015	1:75	0.45	73.34
0.018	1:90	0.37	72.89

4.4 Cost analysis

The socio-economic benefit of academic research whether scientific or humanities is always a prior goal. The various scholarly articles aimed at the development of the society, science and technology, and economic strengthening of any nation. It is very important to define research work in terms of time and economic benefit. Statistical tools are very useful to describe the financial aspect of the project or research work. Some of the tools are the Break-Even Analysis, the Net present value Method, the Return On Investment, the Payback Period Method, the Internal Rate of Return Method, *etc*. The proper distribution of capital is the most crucial in the modern financial management system. Cost estimation of the present work has been done to

have an idea of the economic viability of using hydrogen gas as a fuel. A cost comparison statement is also given among electricity, LPG, and hydrogen gas.

4.4.1 Break-Even Analysis (B/E analysis)

It is the most useful financial tool to be applicable in making investment decisions in cost-volume-profit (CVP) analysis. It acts as a powerful technique in profit planning and control. The break-even analysis establishes a relationship between revenues and cost with respect to sales quantity. It allows knowing the level of sales at which point the revenues and cost coincide and that point is termed as break-even point (BEP). At BEP total cost is equal to total revenues making it as no-profit, no-loss zone. Towards the right, it is profit zone and in left it is a loss zone as can be observed in fig. 4.37 below. One assumption of this analysis is that the sum of variable cost (V.C.) and fixed cost (F.C.) always equals to total cost (T.C.). Two approaches exist to evaluate the BEP.

C. The formula approach
D. The chart approach

Both methods are employed here to tally the results.

A. The analytical or formula approach

Estimation

It is found that the price of the H_2 cylinder is Rs 800.00 per 7 m^3. Hence, Rs 0.11 is the price of 1 liter of H_2. Based on the price of commercially available H_2 cylinder the following calculations are performed.

From the best result obtained in the experiment at 5M/333 K, we find

1 gram of Al produces = 1.3 liters of H_2

or, 50 gram of Al produces = 65 liters of H_2

Let us scale up to 100 times,

50 gram Al earns revenues = Rs 7.15

5 kg of Al earns revenues = Rs 715.00

Hence, a revenue of Rs 715.00 is obtained per unit (cylinder) hydrogen gas.

Variable cost (V.C.) = Rs 500.00 per unit hydrogen gas

Fixed cost (F.C.) = Rs 10,000.00

Therefore, BEP (units) = (F.C.)/(Revenue per unit- V.C. per unit) (4.7)

or, = 10,000.00/(715.00-500.00)

or, = 46.51 ≈ 47 units

BEP (Rupees) = (F.C.)/{1- (V.C. per unit/Revenue per unit)} (4.8)

or, = 10,000.00/{1- (500.00/715.00)}

or, = Rs 33,333.33

Assessment of payback period

Since, 50 grams Al is completely consumed in 55 minutes.

Hence, Time required to produce 1 unit of hydrogen gas *i.e.*, consumption of 5 kg of Al in 20 litres tank = 5500 minute

or, Time required to complete 47 units = 2,58,500 minute

or, = 0.5 years

or, = 6 months

Depreciation accounting

Let us assume a depreciation @ 5 % per annum (pa).

In 6 months it is anticipated to earn = Rs 33,333.33

or,1 month earning = Rs 5,555.55

@ 5 % depreciation pa, Rs 33,333.33 is reduced by = Rs 1666.67 pa

Hence, depreciation for 6 months = Rs 833.33

That means due to 5 % pa depreciation the amount has been earned after 6 months

= Rs (33,333.33 – 833.33) = Rs 32,500.00

or, = Rs 5416.67

Hence, the required payback period owed to 5 % pa depreciation for collecting the revenues of Rs 33,333.33 = Rs 33,333.33/5416.67

or, = 6.15 months

or, ≈ 6 months

B. The chart approach

The above BEP in terms of unit and rupees is also determined by the graphical method and the results are verified. Figure 4.37 represents the break-even analysis chart with various elements including the profit and loss zone. X-axis represents the number of cylinder of hydrogen produced and the in the Y-axis cost and revenues are plotted. It is seen that the variable cost line and the total cost line are parallel. The fixed cost line is parallel to the horizontal axis. The intersection of the revenues line and the total cost line is called the break-even point (*Q*). Two perpendicular lines are drawn from point Q to X-axis and Y-axis to indicate the break-even sale unit and break-even revenues. From the graph B/E sale unit is found to be 47 unit and B/E revenues is Rs 33,605.00. A difference of Rs 271.67 is found between the analytical and chart approach. The BEP unit is the same for the two methods though (refer to equation no. (4.7)). The difference in the BEP rupees is due to the consideration of the fractional value (46.51 units) in the case of the analytical approach whereas, in the graphical method the value is round up to the next integer *i.e.*, 47 units.

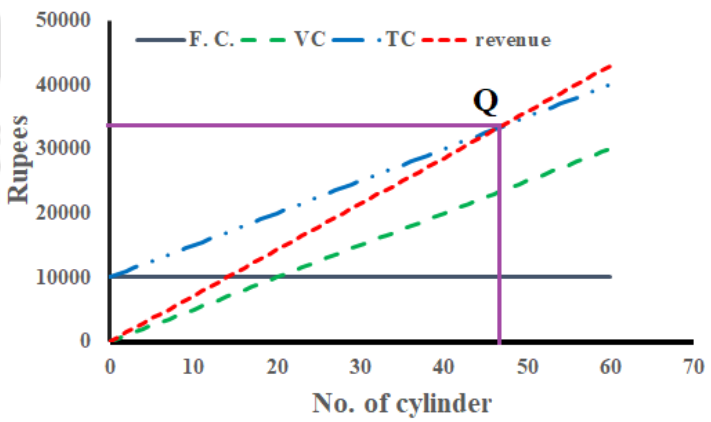

Fig. 4.37 Break-Even analysis of the hydrogen production set up

4.4.2 Comparison study among Electric energy, LPG and Hydrogen energy

The following discussions involve the monetary comparison study of cooking by electrical energy, traditional domestic gas for cooking (LPG), and cooking by hydrogen energy. For this

investigation, 1 kg of water has been considered and allowed to boil. The time requirement and the energy consumption to boil the water in each of the three cases have been evaluated and presented in terms of rupees. The case studies are described one by one below.

i) Estimation of the cost of electricity

Let us consider 1 kg of water at 25 °C. The amount of heat required to boil water at 100 °C

$H = mass\ of\ water \times specific\ heat\ of\ water \times \Delta T$ (T is the temperature in K)

$H = 1 \times 4186 \times 75 = 0.3\ MJ$

Suppose, the capacity of the electrical device is 1.2 kW

That is, 1200 J of energy is transferred = 1 s

or, 1 J of energy is transferred in = 1/1200 s

or, 0.3×10^6 J of energy is transferred in = $({}^{1}/_{1200} \times 0.3 \times 10^6)$ s

= 250 s ≈ 4 minute

Electrical energy consumed in 4 min. = $1.2\ kW \times {}^{4}/_{60}\ h = 0.08\ kWh \approx 0.1\ unit$

or, = $1.2\ kW \times (5/60)\ hr$

or, = 0.1 kWh

Assume, cost of electricity per unit = Rs 10.50

or, cost of 0.1 unit = Rs 1.1

ii) Estimation of cost of LPG

Suppose, daily consumption of LPG in household use be 7 hours on an average in a family consists of four members. Also it is assumed that a cylinder of mass 14.2 kg can sustain for 30 days. It is to be noted that a full LPG cylinder in India contains 14.2 kg of gas.

Therefore, in a month of 30 days, the consumption of LPG (in hour) = $7 \times 30 = 210\ h$

That means, in 210 hours the amount of LPG consumed = 14.2 kg

or, in 1 hour the amount of LPG consumed = 14.2/210 $kg.h^{-1}$

or, = 0.068 $kg.h^{-1}$

or, = 0.068/60 $kg.min^{-1}$

or, = 0.001 $kg.min^{-1}$

Water boils at 100 °C in 10 min. on LPG burner

Therefore, the consumption of LPG in 10 minutes $=0.001\ kg/min \times 10\ min$

or, = 0.01 kg

Consider, the price of a full LPG cylinder be Rs 1100.00

Hence, the price of 14.2 kg of LPG = Rs 1100.00

or, the price of 0.01 kg of LPG = $\frac{1100\times0.01}{14.2} = 0.77 \approx 80\ paisa$

iii) Estimation of the cost of hydrogen gas

The energy required to boil water at 100 °C, H = 3,13,950 J

= 0.3 MJ

Lower heating value of hydrogen = 120 MJ/kg [as in Appendix I]

120 MJ of heat is evolved from the complete combustion of = 1 kg H_2

or, 0.3 MJ of heat is evolved from the complete combustion of = 0.3/120 kg H_2

or, = 0.0025 kg H_2

or, = 0.003 kg H_2

Stoichiometric molar ratio of Al: H_2 = 1:1.5

= 27: 40.5

Market price of aluminium scrap per kg = Rs. 150

or, cost of 0.003 kg H_2 $= Rs\ 150 \left[\frac{(27 \times 0.003)}{40.5}\right] = Rs\ 0.3 = 30\ paisa$

The analysis of the cost estimation for electricity, LPG, and hydrogen gas has been found as Rs 1.10, 80 paisa, and 30 paisa respectively. Hence, hydrogen gas produced from aluminium scrap is an economic fuel for domestic cooking. However, it is highly inflammable and explosive. Extreme design of burner and precaution is mandatory for its wide application at houses.

Chapter-5

Conclusions and Future Scope

5.1 Conclusions

The present situation of the energy crisis and pollution occurred globally due to the consumption of fossil fuel is a burning issue to be addressed. The effort to reduce the polluting gases and particles in the atmosphere thereby, clean the environment is a novel process. Many nations and environmental organizations have tried to balance the environmental system by using green fuel. The study of new and renewable sources of energy has been an emerging area in the present day. A substantial amount of such new technologies have been developed from the last few decades. The hydrogen economy is a feasible technology in this regard. The environmentally friendly nature of the by-product of the combustion of hydrogen gas making it a suitable candidate for power generation. There are several methods for hydrogen production exist though, the chemical method is less costly and free from polluting gases. The production of hydrogen gas from Al scrap is a very economic method of production. Moreover, the barrier in the growth of hydrogen economy due to the storage and transportation is ruled out in the present study.

The on-board production and use of hydrogen gas in this research work turn into a novel approach. The study of reaction kinetics by using machine learning techniques to optimize the various parameters which affect the yield of hydrogen gas and the rate of production is another significant dimension in this work. The conclusions also incorporate the application base of hydrogen gas in a hydrogen-fuelled sintering tube furnace. In-situ hydrogen gas is burned inside the furnace and investigated the thermal efficiency at an optimum FAR. The statistical tool called the break-even analysis is employed to observe the cost-volume-profit relation of the production. Further, the economic aspect of the use of hydrogen gas for domestic cooking purposes is also elucidated.

5.1.1 Conclusions drawn from the present study

The conclusions of the thesis work have been listed below:

- A maximum yield of hydrogen gas through the chemical method is found to be ~ 97 % of the stoichiometric yield.
- As the concentration of aq. NaOH increases from 1M to 5M, a significant increase of ~ 44 % in the yield of H_2 is observed.
- The rate of chemical reaction between Al and water is affected by the size of the Al pellets. Fine pellets have shown a faster rate of reaction.
- Activation energy obtained from the Arrhenius plot is 57.62 kJ. mol^{-1}. The activation energy reduces from 78.21 $kJ.mol^{-1}$ to 57.62 $kJ.mol^{-1}$ which is 26.33 % reduction as the area of Al pellets reduces from 3950 mm^2 to 925 mm^2.
- Among the three input parameters *viz.* concentration, temperature, and time, concentration is found to be the most influential in the production of hydrogen gas. The corresponding values of influence of each parameter are 37.5 %, 29.7 %, and 22.67 %, respectively.
- The MLR model shows less correlation between the experimental result and the simulated result. R_{cc} varies from 0.90-0.91 and AARE % varies from 0.06-0.08 %.
- 98.61 % of data fall within the confidence level of 95 % for the ANN model. The values of R_{cc} and AARE % for the ANN model are in the range of 0.98-0.99 and 1.33-1.37 % respectively. Thus ANN model can predict the nature of the curve with high accuracy.
- The acceptability of the ANN model is higher than the MLR model for the prediction of the generation of hydrogen gas from Al-water reaction in the presence of aq. NaOH solution.
- Radial basis function neural network provides efficient prediction capability for real-time monitoring and control of H_2 generation by chemical method in industrial uses.
- Maximum thermal efficiency of the sintering tube furnace is 76.22 % corresponding to FAR_{ac} = 1:60.
- Hydrogen-induced sintering tube furnace is a sustainable energy system for many industrial applications.
- The analysis of the cost estimation for electricity, LPG, and hydrogen gas has been found as Rs 1.10, Rs 0.80 and Rs 0.30 respectively. Hydrogen gas produced from aluminium scrap is an economic fuel for domestic cooking.

5.2 Scope for future work

The concept of green technology is a new idea with lots of prospects. This field of research needs inclusive exploration to get rid of the dependency on fossil fuel. The environment benign nature of the waste product of green energy is significant to the environment. In connection with the present work, many scopes are awaited, which must be addressed. The thorough research includes the alternation of various parameters *e.g.*, the concentration of NaOH solution, temperature, morphology, size and shape of the raw metals, *etc.* The material characterization of the residue of the Al pellets can be carried out to acknowledge different phenomena. The appropriate alloying of Al with other metals can be a good source of hydrogen gas. In a nutshell, the technical development of the Al metal to be used in the reaction with water to produce hydrogen gas is a scope to extend the research. The effective treatment of the water is necessary because of the salt level present in the water. Water containing more salt particles are efficient to produce hydrogen from Al.

A well designed and fabricated hydrogen gas reactor is essential to generate hydrogen. A cylindrical reactor made of stainless steel with a thin inner liner of Teflon or such inert material can be effective in this regard. The primary importance is given to the non-diffusion nature of the setup material. The complete automation of the reactor is considered as the substantial development of the setup to satisfy the condition for the on-board application of hydrogen gas. The on-board application of hydrogen gas in the internal combustion engine is another incipient topic for research. Very few works have been reported in this area. The development of this technology can lead to a pollutant-free scenario with almost zero percentage of risk associated with the storage and transportation of hydrogen gas.

The economic and effective production of hydrogen gas is anticipated. The hydrogen economy is forced to stagnant due to the reluctance of the oil industries based on crude oil and Government agencies. The wide application of hydrogen gas needs a lot of technical modifications to the existing systems. Which incur lots of money of course. However, it is the mind-set and due to political misuse of power, the advancement of the new technologies is suppressed. Though hydrogen gas is green energy and can fulfil the criteria as a dream fuel still it is not regarded as fuel in the present days. Hence, researchers and scientists are devoting their time and efforts to the economic manufacturing of hydrogen-fuelled engines and furnaces. The use of hydrogen may also cut short the wide use of electricity and fossil fuel as well. Therefore, an optimum condition for hydrogen production with a brand new design of a mechanical

system is expected to establish a hydrogen economy in the world. Thus, it is justified that an ample amount of works is waiting to be performed and completed within a very short period to be free from the global environmental problems and smooth running of the society around the different corners of the world.

References

[1] B. Petroleum, *Statistical review of world energy 2020*, no. 69th Edition. 2020.

[2] K. E. Muroyama, Hiroki, Yuji Tsuda, Toshiki Asakoshi, Hasan Masitah, Takeou Okanishi, Toshiaki Matsui, "Carbon dioxide methanation over Ni catalysts supported on various metal oxides," *J. Catal.*, vol. 343, pp. 178–184, 2016, doi: 10.1016/j.jcat.2016.07.018.

[3] P. C. Hallenbeck and D. Ghosh, "Improvements in fermentative biological hydrogen production through metabolic engineering," *J. Environ. Manage.*, vol. 95, no. SUPPL., pp. S360–S364, 2012, doi: 10.1016/j.jenvman.2010.07.021.

[4] M. K. Yogeswari, K. Dharmalingam, and P. Mullai, "Implementation of artificial neural network model for continuous hydrogen production using confectionery wastewater," *J. Environ. Manage.*, vol. 252, no. March, p. 109684, 2019, doi: 10.1016/j.jenvman.2019.109684.

[5] B. L. S. Fan, X. Wang, S. Cao, Y. Wang, Y. Zhang, "A novel model to determine the relationship between dust concentration and energy conversion efficiency of photovoltaic (PV) panels," *Energy*, vol. 252, p. 123927, 2022, doi: 10.1016/j.energy.2022.123927.

[6] S. C. S. Fan, W. Liang, G. Wang, Y. Zhang, "A novel water-free cleaning robot for dust removal from distributed photovoltaic (PV) in water-scarce areas," *Sol Energy*, vol. 241, pp. 553–563, 2022, doi: 10.1016/J.SOLENER.2022.06.024.

[7] W. Wang, D. M. Chen, and K. Yang, "Investigation on microstructure and hydrogen generation performance of Al-rich alloys," *Int. J. Hydrogen Energy*, vol. 35, no. 21, pp. 12011–12019, 2010, doi: 10.1016/j.ijhydene.2010.08.089.

[8] Y. Yavor, S. Goroshin, J. M. Bergthorson, D. L. Frost, R. Stowe, and S. Ringuette, "Enhanced hydrogen generation from aluminum-water reactions," *Int. J. Hydrogen Energy*, vol. 38, no. 35, pp. 14992–15002, 2013, doi: 10.1016/j.ijhydene.2013.09.070.

[9] M. Q. Fan, L. X. Sun, and F. Xu, "Experiment assessment of hydrogen production from activated aluminum alloys in portable generator for fuel cell applications," *Energy*, vol. 35, no. 7, pp. 2922–2926, 2010, doi: 10.1016/j.energy.2010.03.023.

[10] P. Hoffmann, “Tomorrow’s Energy: Hydrogen, Fuel Cells, and the Prospects for a Cleaner Planet,” *RISK Heal. Saf. Environ.*, p. [289, 2002.

[11] V. Y. Jose Garcia, Gabriel Villavicencio, Francisco Altimiras, Broderick Crawford, Ricardo Soto, Vinicius Minatogawa, Matheus Franco, David Martínez-Muñoz, “Machine learning techniques applied to construction: A hybrid bibliometric analysis of advances and future directions,” *Autom. Constr.*, vol. 142, p. 104532, 2022, doi: 10.1016/j.autcon.2022.104532.

[12] S. W. and J. R. J. Enrico Camporeale, *Machine Learning Techniques for Space Weather*. 2018. doi: 10.1016/C2016-0-01976-9.

[13] ZhimingFengaJianHuangaShanJinbGuanqiWangaYiChena, “Artificial intelligence-based multi-objective optimisation for proton exchange membrane fuel cell: A literature review,” *J. Power Sources*, vol. 520, p. 230808, 2022, doi: 10.1016/j.jpowsour.2021.230808.

[14] P. S. V. Masson-Delmotte, P. Zhai, H. Pörtner, D. Roberts, J. Skea, “Summary for policymakers.” IPCC, 2018.

[15] JianGongFengqiYou, “Sustainable design and synthesis of energy systems,” *Curr. Opin. Chem. Eng.*, vol. 10, pp. 77–86, 2015, doi: 10.1016/j.coche.2015.09.001.

[16] S. Kr.JhaaJasminBilalovicbAnjuJhabNileshPatelcHanZhang, “Renewable energy: Present research and future scope of Artificial Intelligence,” *Renew. Sustain. Energy Rev.*, vol. 77, pp. 297–317, 2017, doi: 10.1016/j.rser.2017.04.018.

[17] H. C. Ahmad, Tanveer, Dongdong Zhang, Chao Huang, Hongcai Zhang, Ningyi Dai, Yonghua Song, “Artificial intelligence in sustainable energy industry: Status Quo, challenges and opportunities,” *J. Clean. Prod.*, vol. 289, p. 125834, 2021, doi: 10.1016/j.jclepro.2021.125834.

[18] “Quantum supremacy using a programmable superconducting processor,” *Nature*, vol. 574, pp. 505–510, 2019.

[19] Y. Wu, W.-S. Bao, S. Cao, F. Chen, M.-C. Chen, X. Chen, “Strong quantum computational advantage using a superconducting quantum processor,” *Phys. Rev. Lett.*, vol. 127, p. 180501, 2021.

[20] RománOrúsabcdSamuelMugeldeEnriqueLizasod, "Quantum computing for finance: overview and prospects," *Rev. Phys.*, vol. 4, p. 100028, 2019, doi: 10.1016/j.revip.2019.100028.

[21] A. A.-G. Y. Cao, J. Romero, "Potential of quantum computing for drug discovery," *IBM J. Res. Dev.*, vol. 62, no. 6, pp. 1–6, 2018.

[22] S. S. M. M.P. Andersson, M.N. Jones, K.V. Mikkelsen, F. You, "Quantum computing for chemical and biomolecular product design," *Curr. Opin. Chem. Eng.*, vol. 36, p. 100754, 2022.

[23] V. H. C. D. A. A.H. Sodhro, S. Pirbhulal, "Artificial intelligence-driven mechanism for edge computing-based industrial applications," *IEEE Trans. Ind. Informatics*, vol. 15, pp. 4235–4243, 2019, doi: 10.1109/TII.2019.2902878.

[24] B. K. Bose, "Artificial intelligence techniques in smart grid and renewable energy systems - some example applications," *Proc. IEEE*, vol. 105, pp. 2262-2273, 2017, doi: 10.1109/JPROC.2017.2756596.

[25] C. J. Winter, "Into the hydrogen energy economy - Milestones," *Int. J. Hydrogen Energy*, vol. 30, no. 7, pp. 681–685, 2005, doi: 10.1016/j.ijhydene.2004.12.011.

[26] T. A. Milne, C. C. Elam, and R. J. Evans, "Hydrogen from biomass: state of the art and research challenges," *Energy Policy*, vol. 36, no. 12, pp. 4356–4362, 2008, doi: 10.2172/792221.

[27] P. P. Edwards, V. L. Kuznetsov, W. I. F. David, and N. P. Brandon, "Hydrogen and fuel cells: Towards a sustainable energy future," *Energy Policy*, 2008, doi: 10.1016/j.enpol.2008.09.036.

[28] S. Sharma and S. K. Ghoshal, "Hydrogen the future transportation fuel: From production to applications," *Renewable and Sustainable Energy Reviews*, vol. 43. pp. 1151–1158, 2015. doi: 10.1016/j.rser.2014.11.093.

[29] M. Balat, "Potential importance of hydrogen as a future solution to environmental and transportation problems," *Int. J. Hydrogen Energy*, 2008, doi: 10.1016/j.ijhydene.2008.05.047.

[30] BP, "BP Statistical Review of World Energy 2019|68th Edition," *BP World Energy*. 2019. doi: 10.2307/3324639.

[31] M. I. (Lead A. Hegglin, D. W. Fahey, M. McFarland, S. A. Montzka, and E. R. Nash, "Twenty Questions and Answers About the Ozone Layer: 2014 Update," 2015. doi: 10.1016/j.jemermed.2013.11.043.

[32] C. B. Raupach, Michael R., Gregg Marland, Philippe Ciais, "Global and regional drivers of accelerating CO2 emissions," *Proc. Natl. Acad. Sci. U. S. A.*, 2007, doi: 10.1073/pnas.0700609104.

[33] L. Schlapbach and A. Züttel, "Hydrogen-storage materials for mobile applications," *Nature*. 2001. doi: 10.1038/35104634.

[34] G. Principi, F. Agresti, A. Maddalena, and S. Lo Russo, "The problem of solid state hydrogen storage," *Energy*, 2009, doi: 10.1016/j.energy.2008.08.027.

[35] Wood, E.., Tappan, G.., Hadj, A., 2004. Understanding the drivers of agricultural land use change in south-central Senegal. J. Arid Environ. 59 *et al.*, "Urban Forest and Rural Cities: Multi-sited Households, Consumption Patterns, and Forest Resources in Amazonia," *Ecol. Soc.*, 2008, doi: 10.1186/1556-276X-7-150.

[36] I. P. Jain, "Hydrogen the fuel for 21st century," *Int. J. Hydrogen Energy*, 2009, doi: 10.1016/j.ijhydene.2009.05.093.

[37] C. C. Elam, C. E. G. Padró, G. Sandrock, A. Luzzi, P. Lindblad, and E. F. Hagen, "Realizing the hydrogen future: The International Energy Agency's efforts to advance hydrogen energy technologies," *Int. J. Hydrogen Energy*, 2003, doi: 10.1016/S0360-3199(02)00147-7.

[38] C. B. Porciúncula, N. R. Marcilio, I. C. Tessaro, and M. Gerchmann, "Production of hydrogen in the reaction between aluminum and water in the presence of NaOH and KOH," *Brazilian J. Chem. Eng.*, vol. 29, no. 2, pp. 337–348, 2012, doi: 10.1590/S0104-66322012000200014.

[39] W. Z. Gai, W. H. Liu, Z. Y. Deng, and J. G. Zhou, "Reaction of Al powder with water for hydrogen generation under ambient condition," *Int. J. Hydrogen Energy*, vol. 37, no. 17, pp. 13132–13140, 2012, doi: 10.1016/j.ijhydene.2012.04.025.

[40] Y. H. Huang, X, T Gao, X Pan, D Wei, C Lv, L Qin, "A review: Feasibility of hydrogen generation from the reaction between aluminum and water for fuel cell applications," *J. Power Sources*, vol. 229, pp. 133–140, 2013, doi: 10.1016/j.jpowsour.2012.12.016.

[41] S. Meher Kotay and D. Das, "Biohydrogen as a renewable energy resource-Prospects and potentials," *Int. J. Hydrogen Energy*, 2008, doi: 10.1016/j.ijhydene.2007.07.031.

[42] H. Torres-Silva, J. López-Bonilla, R. López-Vázquez, and J. Rivera-Rebolledo, "Weber's electrodynamics for the hydrogen atom," *Indones. J. Appl. Phys.*, 2015, doi: 10.13057/ijap.v5i01.260.

[43] R. Chaubey, S. Sahu, O. O. James, and S. Maity, "A review on development of industrial processes and emerging techniques for production of hydrogen from renewable and sustainable sources," *Renewable and Sustainable Energy Reviews*. 2013. doi: 10.1016/j.rser.2013.02.019.

[44] A. Fujishima and K. Honda, "Electrochemical photolysis of water at a semiconductor electrode," *Nature*, vol. 238, pp. 37–38, 1972, doi: 10.1038/238037a0.

[45] W. H. Cheng, C. Y. Shiau, T. H. Liu, H. L. Tung, J. F. Lu, and C. C. Hsu, "Promotion of Cu/Cr/Mn catalyst by alkali additives in methanol decomposition," *Appl. Catal. A Gen.*, vol. 170, no. 2, pp. 215–224, 1998, doi: 10.1016/S0926-860X(98)00055-6.

[46] L. F. Brown, "A comparative study of fuels for on-board hydrogen production for fuel-cell-powered automobiles," *Int. J. Hydrogen Energy*, vol. 26, no. 4, pp. 381–397, 2001, doi: 10.1016/S0360-3199(00)00092-6.

[47] J. H. Wee, "Which type of fuel cell is more competitive for portable application: Direct methanol fuel cells or direct borohydride fuel cells?," *Journal of Power Sources*. pp. 1–10, 2006. doi: 10.1016/j.jpowsour.2006.07.032.

[48] P. Nikolaidis and A. Poullikkas, "A comparative overview of hydrogen production processes," *Renew. Sustain. Energy Rev.*, vol. 67, pp. 597–611, 2017, doi: 10.1016/j.rser.2016.09.044.

[49] D. Belitskus, "Reaction of Aluminum with Sodium Hydroxide Solution as a Source of Hydrogen," *J. Electrochem. Soc.*, vol. 117, p. 1097, 1970, doi: 10.1149/1.2407730.

[50] New York State Energy Research and Development Authority, "Hydrogen Production - Steam Methane Reforming (SMR)," *Fuel*, 2008.

[51] M. Ni, M. K. H. Leung, D. Y. C. Leung, and K. Sumathy, "A review and recent developments in photocatalytic water-splitting using TiO2 for hydrogen production," *Renew. Sustain. Energy Rev.*, vol. 11, no. 3, pp. 401–425, 2007, doi: 10.1016/j.rser.2005.01.009.

[52] Q. Li, S. Ji, J. Hu, and S. Jiang, "Catalytic steam reforming of rice straw biomass to hydrogen-rich syngas over Ni-based catalysts," *Chinese J. Catal.*, 2013, doi: 10.1016/S1872-2067(12)60618-4.

[53] C. Y. Cho, K. H. Wang, and J. Y. Uan, "Evaluation of a new hydrogen generating system: Ni-rich magnesium alloy catalyzed by platinum wire in sodium chloride solutio," 2005. doi: 10.2320/matertrans.46.2704.

[54] M. H. Grosjean, M. Zidoune, L. Roué, and J. Y. Huot, "Hydrogen production via hydrolysis reaction from ball-milled Mg-based materials," *Int. J. Hydrogen Energy*, 2006, doi: 10.1016/j.ijhydene.2005.01.001.

[55] M. H. Grosjean and L. Roué, "Hydrolysis of Mg-salt and MgH2-salt mixtures prepared by ball milling for hydrogen production," *J. Alloys Compd.*, 2006, doi: 10.1016/j.jallcom.2005.09.008.

[56] J. Y. Uan, C. Y. Cho, and K. T. Liu, "Generation of hydrogen from magnesium alloy scraps catalyzed by platinum-coated titanium net in NaCl aqueous solution," *Int. J. Hydrogen Energy*, vol. 32, no. 13, pp. 2337–2343, 2007, doi: 10.1016/j.ijhydene.2007.03.014.

[57] O. V. Kravchenko, K. N. Semenenko, B. M. Bulychev, and K. B. Kalmykov, "Activation of aluminum metal and its reaction with water," *J. Alloys Compd.*, vol. 397, no. 1–2, pp. 58–62, 2005, doi: 10.1016/j.jallcom.2004.11.065.

[58] C. R. Jung, A. Kundu, B. Ku, J. H. Gil, H. R. Lee, and J. H. Jang, "Hydrogen from aluminium in a flow reactor for fuel cell applications," *J. Power Sources*, 2008, doi: 10.1016/j.jpowsour.2007.09.064.

[59] H. W. Wang, H. W. Chung, H. Te Teng, and G. Cao, "Generation of hydrogen from aluminum and water - Effect of metal oxide nanocrystals and water quality," *Int. J. Hydrogen Energy*, vol. 36, no. 23, pp. 15136–15144, 2011, doi: 10.1016/j.ijhydene.2011.08.077.

[60] H. Wang, Z. Wang, Z. Shi, X. Gong, J. Cao, and M. Wang, "Facile hydrogen production from Al-water reaction promoted by choline hydroxide," *Energy*, 2017, doi: 10.1016/j.energy.2017.05.031.

[61] J. Z. & J. Tianyou Zhang, Weijuan Yang, Shengsheng Zhang and Liu, "Hydrogen production by the reaction of Al-based metals with water vapor," *Energy sources*, 2018.

[62] M. Q. Fan, F. Xu, L. X. Sun, J. N. Zhao, T. Jiang, and W. X. Li, "Hydrolysis of ball milling Al-Bi-hydride and Al-Bi-salt mixture for hydrogen generation," *J. Alloys Compd.*, 2008, doi: 10.1016/j.jallcom.2007.05.077.

[63] S. Elitzur, V. Rosenband, and A. Gany, "Study of hydrogen production and storage based on aluminum-water reaction," *Int. J. Hydrogen Energy*, vol. 39, no. 12, pp. 6328–6334, 2014, doi: 10.1016/j.ijhydene.2014.02.037.

[64] A. V. Parmuzina and O. V. Kravchenko, "Activation of aluminium metal to evolve hydrogen from water," *Int. J. Hydrogen Energy*, vol. 33, no. 12, pp. 3073–3076, 2008, doi: 10.1016/j.ijhydene.2008.02.025.

[65] J. T. Slocum, *Characterization and Science of an Aluminum Fuel Treatment Process*, vol. Dissertati. 2107, p. MIT, US.

[66] J. L. S. Xu, X. Yang, S. Tang, "Liquid metal activated hydrogen production from waste aluminum for power supply and its life cycle assessment," *Int. J. Hydrog. Energy*, vol. 44, no. 33, pp. 17506–17514, 2019.

[67] L. Soler, A. M. Candela, J. Macanás, M. Muñoz, and J. Casado, "In situ generation of hydrogen from water by aluminum corrosion in solutions of sodium aluminate," *J. Power Sources*, vol. 192, no. 1, pp. 21–26, 2009, doi: 10.1016/j.jpowsour.2008.11.009.

[68] X. N. Huang, C. J. Lv, Y. X. Huang, S. Liu, C. Wang, and D. Chen, "Effects of amalgam on hydrogen generation by hydrolysis of aluminum with water," *Int. J. Hydrogen Energy*, vol. 36, no. 23, pp. 15119–15124, 2011, doi: 10.1016/j.ijhydene.2011.08.073.

[69] X. Z. Hu, Huarong, Minghua Qiao, Yan Pei, Kangnian Fan, Hexing Li, Baoning Zong, "Kinetics of hydrogen evolution in alkali leaching of rapidly quenched Ni-Al alloy," *Appl. Catal. A Gen.*, 2003, doi: 10.1016/S0926-860X(03)00416-2.

[70] B. Alinejad and K. Mahmoodi, “A novel method for generating hydrogen by hydrolysis of highly activated aluminum nanoparticles in pure water,” *Int. J. Hydrogen Energy*, 2009, doi: 10.1016/j.ijhydene.2009.07.028.

[71] Z. Y. Deng, Y. F. Liu, Y. Tanaka, J. Ye, and Y. Sakka, “Modification of AI particle surfaces by γ-Al 2O 3 and its effect on the corrosion behavior of Al,” *J. Am. Ceram. Soc.*, vol. 88, no. 4, pp. 977–979, 2005, doi: 10.1111/j.1551-2916.2005.00154.x.

[72] H. Z. Wang, D. Y. C. Leung, M. K. H. Leung, and M. Ni, “A review on hydrogen production using aluminum and aluminum alloys,” *Renew. Sustain. Energy Rev.*, vol. 13, no. 4, pp. 845–853, 2009, doi: 10.1016/j.rser.2008.02.009.

[73] J. T. Ziebarth, J. M. Woodall, R. A. Kramer, and G. Choi, “Liquid phase-enabled reaction of Al-Ga and Al-Ga-In-Sn alloys with water,” *Int. J. Hydrogen Energy*, 2011, doi: 10.1016/j.ijhydene.2011.01.127.

[74] K. Mahmoodi and B. Alinejad, “Enhancement of hydrogen generation rate in reaction of aluminum with water,” *Int. J. Hydrogen Energy*, vol. 35, no. 11, pp. 5227–5232, 2010, doi: 10.1016/j.ijhydene.2010.03.016.

[75] M. Q. Fan, F. Xu, and L. X. Sun, “Studies on hydrogen generation characteristics of hydrolysis of the ball milling Al-based materials in pure water,” *Int. J. Hydrogen Energy*, 2007, doi: 10.1016/j.ijhydene.2006.12.020.

[76] A. Z. Zhuk, A. E. Sheindlin, B. V. Kleymenov, E. I. Shkolnikov, and M. Y. Lopatin, “Use of low-cost aluminum in electric energy production,” *J. Power Sources*, 2006, doi: 10.1016/j.jpowsour.2005.11.097.

[77] L. Soler, J. Macanás, M. Muñoz, and J. Casado, “Hydrogen Generation From Aluminum In A Non-Consumable Potassium Hydroxide Solution,” *Energy*, 2005.

[78] S. R. Yinon Yavor, Sam Goroshin, Jeffrey M. Bergthorson, David L. Frost, Robert Stowe, “Enhanced hydrogen generation from aluminumewater reactions,” *Int. J. Hydrogen Energy*, vol. 38, no. 35, pp. 14992–15002, 2013, doi: 10.1016/j.ijhydene.2013.09.070.

[79] M. S. Vlaskin, E. I. Shkolnikov, and A. V. Bersh, “Oxidation kinetics of micron-sized aluminum powder in high-temperature boiling water,” *Int. J. Hydrogen Energy*, 2011, doi: 10.1016/j.ijhydene.2011.02.131.

[80] J. C. Lluís Solera, Jorge Macanása, Maria Muñoza, “Synergistic hydrogen generation from aluminum, aluminum alloys and sodium borohydride in aqueous solutions,” *Int. J. Hydrogen Energy*, vol. 32, pp. 4702–4710, 2007.

[81] S. S. Martínez, L. Albañil Sánchez, A. A. Álvarez Gallegos, and P. J. Sebastian, “Coupling a PEM fuel cell and the hydrogen generation from aluminum waste cans,” *Int. J. Hydrogen Energy*, vol. 32, no. 15, pp. 3159–3162, 2007, doi: 10.1016/j.ijhydene.2006.03.015.

[82] V. Rosenband and A. Gany, “Application of activated aluminum powder for generation of hydrogen from water,” *Int. J. Hydrogen Energy*, vol. 35, no. 20, pp. 10898–10904, 2010, doi: 10.1016/j.ijhydene.2010.07.019.

[83] H. Nie, M. Schoenitz, and E. L. Dreizin, “Calorimetric investigation of the aluminum-water reaction,” *Int. J. Hydrogen Energy*, 2012, doi: 10.1016/j.ijhydene.2012.05.012.

[84] A. R. Studart, M. D. M. Innocentini, I. R. Oliveira, and V. C. Pandolfelli, “Reaction of aluminum powder with water in cement-containing refractory castables,” *J. Eur. Ceram. Soc.*, 2005, doi: 10.1016/j.jeurceramsoc.2004.07.004.

[85] T. Hiraki, M. Takeuchi, M. Hisa, and T. Akiyama, “Hydrogen production from waste aluminum at different temperatures, with LCA,” *Mater. Trans.*, vol. 46, no. 5, pp. 1052–1057, 2005, doi: 10.2320/matertrans.46.1052.

[86] H. Te Teng, T. Y. Lee, Y. K. Chen, H. W. Wang, and G. Cao, “Effect of Al(OH) 3 on the hydrogen generation of aluminum-water system,” *J. Power Sources*, vol. 219, pp. 16–21, 2012, doi: 10.1016/j.jpowsour.2012.06.077.

[87] A. V. Ilyukhina, A. S. Ilyukhin, and E. I. Shkolnikov, “Hydrogen generation from water by means of activated aluminum,” *Int. J. Hydrogen Energy*, vol. 37, no. 21, pp. 16382–16387, 2012, doi: 10.1016/j.ijhydene.2012.02.175.

[88] T. Hiraki, S. Yamauchi, M. Iida, H. Uesugi, and T. Akiyama, “Process for recycling waste aluminum with generation of high-pressure hydrogen,” *Environ. Sci. Technol.*, vol. 41, no. 12, pp. 4454–4457, 2007, doi: 10.1021/es062883l.

[89] US DOE, “Reaction of aluminum with water to produce hydrogen,” *US DOE Rep.*, 2008.

[90] M. H. and T. A. Takehito Hiraki1, Masato Takeuchi2, “Hydrogen Production from Waste Aluminum at Different Temperatures, with LCA,” *Mater. Trans.*, vol. 46, no. 5, pp. 1052–1057.

[91] J. M. Woodall, J. T. Ziebarth, C. R. Allen, D. M. Sherman, J. Jeon, and G. Choi, “Recent results on splitting water with aluminum alloys,” 2009. doi: 10.1002/9780470483428.ch13.

[92] V. G. Ivanov, M. N. Safronov, and O. V. Gavrilyuk, “Macrokinetics of oxidation of ultradisperse aluminum by water in the liquid phase,” *Combust. Explos. Shock Waves*, 2001, doi: 10.1023/A:1017505709456.

[93] Z. Y. Deng, J. M. F. Ferreira, and Y. Sakka, “Hydrogen-generation materials for portable applications,” *J. Am. Ceram. Soc.*, 2008, doi: 10.1111/j.1551-2916.2008.02800.x.

[94] R. C. Dante, L. P. Güereca, L. Neri, J. L. Escamilla, L. Aquino, and J. Celis, “Life cycle analysis of hydrogen fuel: A methodology for a strategic approach of decision making,” *Int. J. Hydrogen Energy*, vol. 27, no. 2, pp. 131–133, 2002, doi: 10.1016/S0360-3199(01)00098-2.

[95] M. A. Escalante Soberanis and A. M. Fernandez, “A review on the technical adaptations for internal combustion engines to operate with gas/hydrogen mixtures,” *Int. J. Hydrogen Energy*, vol. 35, no. 21, pp. 12134–12140, 2010, doi: 10.1016/j.ijhydene.2009.09.070.

[96] R. K. Green and N. D. Glasson, “High-pressure hydrogen injection for internal combustion engines,” *Int. J. Hydrogen Energy*, vol. 17, no. 11, pp. 895–901, 1992, doi: 10.1016/0360-3199(92)90041-T.

[97] S. Verhelst, T. Wallner, and R. Sierens, “Hydrogen-Fueled internal combustion engines,” *Handb. Hydrog. Energy*, vol. 35, no. 6, pp. 821–902, 2014, doi: 10.1201/b17226.

[98] L. M. Das, “Hydrogen engine: Research and development (R&D) programmes in Indian Institute of Technology (IIT), Delhi,” *Int. J. Hydrogen Energy*, vol. 27, no. 9, pp. 953–965, 2002, doi: 10.1016/S0360-3199(01)00178-1.

[99] E. Tzimas, C. Filiou, S. D. Peteves, and J. Veyret, *Hydrogen Storage : State-of-the-Art and Future Perspective*. 2003.

[100] J. S. Z.Wen, “Methods and Applications for Artificial Intelligence, Big Data, Internet-of-Things, and Blockchain in Smart Energy Management,” *Energy AI*, p. 100208, 2022, doi: 10.1016/j.egyai.2022.100208.

[101] S. W. Antonopoulos, Ioannis, Valentin Robu, Benoit Couraud, Desen Kirli, Sonam Norbu, A. E. Kiprakis, David Flynn, Sergio Elizondo-Gonzalez, “Artificial intelligence and machine learning approaches to energy demand-side response: A systematic review,” *Renew. Sustain. Energy Rev.*, vol. 130, p. 109899, 2020, doi: 10.1016/j.rser.2020.109899.

[102] S. Kr.JhaaJasminBilalovicbAnjuJhabNileshPatelcHanZhangd, “Renewable energy: Present research and future scope of Artificial Intelligence,” *Renew. Sustain. Energy Rev.*, vol. 77, pp. 297–317, 2017, doi: 10.1016/j.rser.2017.04.018.

[103] S. S. Arumugam, Thangavelu, Sridhar Ramachandran, Sapna Kinattinkara, Sampathkumar Velusamy, Snehmani, Manoj Shanmugamoorthy, “Bayesian networks and intelligence technology applied to climate change: An application of fuzzy logic based simulation in avalanche simulation risk assessment using GIS in a Western Himalayan region,” *Urban Clim.*, vol. 45, p. 101272, 2022, doi: 10.1016/j.uclim.2022.101272.

[104] B. RoodposhtibPiotrJankowskicdThomasBlaschkee, “A GIS-based extended fuzzy multi-criteria evaluation for landslide susceptibility mapping,” *Comput. Geosci.*, vol. 73, pp. 208–221, 2014, doi: doi.org/10.1016/j.cageo.2014.08.001.

[105] ZiqiangShiaRongZhenabJialunLiubc, “Fuzzy logic-based modeling method for regional multi-ship collision risk assessment considering impacts of ship crossing angle and navigational environment,” *Ocean Eng.*, vol. 259, p. 111847, 2022, doi: 10.1016/j.oceaneng.2022.111847.

[106] E.H.MamdaniS.Assilian, “An experiment in linguistic synthesis with a fuzzy logic controller,” *Int. J. Man. Mach. Stud.*, vol. 7, no. 1, pp. 1–13, 1975, doi: 10.1016/S0020-7373(75)80002-2.

[107] S.KaruppusamyaB.SureshkumaraM.KarthebR.Sanjeevic, “Fuzzy logic modelling in drilling operation,” 2022. doi: 10.1016/j.matpr.2022.07.144.

[108] JinqiangLiuXiaoruWangYunLu, “A novel hybrid methodology for short-term wind power forecasting based on adaptive neuro-fuzzy inference system,” *Renew. Energy*, vol. 103, pp. 620–629, 2017, doi: 10.1016/j.renene.2016.10.074.

[109] L. Das Deep, Narasingh, Punyapriya Mishra, “Application of adaptive neuro-fuzzy inference system (ANFIS) for predicting dielectric characteristics of CNT/PMMA nanocomposites,” *Mater. Today Proc.*, vol. 33, pp. 5200–5205, 2020, doi: 10.1016/j.matpr.2020.02.882.

[110] M. Das Ghatak and A. Ghatak, “Artificial neural network model to predict behavior of biogas production curve from mixed lignocellulosic co-substrates,” *Fuel*, vol. 232, no. May 2017, pp. 178–189, 2018, doi: 10.1016/j.fuel.2018.05.051.

[111] F. M. Cavalcanti, M. Schmal, R. Giudici, and R. M. Brito Alves, “A catalyst selection method for hydrogen production through Water-Gas Shift Reaction using artificial neural networks,” *J. Environ. Manage.*, vol. 237, no. October 2018, pp. 585–594, 2019, doi: 10.1016/j.jenvman.2019.02.092.

[112] M. Cervantes-Bobadilla, J. García-Morales, R. F. Escobar-Jiménez, J. A. Hernández-Pérez, J. F. Gómez-Aguilar, and V. H. Olivares-Peregrino, “Experimental implementation of a new control approach using an inverse neural network to on-demand hydrogen production,” *Control Eng. Pract.*, vol. 105, no. September, p. 104631, 2020, doi: 10.1016/j.conengprac.2020.104631.

[113] T. J. K. Xu, Moran, Changping Li, Rendi Kurniawan, GunChul Park, Jielin Chen, “Study on surface integrity of titanium alloy machined by electrical discharge-assisted milling,” *J. Mater. Process. Technol.*, vol. 299, p. 117334, 2022.

[114] G. C. D’Amico, “Building energy performance forecasting: A multiple linear regression approach,” *Appl. Energy*, vol. 253, 2109.

[115] J. Meerasri and R. Sothornvit, “Artificial neural networks (ANNs) and multiple linear regression (MLR) for prediction of moisture content for coated pineapple cubes,” *Case Stud. Therm. Eng.*, vol. 33, p. 101942, May 2022, doi: 10.1016/J.CSITE.2022.101942.

[116] P. S. R. Saptarshi Dutta, “Experimental investigation and modeling of creep curve of Zr-2.5Nb alloy by machine learning techniques,” *Met. Mater. Int.*, 2022.

[117] P. C. Hallenbeck and D. Ghosh, “Advances in fermentative biohydrogen production: the way forward?,” *Trends Biotechnol.*, vol. 27, no. 5, pp. 287–297, 2009, doi: 10.1016/j.tibtech.2009.02.004.

[118] K. Ghasemzadeh, F. Ahmadnejad, A. Aghaeinejad-Meybodi, and A. Basile, “Hydrogen production by a Pd–Ag membrane reactor during glycerol steam reforming: ANN modeling study,” *Int. J. Hydrogen Energy*, vol. 43, no. 15, pp. 7722–7730, 2018, doi: 10.1016/j.ijhydene.2017.09.120.

[119] P. Jha, E. B. G. Kana, and S. Schmidt, “Can artificial neural network and response surface methodology reliably predict hydrogen production and COD removal in an UASB bioreactor?,” *Int. J. Hydrogen Energy*, vol. 42, no. 30, pp. 18875–18883, 2017, doi: 10.1016/j.ijhydene.2017.06.063.

[120] P. S. Robi and U. S. Dixit, “Application of neural networks in generating processing map for hot working,” *J. Mater. Process. Technol.*, vol. 142, no. 1, pp. 289–294, 2003, doi: 10.1016/S0924-0136(03)00579-X.

[121] P. A. C. R. Nogueira, Tiago de Oliveira, Gilderlânio Barbosa Alves Palacio, Fabrício Damasceno Braga, Pedro Paulo Nunes Maia, Elineudo Pinho de Moura, Carla Freitas de Andrade, “Imbalance classification in a scaled-down wind turbine using radial basis function kernel and support vector machines,” *Energy*, vol. 238, 2022, doi: 10.1016/j.energy.2021.122064.

[122] R. D. Junpeng Huang, Sixiang Ling, Xiyong Wu, “Gis-based comparative study of the bayesian network, decision table, radial basis function network and stochastic gradient descent for the spatial prediction of landslide susceptibility,” vol. 11, no. 3, 2022, doi: 10.3390/land11030436.

[123] G. Chen, “Multimedia Security Situation Prediction Based on Optimization of Radial Basis Function Neural Network Algorithm,” *Comput. Intell. Neurosci.*, 2022, doi: 10.1155/2022/6314262.

[124] M. M. Manoj A. Patil, “Enhanced radial basis function neural network for tomato plant disease leaf image segmentation,” *Ecol. Inform.*, vol. 70, 2022, doi: 10.1016/j.ecoinf.2022.101752.

[125] S. I. M. b May Ali Alsaffar a, Bamidele Victor Ayodele b, "Scavenging carbon deposition on alumina supported cobalt catalyst during renewable hydrogen-rich syngas production by methane dry reforming using artificial intelligence modeling technique," *J. Clean. Prod.*, vol. 247, 2020, doi: 10.1016/j.jclepro.2019.119168.

[126] D.-I. S. c Donglei Liu a, Shunli Wang a b, Yongcun Fan a, Yawen Liang a, Carlos Fernandez d, "State of energy estimation for lithium-ion batteries using adaptive fuzzy control and forgetting factor recursive least squares combined with AEKF considering temperature," *J. Energy Storage*, vol. 70, 2023, doi: 10.1016/j.est.2023.108040.

[127] A. A.-O. c Muhammad Tawalbeh a b, Afifa Farooq c, Remston Martis c, "Optimization techniques for electrochemical devices for hydrogen production and energy storage applications," *Int. J. Hydrogen Energy*, 2023, doi: 10.1016/j.ijhydene.2023.06.264.

[128] H. R. Jinling Lu, Dingyue Huang, "Data-driven source-load robust optimal scheduling of integrated energy production unit including hydrogen energy coupling," *Glob. Energy Interconnect.*, vol. 6, no. 4, pp. 375–388, 2023, doi: 10.1016/j.gloei.2023.08.001.

[129] R. W. b Hans Dembinski a, Michael Schmelling a, "Application of the iterated weighted least-squares fit to counting experiments," *Nucl. Instruments Methods Phys. Res. Sect. A Accel. Spectrometers, Detect. Assoc. Equip.*, vol. 940, pp. 135–141, 2019, doi: 10.1016/j.nima.2019.05.086.

[130] R. K. Jr, "Data smoothing using a least squares fit C++ class," *ISA Trans.*, vol. 37, pp. 3–19, 1998, doi: 10.1016/S0019-0578(98)00008-1.

[131] International Energy Agency, "World Energy Outlook 2017 - Chapter 1: Introduction and scope," *World Energy Outlook 2017*, 2017, doi: 10.1787/weo-2017-en.

[132] E. Morsch Filho, T. S. Possamai, V. de P. Nicolau, and R. Oba, "Experimental investigation of the thermal behavior for oxy-fired and air-fired high temperature furnaces for the vitreous ceramic industry," *Therm. Sci. Eng. Prog.*, 2020, doi: 10.1016/j.tsep.2019.100455.

[133] H. L. Ji, Zhiyun, Haoyu Zhou, Xiaohui Fan, Min Gan, Qian Liu, Xiaoxian Huang, Xuling Chen, "Insight into the application of hydrogen-rich energy in iron ore sintering: Parameters optimization and function mechanism," *Process Saf. Environ. Prot.*, 2020, doi: 10.1016/j.psep.2019.12.016.

[134] J. M. F. Clout and J. R. Manuel, “Fundamental investigations of differences in bonding mechanisms in iron ore sinter formed from magnetite concentrates and hematite ores,” 2003. doi: 10.1016/S0032-5910(02)00241-3.

[135] I. Pisa, G. Lazaroiu, and T. Prisecaru, “Influence of hydrogen enriched gas injection upon polluting emissions from pulverized coal combustion,” 2014. doi: 10.1016/j.ijhydene.2014.08.119.

[136] J. K. Daho, Tizane, Gilles Vaitilingom, Oumar Sanogo, Salifou K. Ouiminga, Augustin S. Zongo, Bruno Piriou, “Combustion of vegetable oils under optimized conditions of atomization and granulometry in a modified fuel oil burner,” *Fuel*, 2014, doi: 10.1016/j.fuel.2013.11.009.

[137] J. S. Kim, W. Yang, Y. Kim, and S. H. Won, “Behavior of buoyancy and momentum controlled hydrogen jets and flames emitted into the quiescent atmosphere,” *J. Loss Prev. Process Ind.*, 2009, doi: 10.1016/j.jlp.2009.08.018.

[138] B. Sakintuna, F. Lamari-Darkrim, and M. Hirscher, “Metal hydride materials for solid hydrogen storage: A review,” *International Journal of Hydrogen Energy*, vol. 32, no. 9. pp. 1121–1140, 2007. doi: 10.1016/j.ijhydene.2006.11.022.

[139] P. Muthukumar, U. Madhavakrishna, and A. Dewan, “Parametric studies on a metal hydride based hydrogen storage device,” *Int. J. Hydrogen Energy*, 2007, doi: 10.1016/j.ijhydene.2007.08.010.

[140] J. M. Ogden, “Developing an infrastructure for hydrogen vehicles: A Southern California case study,” *Int. J. Hydrogen Energy*, 1999, doi: 10.1016/S0360-3199(98)00131-1.

[141] D. P, “CRC Handbook of Chemistry and Physics,” *J. Mol. Struct.*, 1992, doi: 10.1016/0022-2860(92)85083-s.

[142] C. Liu, F. Li, M. Lai-Peng, and H. M. Cheng, “Advanced materials for energy storage,” *Advanced Materials*. 2010. doi: 10.1002/adma.200903328.

[143] US Department of Energy, “EnergyPlus Engineering Reference: The Reference to EnergyPlus Calculations,” *US Dep. Energy*, 2010, doi: citeulike-article-id:10579266.

[144] H. M. Cheng, Q. H. Yang, and C. Liu, “Hydrogen storage in carbon nanotubes,” *Carbon N. Y.*, 2001, doi: 10.1016/S0008-6223(00)00306-7.

[145] I. P. Jain, C. Lal, and A. Jain, “Hydrogen storage in Mg: A most promising material,” *Int. J. Hydrogen Energy*, vol. 35, no. 10, pp. 5133–5144, 2010, doi: 10.1016/j.ijhydene.2009.08.088.

[146] U. B. Demirci and P. Miele, “Sodium borohydride versus ammonia borane, in hydrogen storage and direct fuel cell applications,” *Energy and Environmental Science*. 2009. doi: 10.1039/b900595a.

[147] B. S. L.-D. Hirscher, “Metal hydride materials for solid hydrogen storage: A reviewNo Title,” *Int. J. Hydrogen Energy*, vol. 32, pp. 1121–1140, 2007.

[148] T. Nakayama, S. Tomura, M. Ozaki, R. Ohmura, and Y. H. Mori, “Engineering investigation of hydrogen storage in the form of clathrate hydrates: Conceptual design of hydrate production plants,” *Energy and Fuels*, vol. 24, no. 4, pp. 2576–2588, 2010, doi: 10.1021/ef100039a.

[149] W. L. Vos, L. W. Finger, R. J. Hemley, and H. K. Mao, “Novel H2-H2O clathrates at high pressures,” *Phys. Rev. Lett.*, 1993, doi: 10.1103/PhysRevLett.71.3150.

[150] Neil Glasson, “HYDROGEN FUELLING OFAN INTERNAL COMBUSTION ENGINE,” *Dep. Mech. Eng. Univ. Canterbury Christchurch NEW Zeal.*, 1992.

[151] R. Reider and F. J. Edeskuty, “Hydrogen safety problems,” *Int. J. Hydrogen Energy*, 1979, doi: 10.1016/0360-3199(79)90128-9.

[152] L. Segal, J. S. Wallace, and J. F. Keffer, “Safety considerations in the design of a gaseous hydrogen fuel supply for engine testing,” *Int. J. Hydrogen Energy*, 1986, doi: 10.1016/0360-3199(86)90143-6.

[153] L. M. Das, “Safety aspects of a hydrogen-fuelled engine system development,” *Int. J. Hydrogen Energy*, 1991, doi: 10.1016/0360-3199(91)90086-X.

[154] G.E.Dieter, “Mechanical Metallurgy 1998”.

[155] G. GD, “Interpreting neural-network connection weights,” p. Artif Intell Expert 6:47–51, 1991.

[156] S. Moradkhani, H., Hsu, K.-l., Gupta, H.V., Sorooshian, “Improved streamflow forecasting using self-organizing radial basis function artificial neural networks,” *J. Hydrol.*, vol. 295, no. 1, p. 246e262., 2004.

[157] H. H. a Xiaoling Zhou a 1, Lili Zheng a 1, Shiyan Chen a, Hongwei Du b, Benimana Muhire Gakoko Raphael a, Qianyun Song a, Fuyong Wu c, Jianrong Chen a, Hongjun Lin a, "Factors influencing DBPs occurrence in tap water of Jinhua Region in Zhejiang Province, China," *Ecotoxicol. Environ. Saf.*, vol. 171, pp. 813–822, 2019, doi: https://doi.org/10.1016/j.ecoenv.2018.12.106.

[158] F. W. Lin, Hongjun, Qunyun Dai, Lili Zheng, Huachang Hong, Wenjing Deng, "Radial basis function artificial neural network able to accurately predict disinfection by-product levels in tap water: Taking haloacetic acids as a case study," *Chemosphere*, vol. 248, p. 125999, 2020, doi: https://doi.org/10.1016/j.chemosphere.2020.125999.

[159] H. A. Azam Safarnejad a, M. Reza Hormozi-Nezhad b, c, "Radial basis function-artificial neural network (RBF-ANN) for simultaneous fluorescent determination of cysteine enantiomers in mixtures," *Spectrochim. Acta Part A Mol. Biomol. Spectrosc.*, vol. 261, p. 120029, 2021, doi: https://doi.org/10.1016/j.saa.2021.120029.

[160] H. L. a Yifeng Chen a, Genying Yu a, Ying Long a, Jiaheng Teng a, Xiujia You a, Bao-Qiang Liao b, "Application of radial basis function artificial neural network to quantify interfacial energies related to membrane fouling in a membrane bioreactor," *Bioresour. Technol.*, vol. 293, p. 122103, 2019, doi: https://doi.org/10.1016/j.biortech.2019.122103.

[161] P. B. Liangjie Jin, "QSPR study on normal boiling point of acyclic oxygen containing organic compounds by radial basis function artificial neural network," *Chemom. Intell. Lab. Syst.*, vol. 157, pp. 127–132, 2016, doi: https://doi.org/10.1016/j.chemolab.2016.07.007.

[162] J. C. Yifeng Chen, Liguo Shen, Renjie Li, Xianchao Xu, Huachang Hong, Hongjun Lin, "Quantification of interfacial energies associated with membrane fouling in a membrane bioreactor by using BP and GRNN artificial neural networks," *J. Colloid Interface Sci.*, vol. 565, pp. 1–10, 2020, doi: https://doi.org/10.1016/j.jcis.2020.01.003.

[163] A. A. A. Surajdeen A. Iliyas, Moustafa. Elshafei, Mohamed A. Habib, "RBF neural network inferential sensor for process emission monitoring," *Control Eng. Pract.*, vol. 21, no. 7, pp. 962–970, 2013, doi: https://doi.org/10.1016/j.conengprac.2013.01.007.

[164] S. C. a b 2 Pranav Kulkarni a 1, "Disinfection by-product formation following chlorination of drinking water: Artificial neural network models and changes in

speciation with treatment," *Sci. Total Environ.*, vol. 408, no. 19, pp. 4202–4210, 2010, doi: https://doi.org/10.1016/j.scitotenv.2010.05.040.

[165] H. F. C. Engines, "MODULE 3: HYDROGEN USE IN INTERNAL COMBUSTION ENG," 2001.

[166] O. S. Kunte, "USE OF HYDOGEN IN IC ENGINES," *Int. J. Adv. Res. Sci. Eng.*, vol. 5, no. 3, 2016.

[167] V. Ganesan, *Internal Combustion Engines*, 20th ed. Mc Graw Hill Education, 2018.

[168] İ. G. Jayaraman Kandasamy a, Rasiha Nefise Mutlu a, Esra Eroğlu a c, Mehmet Karaca b, Hande Toffoli c, "Hydrogen production using aluminum-water splitting: A combined experimental and theoretical approach," *Int. J. Hydrogen Energy*, 2023, doi: https://doi.org/10.1016/j.ijhydene.2023.04.068.

[169] Z. Y. Deng, L. L. Zhu, Y. Bin Tang, Y. Sakka, J. Ye, and R. J. Xie, "Role of particle sizes in hydrogen generation by the reaction of Al with water," *J. Am. Ceram. Soc.*, 2010, doi: 10.1111/j.1551-2916.2010.03969.x.

[170] J. Y. Teng Su, Changwei Ji, Shuofeng Wang, Xiaoyu Cong, Lei Shi, "Improving the lean performance of an n-butanol rotary engine by hydrogen enrichment," *Energy Convers. Manag.*, vol. 157, pp. 96–102, 2018, doi: https://doi.org/10.1016/j.enconman.2017.12.005.

[171] K. Z. Long Wanga, Zhanming Chena, Tiancong Zhangb, "Effect of excess air/fuel ratio and methanol addition on the performance, emissions, and combustion characteristics of a natural gas/methanol dualfuel engine," *Fuel*, vol. 255, p. 115799, 2019, doi: https://doi.org/10.1016/j.fuel.2019.115799.

[172] G. X. Hao Meng, Changwei Ji*, Jinxin Yang, Shuofeng Wang, Ke Chang, "Experimental study of the effects of excess air ratio on combustion and emission characteristics of the hydrogen-fueled rotary engine," *i n t e r n a t i o n a l J. o f Hydrog. energy*, vol. 46, pp. 3 2 2 6 1-3 2 2 7 2, 2021, doi: https://doi.org/10.1016/j.ijhydene.2021.06.208.

[173] L. M. Das, "Hydrogen–oxygen reaction mechanism and is implication to hydrogen engine combustion methane – hydrogen mixtures as fuel," *Int. J. Hydrogen Energy*, vol. 21, p. 70, 1996.

Publications from the Thesis

Journals

1) **Biswajyoti Das**, P.S. Robi, P. Mahanta, "Experimental Investigation and Modelling by Machine Learning Techniques for Hydrogen Generation by Reacting Aluminium with Aqueous NaOH Solution," *Fuel*, vol. 351, 2023, doi.org/10.1016/j.fuel.2023.128924.
2) **Biswajyoti Das**, P.S. Robi, P. Mahanta, "Data-Driven Models for the Prediction of H_2 Generation through Chemical Reaction and Performance Evaluation of On-Board Hydrogen Fuelled Sintering Tube Furnace", *Renewable Energy*, vol. 235, 2024, doi.org/10.1016/j.renene.2024.121324.

Book Chapters

1) **Biswajyoti Das**, P. Mahanta, P.S. Robi, "Production of Hydrogen Gas from Al-Water Reaction in the Presence of Aqueous NaOH—An Experimental Approach", Advances in Thermofluids and Renewable Energy: Select Proceedings of TFRE 2020, Springer Singapore, pp 303-309, (2022).
2) **Biswajyoti Das**, P. Mahanta, P.S. Robi, "An overview of the methods of enhancement of the reaction kinetics of Al-water reaction in an aqueous medium and the prospect of the economic viability", Advances in Thermofluids and Renewable Energy: Select Proceedings of TFRE 2020, Springer Singapore, pp 591-596, (2022).

Appendix I

Physical property chart for hydrogen [98]

Property	Measure
Molecular Formula	H_2
Molecular Weight	2.016 g/mol
Boiling Point (at 1 atm)	-253° C
Freezing Point (at 1 atm)	-259° C
Vapour Density (at 20° C, 1 atm)	0.08376 kg/m^3
Liquid Density (at normal boiling point, 1 atm)	70.86 kg/m^3
Specific Volume (Gaseous state at 20° C, 1 atm)	11.9 m^3/kg
Specific Volume (Liquid state at -253° C, 1 atm)	0.014 m^3/kg
Specific Gravity (Gaseous state at 20° C, 1 atm)	0.0696 (approx. 7% the density of air)
Specific Gravity (Liquid state at -253° C, 1 atm)	0.0708 (approx.. 7% the density of water)
Expansion Ratio	1:848
Higher Heating Value (at 25° C, 1 atm)	141.86 MJ/kg
Lower Heating Value (at 25° C, 1 atm)	119.93 MJ/kg
Energy density (LHV) (at 15° C, 1 atm)	10.050 KJ/m^3
	1,825,000 KJ/m^3
(at 15° C, 200 bar)	4,500,000 KJ/m^3
(at 15° C, 690 bar) (liquid)	8,491,000 KJ/m^3
Flashpoint	< -253° C
Auto-ignition Temperature	585° C
Octane Number	130+ (lean burn)
Ignition Energy	0.02mJ
Burning Speed	2.65-3.25 m/s

Appendix II

Comparison of hydrogen as a fuel [173]

Property	**Gasoline**	**CNG**	**H_2**	**Advantages of H_2 fuel**
Flammability limits (%)	1-7.5	5.3-15	9.75	Lean AFR can be used
Diffusivity	0.05	0.16	0.61	Homogeneous mixture
Auto ignition temperature (^{0} C)	230-480	540	585	Knock resistance
Emission product	HC, CO, CO_2, No_x, H_2O	HC, CO, CO_2, No_x, H_2O	H_2O	Zero emission
Energy density (MJ/m^3)	31.15	32.56	10.05	Large tank is required for storage
Quenching gap in air (mm)	2	2.03	0.64	Responsible for back-fire
Flammability limits (%)	1-7.5	5.3-15	9.75	Lean AFR can be used

Diffusivity	0.05	0.16	0.61	Homogeneous mixture
Auto ignition temperature (^{0} C)	230-480	540	585	Knock resistance
Emission product	HC, CO, CO_2, No_x, H_2O	HC, CO, CO_2, No_x, H_2O	H_2O	Zero emission
Energy density (MJ/m^3)	31.15	32.56	10.05	Large tank is required for storage
Quenching gap in air (mm)	2	2.03	0.64	Responsible for back-fire

Appendix III

Comparative results obtained during the ANN training and testing of process

SL No	File Name	1st TF	2nd TF	neurons	epochs	goal	TR_ Dev-M	TST_ DEV_M	NTR_10	NTR_5	NTst_10	NTst_5	RMS_Tr	RMS_Ts
1	Weight_H1	Tansig	Purelin	35	10	0.001	22.23	15.77	6	37	2	16	0.0035	0.0036
2	Weight_H2	Tansig	Purelin	35	9	0.001	14.25	10.34	4	60	3	30	0.0035	0.0035
3	Weight_H3	Tansig	Purelin	35	1030	0.00001	2.65	4.39	0	0	0	0	0.00034	0.00042
4	Weight_H4	Tansig	Purelin	35	514	0.00001	3.06	4.46	0	0	0	0	0.00028	0.00038
5	Weight_H5	Tansig	Purelin	5	58	0.00001	65.00	47.00	105	197	57	105	0.0052	0.0052
6	Weight_H6	Tansig	Purelin	10	3000	0.00001	57.00	47.00	31	110	11	56	0.0035	0.0036
7	Weight_H7	Tansig	Purelin	5	713	0.00001	114.70	67.02	102	203	50	107	0.0076	0.0082
8	Weight_H8	Tansig	Purelin	25	1365	0.00001	2.81	3.49	0	0	0	0	0.00037	0.00049
9	Weight_H9	Tansig	Purelin	25	3000	0.00001	2.73	5.37	0	0	0	2	0.00037	0.00047
10	Weight_H10	Tansig	Purelin	25	1213	0.00001	2.95	5.47	0	0	0	2	0.00048	0.00051
11	Weight_H11	Tansig	Purelin	30	1711	0.00001	3.23	5.73	0	0	0	2	0.00033	0.00041
12	Weight_H12	Tansig	Purelin	35	1414	0.00001	1.97	7.11	0	0	0	2	0.00036	0.00045
13	Weight_H13	Tansig	Purelin	35	1500	0.00001	2.85	4.59	0	0	0	0	0.00035	0.00045
14	Weight_H14	Purelin	Tansig	25	2	0.00001	5.27×10^3	$3.35. \times 10^3$	336	337	184	185	0.194	0.1936
15	Weight_H15	Purelin	Tansig	35	2	0.00001	5.27×10^3	$3.35. \times 10^3$	336	337	184	185	0.194	0.1936
16	Weight_H16	Purelin	Tansig	30	2	0.00001	5.27×10^3	$3.35. \times 10^3$	336	337	184	185	0.194	0.1936
17	Weight_H17	Purelin	Tansig	20	2	0.00001	5.27×10^3	$3.35. \times 10^3$	336	337	184	185	0.194	0.1936
18	Weight_H18	Purelin	Tansig	15	2	0.00001	5.27×10^3	$3.35. \times 10^3$	336	337	184	185	0.194	0.1936
19	Weight_H19	logsig	Purelin	5	3000	0.00001	177.45	134.94	167	244	90	136	0.0072	0.0075
20	Weight_H20	logsig	Purelin	10	1394	0.00001	26.68	19.86	21	71	10	39	0.0034	0.0038
21	Weight_H21	logsig	Purelin	15	2100	0.00001	11.10	7.39	2	9	0	6	0.0016	0.0017
22	Weight_H22	logsig	Purelin	20	1502	0.00001	2.86	5.74	0	0	0	1	0.00077	0.0008
23	Weight_H23	logsig	Purelin	30	1128	0.00001	2.68	4.71	0	0	0	0	0.00031	0.00051

24	Weight_H24	logsig	Purelin	35	1012	0.00001	2.34	5.51	0	0	0	1	0.0003	0.00045
25	Weight_H25	Purelin	logsig	5	2	0.00001	$2.24. \times 10^4$	1.31×10^4	337	337	185	185	0.8327	0.832
26	Weight_H26	Purelin	logsig	10	4	0.00001	$2.24. \times 10^4$	1.31×10^4	337	337	185	185	0.8327	0.832
27	Weight_H27	Purelin	logsig	25	4	0.00001	$2.24. \times 10^4$	1.31×10^4	337	337	185	185	0.8327	0.832
28	Weight_H28	Tansig	logsig	5	5	0.00001	$2.24. \times 10^4$	1.31×10^4	337	337	185	185	0.8327	0.832
29	Weight_H29	Tansig	logsig	15	5	0.00001	$2.24. \times 10^4$	1.31×10^4	337	337	185	185	0.8327	0.832
30	Weight_H30	Tansig	logsig	25	2	0.00001	$2.24. \times 10^4$	1.31×10^4	337	337	185	185	0.8327	0.832
31	Weight_H31	Tansig	logsig	30	2	0.00001	$2.24. \times 10^4$	1.31×10^4	337	337	185	185	0.8327	0.832
32	Weight_H32	Tansig	logsig	35	4	0.00001	$2.24. \times 10^4$	1.31×10^4	337	337	185	185	0.8327	0.832
33	Weight_H33	logsig	Tansig	5	2	0.00001	5.27×10^3	$3.35. \times 10^3$	336	337	185	185	0.194	0.1936
34	Weight_H34	logsig	Tansig	15	2	0.00001	5.27×10^3	$3.35. \times 10^3$	336	337	186	185	0.194	0.1936
35	Weight_H35	logsig	Tansig	20	2	0.00001	5.27×10^3	$3.35. \times 10^3$	336	337	186	185	0.194	0.1936
36	Weight_H36	logsig	Tansig	35	3	0.00001	5.27×10^3	$3.35. \times 10^3$	336	337	186	185	0.194	0.1936
37	Weight_H37	Tansig	Purelin	5	1432	0.00001	467.64	148.12	195	246	100	132	0.0216	0.0213
38	Weight_H38	Tansig	Purelin	5	54	0.0001	123.83	90.47	118	216	68	124	0.0216	0.0132
39	Weight_H39	Tansig	Purelin	10	1433	0.0001	52.35	42.76	8	67	5	38	0.0029	0.0028
40	Weight_H40	Tansig	Purelin	35	2601	0.0001	8.69	6.27	0	4	0	2	0.00079	0.00093
41	Weight_H41	Tansig	Purelin	40	1538	0.00001	2.82	12.35	0	0	1	1	0.0004	0.00056
42	Weight_H42	Tansig	Purelin	45	1198	0.00001	3.06	4.32	0	0	0	0	0.0005	0.00059
43	Weight_H43	Tansig	Purelin	35	1460	0.00001	2.86	4.47	0	0	0	0	0.00036	0.00048
44	Weight_H44	Tansig	Purelin	35	1694	0.00001	2.19	4.41	0	0	0	0	0.00036	0.00051
45	Weight_H45	Tansig	Purelin	35	1105	0.00001	2.41	5.01	0	4	0	15	0.00014	0.00021
46	Weight_H46	Tansig	Purelin	30	1223	0.0001	3.02	5.31	0	0	0	1	0.00015	0.00021

47	Weight_H47	Tansig	Purelin	35	2500	0.0001	2.38	6.55	0	0	0	2	0.00012	0.00021
48	Weight_H48	Tansig	Purelin	35	2470	0.0001	2.09	4.90	0	0	0	0	0.00012	0.00021